COPPE
Instituto Alberto Luiz Coimbra de Pós-Graduação e Pesquisa de Engenharia
UFRJ

APPLICATION OF THE MODAL EXPANSION METHOD IN THE PREDICTION OF DYNAMIC RESPONSES IN A RECIPROCATING COMPRESSOR INTERSTAGE PIPING SYSTEM

Claudio de Oliveira Mendonça

Dissertação de Mestrado apresentada ao Programa de Pós-graduação em Engenharia Oceânica, COPPE, da Universidade Federal do Rio de Janeiro, como parte dos requisitos necessários à obtenção do título de Mestre em Engenharia Oceânica.

Orientador: Luiz Antônio Vaz Pinto

Rio de Janeiro
Setembro de 2020

APPLICATION OF THE MODAL EXPANSION METHOD IN THE PREDICTION OF DYNAMIC RESPONSES IN A RECIPROCATING COMPRESSOR INTERSTAGE PIPING SYSTEM

Claudio de Oliveira Mendonça

DISSERTAÇÃO SUBMETIDA AO CORPO DOCENTE DO INSTITUTO ALBERTO LUIZ COIMBRA DE PÓS-GRADUAÇÃO E PESQUISA DE ENGENHARIA DA UNIVERSIDADE FEDERAL DO RIO DE JANEIRO COMO PARTE DOS REQUISITOS NECESSÁRIOS PARA A OBTENÇÃO DO GRAU DE MESTRE EM CIÊNCIAS EM ENGENHARIA OCEÂNICA.

Orientador: Luiz Antônio Vaz Pinto

Aprovada por: Prof. Luiz Antônio Vaz Pinto
Prof. Ulisses Admar Barbosa Vicente Monteiro
Prof. Marcelo Igor Lourenço de Souza
Prof. Fernando Agusto de Noronha Castro Pinto
Eng. Ricardo Homero Ramirez Gutiérrez

RIO DE JANEIRO, RJ – BRASIL
SETEMBRO DE 2020

Mendonça, Claudio de Oliveira

Application Of The Modal Expansion Method In The Prediction Of Dynamic Responses In A Reciprocating Compressor Interstage Piping System/Claudio de Oliveira Mendonça. – Rio de Janeiro: UFRJ/COPPE, 2020.

XVI, 91 p.: il.; 29, 7cm.

Orientador: Luiz Antônio Vaz Pinto

Dissertação (mestrado) – UFRJ/COPPE/Programa de Engenharia Oceânica, 2020.

Referências Bibliográficas: p. 87 – 91.

1. Pipe vibration. 2. Substructuring. 3. Numeric-Experimental correlation. I. Pinto, Luiz Antônio Vaz. II. Universidade Federal do Rio de Janeiro, COPPE, Programa de Engenharia Oceânica. III. Título.

Dedico este trabalho à minha esposa Nayara, que me apoiou com muita compreensão durante todo o período do desenvolvimento de trabalho.

Agradecimentos

À Nayara, que além de compreender minha ausência em vários momentos durante todo transcorrer deste projeto, sempre me apoia e segue ao meu lado nas horas mais difíceis e felizes da vida.

Aos meus pais, que sempre se esforçaram para que eu tivesse as melhores condições de estudo e sempre me apoiaram em todas as minhas escolhas.

Aos amigos Ulisses e Ricardo Homero, pela dedicação ímpar ao meu desenvolvimento acadêmico, por todas as discussões teóricas e práticas, presenciais e por videoconferências, e por tornarem essa caminhada de pesquisa acadêmica um percurso prazeroso do qual nasceu uma grande amizade.

À UFRJ/COPPE e ao Professor Luiz Vaz, pela oportunidade de me desenvolver na área acadêmica e por ter ajudado a viabilizar os experimentos de campo.

Ao amigo Ricardo Minette, por ter me apresentado a Engenharia Naval da COPPE e pelo compartilhamento de ideias e interesses acadêmicos.

Aos colegas de trabalho Jorivaldo Medeiros, Ediberto Tinoco, Rubem Yuan e Nelson Patricio, pela grande inspiração na minha vida profissional, pelo apoio nos momentos de dificuldade na elaboração da pesquisa, pelas discussões teóricas e práticas que tanto me ensinaram, e pela amizade. Ao Ediberto em especial, pela paciência e por não ter medido esforços para me auxiliar no desenvolvimento do modelo númerico da tubulação.

Ao Artur Fernandes, meu agradecimento especial pelo respaldo e pela oportunidade de conciliar a vida profissional e a acadêmica, e pela confiança de que eu poderia trazer uma contribuição para a Petrobras por meio dos meus estudos.

Ao Fred, Sarasa, Hualber, pela excelente preparação e acompanhamento dos experimentos.

Aos colegas do LEDAV, que me sempre me acolheram com muito carinho e se dispuseram a ajudar sempre que foi preciso. Ao Brenno, pela parceria no desenvolvimento dos algoritmos e modelos.

Resumo da Dissertação apresentada à COPPE/UFRJ como parte dos requisitos necessários para a obtenção do grau de Mestre em Ciências (M.Sc.)

APLICAÇÃO DO MÉTODO DA EXPANSÃO MODAL NA PREDIÇÃO DE RESPOSTAS DINÂMICAS NUM SISTEMA DE TUBULAÇÃO DE INTERESTÁGIO DE COMPRESSOR ALTERNATIVO

Claudio de Oliveira Mendonça

Setembro/2020

Orientador: Luiz Antônio Vaz Pinto

Programa: Engenharia Oceânica

Estruturas e equipamentos sujeitos a carregamento dinâmico estão sujeitos a uma vida útil reduzida devido a níveis excessivos de vibração, que podem levar à falha por fadiga de seus componentes. O monitoramento contínuo desses sistemas pode ser uma tarefa complicada e cara, devido à complexidade e pouca ou nenhuma acessibilidade a alguns locais, o que dificulta a avaliação da integridade estrutural. Uma maneira de lidar com esse problema é usar o modelo de elementos finitos, a análise modal e o método de expansão modal para prever respostas dinâmicas em locais que não foram medidos. Neste trabalho, três estudos de caso são analisados. Os dois primeiros estudos de caso são desenvolvidos usando uma viga retangular de alumínio, cada um com sua respectiva condição de contorno e o terceiro estudo de caso foi de um sistema real da indústria. A matriz modal experimental foi obtida através de análise modal e um processo de redução mista usando a técnica de Guyan e do método System Equivalent Reduction Expansion Process (SEREP) foi utilizada para reduzir o modelo de Elementos Finitos para cada caso estudado, garantindo assim a compatibilidade entre os graus de liberdade numéricos e experimentais. A suavização do modelo foi realizada usando a correspondência local para modos e coordenadas, uma extensão do método LC. Finalmente, usando o método de expansão modal, o modelo modal suavizado foi usado para predizer respostas dinâmicas. Os resultados mostraram alta precisão entre os sinais de aceleração medidos e previstos para todos os três casos apresentados

Abstract of Dissertation presented to COPPE/UFRJ as a partial fulfillment of the requirements for the degree of Master of Science (M.Sc.)

APPLICATION OF THE MODAL EXPANSION METHOD IN THE PREDICTION OF DYNAMIC RESPONSES IN A RECIPROCATING COMPRESSOR INTERSTAGE PIPING SYSTEM

Claudio de Oliveira Mendonça

September/2020

Advisor: Luiz Antônio Vaz Pinto

Department: Ocean Engineering

Structures and equipment subject to dynamic loading are prone to a shortened life span due to excessive vibration levels, which can lead to fatigue failure of its components. Continuous monitoring of those systems can be a complicated and expensive task, due to the complexity and little or no accessibility to some locations, which makes it difficult to assess the structural integrity. One way to deal with this issue is to use finite element model, output-only modal analysis and the modal expansion method to predict dynamic responses in locations that have not been measured. In this work, three case studies are analyzed. The first two case studies are developed using an aluminum rectangular beam, each one with its respective boundary condition and the third case study was of a real industry system. The experimental modal matrix was obtained through output-only modal analysis and a mixed reduction process using Guyan and the System Equivalent Reduction Expansion Method (SEREP) technique was used to reduce the Finite Element model for each case studied, thus ensuring the compatibility between numerical and experimental degrees of freedom. Model smoothing was carried out using the local correspondence for modes and coordinates, an extension of the LC method. Finally, by using the modal expansion method, the smoothed modal model was used to predict dynamic responses. Results showed high accuracy between the measured and the predicted acceleration signals for all three cases presented.

Contents

List of Figures **xi**

List of Tables **xiv**

List of Symbols **xv**

1 Introduction **1**

1.1 Introduction 1
1.2 Motivation 3
1.3 Objectives and Contributions 4
1.4 Dissertation Outline 5

2 Literature Review **7**

2.1 Output-Only Modal Analysis (O-OMA) 7
2.2 Model Reduction 8
2.3 Modal Expansion and Smoothing 9
2.4 Dynamic Response Prediction 10

3 Theoretical Framework **12**

3.1 Modal Analysis 12
3.2 Output-Only Modal Analysis (O-OMA) 13
3.2.1 Enhanced Frequency Domain Decomposition (EFDD) Method 13
3.3 Model Reduction Methods 15
3.3.1 Static Reduction by Guyan 16
3.3.2 System Equivalent Reduction Expansion Process (SEREP) . . 18
3.4 Experimental Mode Shapes Smoothing and Expansion Method 20
3.4.1 Local Correspondence Principle (LC) 20
3.4.2 Local Correspondence Principle for Modes and Coordinates (LCMC) 21
3.5 Dynamic Response Prediction 21
3.6 Criteria Used for Model Assessment 22
3.6.1 Model Assurance Criteria (MAC) 23

3.6.2 Co-Ordinate Modal Assurance Criterion (COMAC) 23
3.6.3 Relative Difference Between Modes (RD) 23
3.6.4 Time Response Assurance Criterion (TRAC) 24
3.6.5 Frequency Response Assurance Criterion (FRAC) 24
3.6.6 Mean Absolute Error (MAE) 24
3.6.7 Root Mean Squared error($RMSE$) 25

4 Methodology for Response Prediction Using the Modal Expansion Method 26
4.1 Finite Element Model 26
4.2 Experiment and O-OMA 29
4.2.1 Complex to Real Operation to the Experimental Mode Shapes 30
4.3 Model Post-Processing and Reduction 30
4.4 Model Reduction Using Guyan-SEREP 31
4.5 Local Correspondence Principle 32
4.5.1 Local Correspondence for Modes and Coordinates 32
4.6 Dynamic Response Prediction 32

5 Case Studies 34
5.1 Rectangular Beam in Free-Free Boundary Condition 34
5.1.1 Finite Element Model (FEM) 34
5.1.2 Experimental Setup 35
5.1.3 Output-Only Modal Analysis (O-OMA) 37
5.1.4 Model Reduction using Guyan-SEREP 39
5.1.5 Modal Expansion and Smoothing Using Experimental Mode Shapes 42
5.1.6 Virtual Sensing 43
5.1.7 Results Discussion 47
5.2 Rectangular Cantilever Beam 49
5.2.1 Finite Element Model (FEM) 49
5.2.2 Experimental Setup 51
5.2.3 Output-Only Modal Analysis (O-OMA) 52
5.2.4 Model Reduction using Guyan-SEREP 53
5.2.5 Smoothing of the Experimental Modal Matrix 57
5.2.6 Virtual Sensing 57
5.2.7 Response Prediction in DOF 5 using Multiple Acceleration Measurements 59
5.2.8 Results Discussion 60
5.3 Interstage Compressor Pipe System 61
5.3.1 FEM Model 62

5.3.2 Experimental Setup 64
5.3.3 Output-Only Modal Analysis (O-OMA) 66
5.3.4 Model Reduction using Guyan-SEREP 67
5.3.5 Modal Smoothing Using Experimental Mode Shapes 71
5.3.6 Virtual Sensing 77
5.3.7 Results Discussion 82

6 Conclusions and Recommendations **84**

References **87**

List of Figures

1.1 Reciprocating compressor, image taken from the 3D model of the process plant. 5

3.1 Schematic representation of the reduction process. Source: AVITABILE (1998). 15
3.2 Schematic representation of the reduction of the complete modal matrix in the active degrees of freedom. Source: AVITABILE (1998) . . 19

4.1 Diagram with the steps applied in the methodology for the aluminum beam 27
4.2 Diagram with the steps applied in the methodology for the pipe system 28

5.1 Aluminum beam finite element model. 34
5.2 Rectangular beam suspended in Free-Free boundary condition and instrumented with 09 accelerometers. 36
5.3 Schematic of the positioning of accelerometers. 37
5.4 Detailed view of the sensor positioning 37
5.5 Aluminum beam being excited by impact hammer. 38
5.6 Impact Hammer Brüel e Kjaer model 8200. 38
5.7 Data acquisition board from *National Instruments* model NI 9234. . . 39
5.8 SEREP reduced and full numerical mode shapes comparison. 40
5.9 MAC for SEREP reduced and full numerical mode shapes comparison. 40
5.10 Experimental and FE reduced mode shapes. 41
5.11 MAC for SEREP and experimental modes. 41
5.12 COMAC and RD between SEREP and experimental modes 42
5.13 LC estimate of optimum number mode shapes for correlation. 42
5.14 Modal plots for calibrated, non-fitted and experimental mode shapes. 43
5.15 MAC improvements from LC correlation procedure. 44
5.16 MAC improvements from LC correlation procedure for higher modes. 44
5.17 Rectangular beam configuration(F_i: force, a_i: accelerometer). 44
5.18 Time domain comparison of predicted and measured accelerations at the ninth DOF. 46

5.19 Frequency domain comparison of predicted and measured accelerations at the ninth DOF. 46
5.20 Time domain comparison of predicted and measured accelerations at the ninth DOF. 47
5.21 Frequency domain comparison of predicted and measured accelerations at the ninth DOF. 47
5.22 Comparison between predicted and estimated signals. 47
5.23 Root mean squared error on time and frequency domains. 48
5.24 MAC improvements comparing LC and LCMC smoothing methods. . 49
5.25 Measuring Instruments: a) A/D NI® board b) Waterproof piezoelectric accelerometer. 51
5.26 Rectangular beam in cantilever boundary condition and instrumented with 05 accelerometers. 52
5.27 Rectangular beam configuration(F_i: force, a_i: accelerometer). 53
5.28 SEREP reduced and full numerical mode shapes comparison. 55
5.29 MAC for SEREP reduced and full numerical mode shapes. 55
5.30 Experimental and SEREP reduced mode shapes comparison. 56
5.31 MAC for SEREP and experimental modes. 56
5.32 COMAC and RD between SEREP and experimental modes 57
5.33 Modal plots for calibrated, non-fitted and experimental mode shapes. 58
5.34 MAC improvements from LC correlation procedure. 58
5.35 Time domain comparison of predicted and measured accelerations at the fifth DOF. 59
5.36 Frequency domain comparison of predicted and measured accelerations at the fifth DOF. 59
5.37 Time domain comparison of predicted and measured accelerations at the fifth DOF. 60
5.38 Frequency domain comparison of predicted and measured accelerations at the fifth DOF. 61
5.39 Second stage suction pipe, image taken from the 3D model of the process plant. Accelerometer installation positions marked in red. . . 62
5.40 Pipe dimensions and identification of accelerometer and impact positions. 63
5.41 Finite element full model. 63
5.42 Intermediary pipe support. 64
5.43 Pulsation damper model for boundary condition stiffness calculation. 65
5.44 Second stage suction pipe with accelerometer installed highlighted with red circles. 67
5.45 SVD - Impacts in P1 and P2, X direction. 68

5.46 Guyan reduction model showing active DOFs. 69
5.47 MAC for reduced and full modes. 70
5.48 Guyan-SEREP reduced and full mode shape for the first mode. . . . 70
5.49 Guyan-SEREP reduced and full mode shape for the second mode. . . 71
5.50 Guyan-SEREP reduced and full mode shape for the third mode. . . . 71
5.51 Guyan-SEREP reduced and full mode shape for the fourth mode. . . 72
5.52 MAC for reduced and experimental modes. 72
5.53 MAC for reduced and experimental modes. 72
5.54 Guyan-SEREP reduced and experimental mode shape for the first mode. 73
5.55 Guyan-SEREP reduced and experimental mode shape for the second mode. 73
5.56 Guyan-SEREP reduced and experimental mode shape for the third mode. 74
5.57 Guyan-SEREP reduced and experimental mode shape for the fourth mode. 74
5.58 MAC for Fitted and experimental modes. 75
5.59 COMAC and RD between fitted and experimental modes 75
5.60 MAC improvements from LCMC correlation procedure. 76
5.61 Experimental and Fitted mode shape for the first mode. 76
5.62 Experimental and Fitted mode shape for the second mode. 77
5.63 Experimental and Fitted mode shape for the third mode. 77
5.64 Experimental and Fitted mode shape for the fourth mode. 78
5.65 Time domain comparison of predicted and measured accelerations at sensor 7 direction X, impact given at point P4 in Z direction. 79
5.66 Frequency domain comparison of predicted and measured accelerations at sensor 7 direction X, impact given at point P4 in Z direction. 80
5.67 Time domain comparison of predicted and measured accelerations at sensor 7 direction Y,impact given at point P4 in Z direction. 80
5.68 Frequency domain comparison of predicted and measured accelerations at sensor 7 direction Y, impact given at point P4 in Z direction. 81
5.69 Time domain comparison of predicted and measured accelerations at sensor 7 direction X. 81
5.70 Frequency domain comparison of predicted and measured accelerations at sensor 7 direction X. 82
5.71 Time domain comparison of predicted and measured accelerations at sensor 7 direction Y. 82
5.72 Frequency domain comparison of predicted and measured accelerations at sensor 7 direction Y. 83

List of Tables

5.1 Mesh convergence by comparison of numerical and experimental natural frequencies. 35
5.2 Dimensions of aluminum beam 36
5.3 Accelerometers specification 36
5.4 Modal parameters estimated using EFDD 39
5.5 FEM model keypoints position in relation to the beam clamped point. 50
5.6 Mesh convergence by comparison of Natural frequencies (f (Hz)) and number of line segment subdivisions (N). 50
5.7 Natural frequencies estimated using EFDD 53
5.8 Analysis of the influence of the number of active degrees-of-freedom in the Guyan natural frequency results. 54
5.9 Difference between numerical and experimental natural frequencies. . 65
5.10 Description and location of the sensors used. 66
5.11 Modal Parameters estimated using EFDD. 68

List of Symbols

Symbols

$[K]$	Stiffness matrix
$[K_r], [M_r]$	Reduced stiffness and mass matrices
$[M]$	Mass matrix
$[T]$	Reduction transformation matrix
ϕ	Experimentally obtained mode shapes (unscaled)
Ψ	Mass normalized mode shape
$\{F\}$	Vector of loads acting on the system
$\{X(t)\}, \{\dot{X}(t)\}, \{\ddot{X}(t)\}$	Displacement, velocity and acceleration vectors
a, d	Active and deleted degrees of freedom
B	Numeric vibration modes cluster
i	Iteration index
p	Number of modes considered in modal truncation
$q(t)$	Modal coordinates
z	Numeric mode adjustment coefficient vector
Φ	Numerically obtained mode shapes
n	Number of possible combinations
r	Degrees of freedom used to check optimization

Abbreviations

DOF	*Degree of Freedom*

EMA	*Experimental Modal Analysis*
ESP	*Electrical Submersible Pump*
FEM	*Finite Element Model*
$FRAC$	*Frequency Response Assurance Criterion*
IEA	*International Energy Agency*
LC	*Local Correspondence Principle*
$LCMC$	*Local Correspondence for Modes and Coordinates*
MAC	*Modal Assurance Criteria*
MAE_{FD}	*Mean Absolute Error in the Frequency Domain*
MAE_{TD}	*Mean Absolute Error in the Time Domain*
$O-OMA$	*Output-Only Modal Analysis*
RD	*Relative difference*
$RMSE_{FD}$	*Root Mean Squared Error in Frequency Domain*
$RMSE_{TD}$	*Root Mean Squared Error in Time Domain*
$SEREP$	*System Equivalent Reduction Expansion Method*
SRM	*Static Reduction Method*
$TRAC$	*Time Response Assurance Criterion*

Chapter 1

Introduction

1.1 Introduction

The oil industry currently accounts for around 40% of the world energy mix IEA (2017). Due to the challenges imposed by the processes necessary to explore, produce and convert oil into clean, safe and efficient by-products, many technological solutions are created for development of a sound and reliable production environment.

One of the most important by-products from the oil chain is the diesel, a very demanded fuel for transportation purposes. As the rules for air pollution emission controls from fossil fuels become more rigid, further processing is necessary to guarantee that the final products meet the necessary requirements.

The hydrotreating unit is responsible for the removal of sulfur and other contaminants from intermediate streams (e.g.: diesel) before blending into a finished product. As emissions and limitations become rigid, hydrotreating units have become more important MCKINSEY (2020).

The hydrotreating process begins with the heating of a mixture of hydrogen to hydrocarbon. This mixture is injected into a reactor vessel containing a specified catalyst where the removal of the sulfur takes place. In order to reduce the coke laydown on the catalyst, high operating pressures are used in this process. The equipment responsible for maintaining this high pressures is a reciprocating hydrogen compressor.

Reciprocating compressors are known sources of dynamic excitation. These machines are responsible for recurrent failure problems in pipes and auxiliary systems connected to it if the design and assembly do not strictly comply with the design recommendations of the relevant technical standards.

Structures and equipment operating under dynamic loads have a high probability of failure, which poses a threat to the health and safety of operators, the environ-

ment, and the companies' productivity and profitability. These risks demand careful equipment inspection and monitoring to prevent accidents.

Controlling excitation forces characteristics is a rather complicated task. Nevertheless, since these forces can cause undesirable system conditions (such as fatigue, stress, high vibration levels, noise, resonance conditions, etc.) in response, it can be interesting to maintain control. These types of conditions can adversely affect system performance, leading to operational problems and component damage.

Knowledge of the system's response to operational load excitation is of great importance for monitoring the reliability of structures CHEN *et al.* (2018). Measurement data is commonly collected to identify operational response characteristics. Although they present important information about system performance, the availability of the necessary amount of sensors for assessment is often limited and difficult accessibility to certain parts may apply CHIPMAN e AVITABILE (2012). In this context, continuous monitoring can be a difficult and expensive task: the technology currently available limits the number of sensors for vibration measurement; the complexity of the system sometimes makes it impossible to continuously measure vibration in locations with higher risk of failure, particularly when these locations have poor accessibility.

According to KULLAA (2016), virtual sensing can be either model-based (analytical) or data-driven (empirical). Analytical virtual sensing techniques use information available from a limited set of physical sensors together with a Finite Element Model (FEM) to calculate an estimate of the quantity of interest. For example, estimating the stress or strain field from acceleration measurements could be useful for fatigue assessment.

Analytical mode shapes from the FEM are typically used as a basis to estimate the response at unmeasured locations by an expansion algorithm KULLAA (2016). Model-based virtual sensing in structural dynamics have been studied by several authors, such as SESTIERI *et al.* (2013), AVITABILE (2005), PINGLE e AVITABILE (2011) and ILIOPOULOS *et al.* (2014).

One way to estimate vibration levels in the structure regions of interest is by using FEM models CHEN *et al.* (2018); QU (2004). However, these models have the disadvantage that they do not always represent the structure properly, as they do not take into account manufacturing errors. According to FRISWELL e MOTTERSHEAD (1995), errors between the model and the actual structure can be minimized by performing calibration using the dynamic behavior of the real structure obtained by modal analysis data, although calibration brings one more challenge: the number of degrees of freedom (DOF) of the FEM is much higher than the number of degrees of freedom that can be monitored, therefore calibration cannot be performed directly.

As long as the modal model is calibrated, the combined use of operational acceleration data and mode shape components is able to provide sufficient information for the prediction of accelerations at different locations along the structure. The prediction is based upon a modal decomposition of the measured accelerations that results in the estimation of the modal coordinates ILIOPOULOS *et al.* (2014). The relation between the modal coordinate and the acceleration in an arbitrary point is established by making use of the calibrated mode shapes ILIOPOULOS *et al.* (2014).

In this work, a methodology for predicting dynamic response is presented in three different case studies. The first two case studies were made in laboratory conditions, each with different boundary conditions for validation. The third was a real industrial application for a reciprocating compressor interstage pipe. In each case study, FEM and output-only modal analysis (O-OMA) mode shapes were used to, after steps of reduction of the FEM model and smoothing of the O-OMA mode shapes, serve as a modal base for the expansion of measured signals allowing the prediction of dynamic responses at unmeasured locations.

1.2 Motivation

Although piping systems are known as static equipment where no dynamic behaviour is expected, these systems can be subjected to different types of loads that make them respond with alternating movements. Examples of these types of loads are: fluid transients, flow induced turbulence, opening and closing of valves, mechanical excitation and many others.

Piping systems presenting these dynamic loading, as the ones imposed by reciprocating compressors like the case study presented in this dissertation, are prone to a shortened life span due to excessive vibration levels, which can lead to fatigue failure of its components.

The piping system object of study in this dissertation presented high values of vibration amplitude and a more thorough analysis was necessary for system assessment.

In the case presented, as in many situations, monitoring of the system can be a complicated and expensive task, due to the complexity and poor accessibility to some locations, which makes it difficult to assess the structural integrity.

Therefore, having a methodology capable of yielding a reliable estimate of vibration response in critical and difficult to reach locations may improve the quality and assertiveness of the assessment, thus improving the piping system safety.

1.3 Objectives and Contributions

This dissertation aims at the definition and validation of a complete methodology to predict dynamic response in structures or equipment's at unmeasured locations. For this purpose, it requires to:

- Develop a FEM of the system object of the analysis;
- Perform an Output-Only modal analysis;
- Reduce the FEM model to match the number of DOFs measured in the modal analysis;
- Validate the reduced model using the appropriate assessment criteria;
- Smooth the experimental mode shapes using the proposed Local Correspondence for Modes and Coordinates (LCMC) method;
- Assess the improvement in the smoothed mode shapes using the MAC criteria;
- Use the smoothed mode shapes to obtain estimates of vibration amplitudes in a non-instrumented location;
- Validate the predicted signal using the adequate assessment criteria. [1]

The methodology proposed will first be validated with two laboratory experiments of an aluminum beam, each with different boundary conditions to check the conditions in the final results. The first experiment will be undertaken with the beam in a free-free condition, while the second will be for a cantilever condition. After validating with the lab experiments, the same methodology will be applied to a industrial example of an interstage pipe of a reciprocating compressor. An image taken from the 3D model of the compressor analysed, showing the second stage piping can be seen in Fig. 1.1. The reduction, smoothing and final signal prediction will be validated using the adequate assessment criteria as FRAC (Frequency Response Assurance Criterion), TRAC (Time Response Assurance Criterion), MAE_{FD} (Mean Absolute Error in the Time Domain),MAE_{TD} (Mean Absolute Error in the Frequency Domain),$RMSE_{FD}$ (Root Mean Squared Error in Frequency Domain) and $RMSE_{TD}$(Root Mean Squared Error in Time Domain) for the predicted signal.

This dissertation contributes to the work currently being developed in the scientific community in the following topics:

[1] Although the main objective of the methodology is to predict dynamic responses at unmeasured locations, the validation in this dissertation is undertaken by prediction of response in a location where an actual sensor was placed only for comparison reasons.

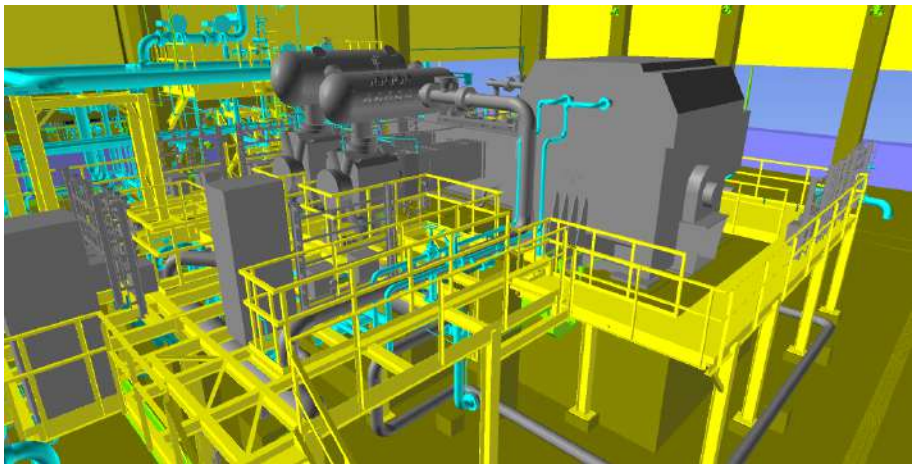

Figure 1.1: Reciprocating compressor, image taken from the 3D model of the process plant.

- Proposition and validation of a mixed reduction method, where part of the reduction is undertaken before exporting the mass an stiffness matrices, from a commercial FEM software, reducing the computational effort;
- Proposition of a variant of the Local Correspondence Principle (LC) described by BRINCKER *et al.* (2014), improving the definition of the optimal number of modes and degrees of freedom to be used in the smoothing of experimental mode shapes;
- Definition and validation of a complete workflow for dynamic signal prediction at unmeasured locations.
- Improvement on the definition of the mode shapes used in the virtual sensing, a similar approach to the LC is used. This proposition diminishes considerably the processing time.

1.4 Dissertation Outline

The research presented in this dissertation is divided in six main chapters:

- The current chapter (introduction) describes an overview of the vibration problems encountered in piping systems connected to reciprocating compressor; the motivation and contributions resulted from the present work.
- The second chapter presents a literature review of the main topics that were used in this work as model reduction and expansion, smoothing of experimental mode shapes and dynamic response prediction at unmeasured locations. It indicates the established fundamentals as well as the most modern works that are currently being developed by the scientific community.

- In the third chapter the theoretical framework is exposed, containing the necessary mathematical development of the methods studied and used in this dissertation.
- Chapter four provides the detailed methodology applied at the subsequent study cases. In addition, the flowchart represented shows in a broader way the steps applied.
- In chapter five the three case studies analyzed in this dissertation are laid out for the validation of the methodology used. The first two case studies for an aluminum rectangular beam, each one with its respective boundary condition and the case study of a real industry condition system is presented. The complete process for each case is structured and the results obtained are discussed.
- Chapter six stands for a comprehensive analysis of the whole work, as well as provides recommendations for future works.

Chapter 2

Literature Review

2.1 Output-Only Modal Analysis (O-OMA)

R. S. MINETTE (2014) presents a methodology for applying output-only modal Analysis to identify modal parameters for an electrical submersible pump (ESP). The ESP is an equipment that is used in the Oil & Gas industry and therefore is located in inaccessible places to pump petroleum, as satellite wells and sub-sea. These locations cause the interventions on those equipment's to be costly and involve undesirable production loss. Therefore the identification of dynamic parameters through modal analysis is of fundamental importance to increase the machines reliability.

RAINIERI e FABBROCINO (2014) proposes an alternative for post-processing modal parameters estimated by O-OMA. Most O-OMA methodologies result in complex eigenvalues and eigenvectors, a consequence of various probable reasons as gyroscopic effects, aerodynamics effects, nonlinearities and nonproporcional damping. As these estimated values are to be compared with FEM results that as they are undamped result in real values. The author proposes a simple methodology to convert the experimentally obtained complex mode shapes to real ones.

ALBUQUERQUE *et al.* (2019) compared two different approaches for the determination of dynamic properties, the *Experimental Modal Analysis* (EMA) where the excitation forces (input) is known as well as the response (output) and the Output-Only Modal Analysis (O-OMA) which uses only the output. While EMA performs a full numerical validation, resulting in a mass normalized modal matrix, in the O-OMA case, the modal matrix could only be normalized to unity. Both methodologies were applied to a beam in a simulated free-free boundary condition, instrumented with 9 (nine) accelerometers and excited with multiple impacts at different positions. The results obtained with both analysis were very close, with natural frequencies differences as high as 0.5% and MAC values higher than 0.9 for the mode shapes correlations. The results were also compared with a FEM, showing

small differences. This indicates that whenever the input is difficult to obtained, as in large structures, the output only modal analysis can be a suitable option for dynamic properties estimation.

2.2 Model Reduction

In determining the natural frequency and modes of vibration of structures, it is generally convenient to reduce the model matrices. GUYAN (1965) presented a methodology for reducing the mass matrix similar to the procedure already used for stiffness matrix, in a procedure based on the elimination of DOFs where the acting forces were zero. The procedure presented by this author allowed the calculation of reduced mass and stiffness matrices, as it was developed as a static method for dynamic cases the solution to the Eigenvalue and Eigenvector problem is close, but not the same, to that of the complete system and is very dependent on the number of degrees of freedom used.

Later, in a complementary development called *Static Reduction Method* (SRM), KIDDER (1973) proposed reduction equations based on the dynamic systems equation. This method is seen as the best extension of the static method proposed by Guyan, but it has a high computational cost.

As the method presented by KIDDER (1973) affects dynamic characteristics, O'CALLAHAN *et al.* (1989) proposed a new methodology capable of reducing models containing arbitrary degrees of freedom. The proposed method, called *System Equivalent Reduction Expansion Process* ("SEREP") maintains natural frequencies and modes of vibration identical to those of the full model. This method is reversible, thus allowing the expansion of the reduced degrees of freedom to the complete space of the model.

Reduction-Expansion methods are also used to estimate the displacements of all DOFs in a FEM based on experimental information. BALMÈS (1999) states that, despite the vast literature on the subject, well-established methods have deficiencies such as the simplification that limits the use of techniques and the consideration that measurements are made at points coinciding with degrees of freedom of the FEM. To resolve this constraint, BALMÈS (1999) proposes an alternative methodology to correlate degrees of freedom and outputs. This methodology presents a theoretical solution to deal with measurements of non-orthogonal to the degrees of freedom of the FEM. The matrix that makes this correlation is called the observation matrix. The author also presents results for expanding measurement data for an engine head and for a test structure, concluding that the use of observation matrices has given good results in expanding structures with non-trivial geometries and that the best expansion methods for cases used were hybrid methods, which combine formulations

using quadratic inequalities with the dynamic method.

KONG *et al.* (2012) proposes a methodology for analyzing a long bridge, with steel x concrete connection, by means of modeling with model reduction techniques. This modeling allows the evaluation of details, such as the connectors between the steel structure and the concrete, without losing dynamic response information of the complete structure. The methodology was validated by computational analysis of a beam with thirty meters in length and a square section. Models were made with solid element, combination of solid element with beam element, beam element and part *substructuring* and the entire structure in solid element. The results obtained indicated that the model made with a bar element was not able to represent the vibration modes characterized by the local buckling of the structure and concludes that the *substructuring* method proved to be simple and accurate not only because of the reduction in computational time but also for maintaining accuracy by extracting sufficient modes. With the validity methodology he proceeded with the numerical analysis of the bridge *jingyue* obtaining positive results.

NONIS *et al.* (2014) presents in his work that although there are several methods for expanding the results of reduced models, SEREP was used due to the preservation of dynamic characteristics regardless of the number of degrees of freedom selected. In this work NONIS *et al.* (2014) successfully uses expansion matrices to expand assembly modes composed of decoupled sub-models. To prove the effectiveness of the method, he compares the results with those obtained by evaluating the complete assembly model

2.3 Modal Expansion and Smoothing

To analyze expansion methods, CHIPMAN e AVITABILE (2012) used a set of 310 (three-hundred and ten) measurements taken on a dryer base plate from laser vibration sensors. The method chosen for the evaluation was SEREP, the transformation matrix was calculated based on a subset of 31 (thirty-one) of the degrees of freedom measured and the expansion of these to the complete system was correlated with the data measured through the correlations MAC and TRAC. The authors concluded that the use of a greater number of degrees of freedom in the calculation of the transformation matrix in relation to the number of vibration modes under evaluation results in better results. They also concluded that similar results were obtained using experimental data for the calculation of the transformation matrix in comparison with the use of data from the computational model. The calculation of the expansion matrix with experimental data proved to be equivalent to that made with numerical data and, the method proved to be excellent in providing expanded information about the system, allowing a more in-depth analysis.

BRINCKER *et al.* (2014) presents, based on the theory of sensitivity, a development to identify the vibration modes of the model to be used in the subspace to smooth experimental modes, a methodology called *"Local Correspondence Principle"* (hereinafter, "LC"). As an example of applying the LC, a test was performed on a plate. The results obtained were compared with the use of SEREP for a fixed subspace of five modes of vibration. For the case studied, in which few degrees of freedom were used to estimate the modes of vibration, the LC method resulted in better results than SEREP. However, it is important to note that the method is limited to cases where the FEM shows close proximity to the real structure.

AENLLE e BRINCKER (2014) proposes a methodology for normalizing the experimental vibration modes from the mass matrix obtained by the FEM. The methodology was validated through simulations of a bridge FEM model and with laboratory tests of a cantilever beam. The results obtained were compared between the mass change method, the FEM mass normalization method and the FEM mass method and the LC smoothed modes. It was observed that the use of LC almost always presents better results, except for conditions in which the mass matrix presents divergence with the real condition.

CHEN *et al.* (2018) proposed the use of the expansion technique for submerged structures. The work in question studied a test structure similar to a fin. Tests were made with the structure inside an aquarium with and without water. It should be noted that the expansion and stress calculation were done with the matrix calculated from the model in the air, without fluid-structure interaction. As expected, the natural frequencies and damping are different, but the stress values found remained close between the measured and the calculated by the model from the expanded displacement field.

2.4 Dynamic Response Prediction

AVITABILE (2005) presents model expansion techniques used today as a mechanism to complete unmeasured DOF from experiments using FEMs. It describes the use of the FEM as a high order polynomial curve fitter used to estimate experimental mode shapes at chosen set of DOF.

MAES *et al.* (2014) compared three different response estimation methods using data from a cantilever beam numerical model with the addition of measurement noise and modeling errors. Joint input-state estimation, Kalman filter and modal interpolation (also known as modal expansion) algorithm were compared, resulting in a better performance for the joint input-state and the modal interpolation when compared to the Kalman filter method. The joint input-state also required a smaller number of output measurements than the modal interpolation but it concluded that

if the number of equivalent forces assumed when applying the joint input-state estimation, large errors may occur.

KULLAA (2016) studied virtual sensing techniques using data available from a limited set of measurements in conjunction with a FEM as a basis of estimation response at unmeasured locations by expansion algorithms. As an alternative to decrease the modelling effort, substructuring techniques were used. The author analysed two examples, a vehicle crane and a floor structure. In both cases better results were found when the physical sensors were installed evenly distributed or close to the virtual sensor being predicted.

Structure health monitoring of wind turbines was undertaken by ILIOPOULOS *et al.* (2016). In his paper, the author uses the prediction of dynamic responses to analyse fatigue sensitive positions in offshore wind turbines that are of difficult accessibility, as points in the mud line below the water level. Response estimations were undertaken using limited set of accelerometers data and a FEM. The technique applied was the modal decomposition and expansion of experimental data. Good results were obtained both in time and frequency domain for acceleration responses, confirmed by TRAC, FRAC and MAE_{TD} criteria. The author indicates that the method is sensitive to operational conditions, as for wind turbines changing operational and ambient conditions affect dynamic behavior of the structure.

TARPØ *et al.* (2020) explored the use of virtual sensing to enable full-field stress/strain for fatigue assessment of offshore structures, which are exposed to fatigue damage. The author applied modal expansion techniques as SEREP, LC and a variant of the LC method proposed in the paper at experimental data obtained from a scaled model of an offshore platform experimented in laboratory conditions. It concluded that expanding mode shapes can increase accuracy of the estimation of unmeasured locations, however as a fitting process, depending on the case can cause over-fitting and should used with care. The author also discussed how the quality measurements TRAC and FRAC might mislead the quality of strain/stress estimation as they assess the shape of the compared values and are independent of amplitude differences which are important in fatigue analysis.

Chapter 3

Theoretical Framework

3.1 Modal Analysis

The methodology used to determine the natural frequencies, damping ratios and vibration modes of a mechanical system is called *Modal Analysis*. The use of this methodology allows the representation of the dynamic behavior of a structure. As noted by OGNO (2013), free vibration fully characterizes the structure's dynamical properties. Therefore, in a linear or linearized system, the response ($\{X(t)\}$) can be expressed as the linear combination of its number n_0 of modes ϕ_i and their time-dependent amplitude or modal coordinates $q_i(t)$, as given in Eq. (3.1):

$$\{X(t)\} = \sum_{i=1}^{n_0} q_i(t)\{\Phi_i\} \quad n_0 \to \infty \tag{3.1}$$

The continuity of a real structure results in infinite degrees of freedom. Nevertheless, as the number of sensor is limited only a certain finite number of modes are possible to be detected. This limitation yields the idea of modal approximation where the Eq. (3.1) is truncated for a certain number of modes (N). The number of modes taken determines the accuracy of the approximation.

$$\{X(t)\} \cong \sum_{i=1}^{N} q_i(t)\{\Phi_i\} \quad N \in \mathbb{N} \tag{3.2}$$

A Modal Analysis is performed to experimentally estimate the modal properties of a structure. This methodology is applied for a broader range of analysis, for example: vibration control, operational stability of turbo machinery, identification of excitation forces, reduction of dynamic models and calibration of finite element method (FEM) models - the focus of this work. In more overall view, the main techniques for Modal Analysis can be categorized in experimental modal analysis (EMA) and output-only modal analysis (O-OMA). In this dissertation, as the methodology

is created to be used in large structures that are difficult to excite with known forces, we applied the output-only modal analysis, to be described on the following section.

3.2 Output-Only Modal Analysis (O-OMA)

As described by BUSSON *et al.* (2019), the biggest limitation of EMA is that the magnitude of the exciting force acting on the system under test must be known in order to estimate its modal parameters. If not impossible, force measurement in large structures may be difficult to accomplish. Applying forces to a complex structure can cause local damages and implies in a considerable economical cost, even in the cases of laboratory tests, where it is hard to reproduce the actual forces in a reliable manner.

For the reasons described above, the Output-Only Modal Analysis was developed in order to (i) bypass the existing limitation of the traditional method and (ii) offer the possibility of modal parameters assessment only from dynamic response information. It is important to mention that this analysis also allows to estimate these parameters in cases of unknown excitation forces (in terms of its magnitude and frequency), applied to linear and time-invariant systems.

The focus of the current work is on *Frequency Domain Technique*. It was determined for the following reasons: (i) easier implementation than time domain technologies; (ii) effectiveness for the expected effect;

The Frequency Domain Technique to be reviewed is Enhanced Frequency Domain Decomposition (EFDD) and it is discussed on the following sub-section.

3.2.1 Enhanced Frequency Domain Decomposition (EFDD) Method

The Enhanced Frequency Domain Decomposition (EFDD) technique in frequency domain is an enhanced version proposed by BRINCKER e VENTURA (2015) of the Frequency Domain Decomposition (FDD) method. The main advantage associated with the FDD method is that it can more accurately evaluate the natural frequency and determine the damping rate.

The essence of the EFDD technique relies on a decomposition of the Power Spectrum Density (PSD) from the measured response. The estimated PSD matrix, $[G_{yy}(\omega)]$ is formed by the estimated PSD's for all sensors. A complex hermitian and positive definite PSD matrix has the following form:

$$[G_{yy}(\omega)] = [H(\omega)][G_{xx}(\omega)][H^{\mathrm{H}}(\omega)] \tag{3.3}$$

Where $[G_{yy}(\omega)]$ and $[G_{xx}(\omega)]$ are the output and input (stochastic) PSD matrices of size $N_m \times N_m$; N_m is the number of measurements and $[H(\omega)]$ is the frequency response function (FRF) matrix, which can be expressed in partial form as (Zhang et al-FSDD):

$$[H(\omega)] = \sum_{m=1}^{N_m} \left(\frac{R_m}{\omega - \lambda_m} + \frac{R_m^*}{\omega - \lambda_m^*} \right) \tag{3.4}$$

Where N_m is the number of modes; λ_m is the mth pole, and are related to the damping factor (σ_m), damped modal frequency (ω_{dm}) and modal damping ratio (ζ_m) as given in Eq. (3.5)

$$\lambda_m = -\sigma_m + \omega_{dm}; \omega_m = \sqrt{\sigma_m^2 + \omega_{dm}^2}; \zeta_m = \frac{\sigma_m}{\sqrt{\sigma_m^2 + \omega_{dm}^2}} \tag{3.5}$$

$[R_m]$ and $[R_m^*]$ are the corresponding conjugate residue matrices pairs and $[R_m]$ is given as:

$$[R_m] = \{\Phi_m\}\{\gamma_m^{\mathrm{T}}\} \tag{3.6}$$

Where, $[\Phi_m]$ and $\{\gamma_m\}$ are the mth mode shape and modal participation factor vectors, respectively. The key step in the EFDD technique is to apply a singular value decomposition (SVD) to the h-PSD estimated at a discrete frequency, $\omega = \omega_k$ JACOBSEN e ANDERSEN (2008):

$$[\widehat{G}_{yy}(\omega_k)] = [U(\omega_k)][S(\omega_k)][U(\omega_k)^{\mathrm{H}}] \tag{3.7}$$

Where the diagonal matrix $[S(\omega_k)]$ is the diagonal matrix of singular values and $[U_k] = [u_{k1}, u_{k2}, \ldots, u_{kM}]$, is the unitary matrix, consisting of unitary vectors u_k, which are interpreted as the modal shape of the system at each natural frequency.

It is observed that singular values are a function of the excitation frequency. When the frequency approaches a modal frequency ω_m, the PSD matrix approximates a rank one matrix as:

$$[\widehat{\mathrm{G}}_{yy_{\omega\rightarrow\omega_m}}(\omega_k)] = [\mathrm{s}_1(\omega_m)][u_1(\omega_m)][u_1^{\mathrm{H}}(\omega_m)] \tag{3.8}$$

The first singular value reaches a maximum, $[s_1(\omega_m)] \rightarrow max$. The corresponding singular vector $[u_1(\omega_m)]$ is an estimate of the mth mode shape $[\widehat{\mathbf{\Phi}}_m] = [u_1(\omega_m)]$ with unitary normalization.

In the vicinity of the natural frequency it is possible to obtain singular vectors having a high MAC value which enable the establishment of a Single-Degree-Of-Freedom (SDOF) spectral density function, for a specific mode, which is transformed to the time domain yielding an auto-correlation function of the SDOF system. From this auto-correlation function, the natural frequency is obtained by determining the

number of zero-crossing as a function of time using a simple least-squares fit. The damping ratio is obtained from the logarithmic decrement of the auto-correlation function again using a simple least-squares fit. JACOBSEN e ANDERSEN (2008).

3.3 Model Reduction Methods

Model Reduction methods are used in various conditions for more efficient analysis. One example of its use is the size reduction of large models, as shown in Fig. 3.1.

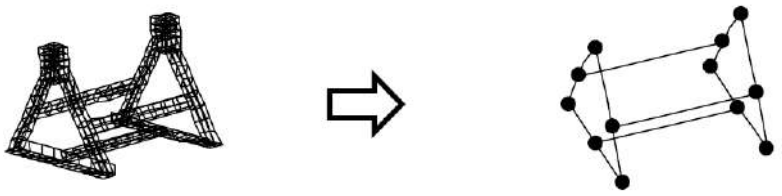

Figure 3.1: Schematic representation of the reduction process. Source: AVITABILE (1998).

In general, the correlation between the degrees of freedom of the full model and the reduced model can be represented by the Eq. (3.9).

$$\{X_{\mathrm{n}}\} = \begin{Bmatrix} X_{\mathrm{a}} \\ X_{\mathrm{d}} \end{Bmatrix} = \Big[T\Big] \{X_{\mathrm{a}}\} \tag{3.9}$$

In Eq. (3.9) the index *'n'* indicates that the degrees of freedom of this vector are from the full model, the index *'a'* represents the active degrees of freedom and the index *'d'* represents the degrees of freedom excluded during the reduction. The $[T]$ matrix is then the correlation matrix between the two sets of degrees of freedom.

Changing the index for the identification of the full model to '1' and the reduced model to '2', the Eq. (3.9) can be rewritten as:

$$\{X_1\} = \Big[T_{12}\Big] \{X_2\} \tag{3.10}$$

Taking in consideration the energy conservation of the system, the energy balance between the full and reduced model can be written as:

$$U = \frac{1}{2} \Big\{x_1\Big\}^T \Big[K_1\Big] \Big\{x_1\Big\} = \frac{1}{2} \Big\{x_2\Big\}^T \Big[K_2\Big] \Big\{x_2\Big\} \tag{3.11}$$

Substituting in the transformation equation, yields:

$$U = \frac{1}{2} \Big\{ \Big[T_{12}\Big] \Big\{x_2\Big\} \Big\}^T \Big[K_1\Big] \Big\{ \Big[T_{12}\Big] \Big\{x_2\Big\} \Big\} = \frac{1}{2} \Big\{x_2\Big\}^T \Big[K_2\Big] \Big\{x_2\Big\} \tag{3.12}$$

Rearranging the terms, we have:

$$U = \frac{1}{2}\left[T_{12}\right]^T \left\{x_2\right\}^T \left[K_1\right] \left[T_{12}\right] \left\{x_2\right\} = \frac{1}{2}\left\{x_2\right\}^T \left[K_2\right] \left\{x_2\right\} \tag{3.13}$$

Thus, the correlation between mass an stiffness equations are given:

$$\left[K_2\right] = \left[T_{12}\right]^T \left[K_1\right] \left[T_{12}\right] \text{ or } \left[K_\mathrm{a}\right] = \left[T\right]^T \left[K_\mathrm{n}\right] \left[T\right] \tag{3.14}$$

$$\left[M_2\right] = \left[T_{12}\right]^T \left[M_1\right] \left[T_{12}\right] \text{ or } \left[M_\mathrm{a}\right] = \left[T\right]^T \left[M_\mathrm{n}\right] \left[T\right] \tag{3.15}$$

The matrix $[T]$ may be obtained by two different reduction methods that will be introduced below.

3.3.1 Static Reduction by Guyan

The methodology of static reduction proposed by GUYAN (1965) is based on the arrangement of the structural Eq. (3.16) in active and deleted Degrees Of Freedom (DOF).

$$\left\{F\right\} = \left[K\right] \left\{X\right\} \tag{3.16}$$

After partitioning in the form:

$$\begin{bmatrix} \begin{bmatrix} K_{\mathrm{aa}} \end{bmatrix} & \begin{bmatrix} K_{\mathrm{ad}} \end{bmatrix} \\ \begin{bmatrix} K_{\mathrm{da}} \end{bmatrix} & \begin{bmatrix} K_{\mathrm{dd}} \end{bmatrix} \end{bmatrix} \begin{Bmatrix} X_\mathrm{a} \\ X_\mathrm{d} \end{Bmatrix} = \begin{Bmatrix} F_\mathrm{a} \\ F_\mathrm{d} \end{Bmatrix} \tag{3.17}$$

Assuming the forces on the deleted DOF F_d to be zero, the resulting equations yields:

$$\left[K_{\mathrm{da}}\right] \left\{X_\mathrm{a}\right\} + \left[K_{\mathrm{dd}}\right] \left\{X_\mathrm{d}\right\} = \left\{0\right\} \tag{3.18}$$

This can be solved for displacement in the deleted DOFs as:

$$\left\{X_\mathrm{d}\right\} = -\left[K_{\mathrm{dd}}\right]^{-1} \left[K_{\mathrm{da}}\right] \left\{X_\mathrm{a}\right\} \tag{3.19}$$

The first equation can be written as:

$$\left[K_{\mathrm{aa}}\right] \left\{X_\mathrm{a}\right\} + \left[K_{\mathrm{ad}}\right] \left\{X_\mathrm{d}\right\} = \left\{F_\mathrm{a}\right\} \tag{3.20}$$

Making the substitution for the excluded degrees of freedom, with the results of Eq. (3.19), we have:

$$\left[K_{\mathrm{aa}}\right]\left\{X_{\mathrm{a}}\right\}+\left[K_{\mathrm{ad}}\right]\left[K_{\mathrm{dd}}\right]^{-1}\left[K_{\mathrm{da}}\right]\left\{X_{\mathrm{a}}\right\}=\left\{F_{\mathrm{a}}\right\} \tag{3.21}$$

The results obtained can be manipulated to obtain the transformation matrix:

$$\left[T_{\mathrm{s}}\right]=\begin{bmatrix}\left[I\right]\\ \left[t_{\mathrm{s}}\right]\end{bmatrix}=\begin{bmatrix}\left[I\right] & \\ -\left[K_{\mathrm{dd}}\right]^{-1} & \left[K_{\mathrm{da}}\right]\end{bmatrix} \tag{3.22}$$

Therefore, the matrices of mass and stiffness reduced by the methodology proposed by Guyan are:

$$\left[K_{\mathrm{a}}{}^{G}\right]=\left[T_{\mathrm{s}}\right]^{T}\left[K_{\mathrm{n}}\right]\left[T_{\mathrm{s}}\right] \tag{3.23}$$

$$\left[M_{\mathrm{a}}{}^{G}\right]=\left[T_{\mathrm{s}}\right]^{T}\left[M_{\mathrm{n}}\right]\left[T_{\mathrm{s}}\right] \tag{3.24}$$

As indicated by AVITABILE (1998), this transformation is only necessary for stiffness reductions, where inertial forces are not preserved. Thus, it cannot be guaranteed that this reduction will be accurate for dynamic applications, and in general results in natural frequency results greater than those of the full model.

Some methodologies emerged later to overcome the difficulties imposed by the static reduction method, such as the derived version proposed by KIDDER (1973). One of the best is the System Equivalent Reduction Expansion Process (SEREP) shown below, as it produces reduced models containing user chosen DOF that preserves the dynamic characteristics fo the original full system at the selected modes of interest.

3.3.2 System Equivalent Reduction Expansion Process (SEREP)

A large and growing body of literature investigates several model reduction methods (FRISWELL e MOTTERSHEAD (1995); QU (2004)). In the present study the SEREP dynamic condensation method (performed in the modal space) is used O'CALLAHAN *et al.* (1989). This method allows the FEM model's reduction to a few degrees of freedom without changing its dynamic characteristics. Consequently, from the general equation of movement, we have:

$$[\mathrm{M}]\{\ddot{\mathrm{X}}(\mathrm{t})\} + [K]\{X(\mathrm{t})\} = \{\mathrm{F}(\mathrm{t})\} \tag{3.25}$$

The solution of Eq. (3.25), using the modal truncation technique and considering p modes in the modal superposition AVITABILE (1998), is as follows:

$$\{X(t)\} = [\Phi_p]\{q_p(t)\} \tag{3.26}$$

Where $[\Phi_p]$ and $\{q_p(t)\}$ are the modal matrix and modal coordinates for the p modes considered, respectively.

Since the total degrees of freedom can be categorized as active, a, and deleted, d, then Eq. (3.26) can be rearranged as follows:

$$\{X(t)\} = \left\{ \begin{array}{c} X_a(t) \\ X_d(t) \end{array} \right\} = \left\{ \begin{array}{c} \Phi_{ap} \\ \Phi_{dp} \end{array} \right\} q_p(t) \tag{3.27}$$

Equation 3.27 is a description of the responses for the active degrees of freedom in terms of the modal matrix of the active DOF themselves. It can also be determined that $[\Phi_{ap}]$ is generally not a square matrix and depends directly on the degrees of freedom and modes considered. However, the SEREP method considers that the number of active degrees of freedom is greater than the number of modes taken into account in the modal superposition ($a > p$)QU (2004). Therefore, Eq. (3.27) can be placed in the normal form, projecting this equation as:

$$\{X_p(t)\} = [\Phi_{ap}]^T\{X_a(t)\} \tag{3.28}$$

Merging Eq.(3.27) into Eq.(3.28) yields:

$$\{X_p(t)\} = [\Phi_{ap}]^T[\Phi_{ap}]\{\tilde{q}_p(t)\} \tag{3.29}$$

Where $\{\tilde{q}_p(t)\}$ is an approximate solution of $\{q_p(t)\}$, and can be calculated by manipulating Eq. (3.29):

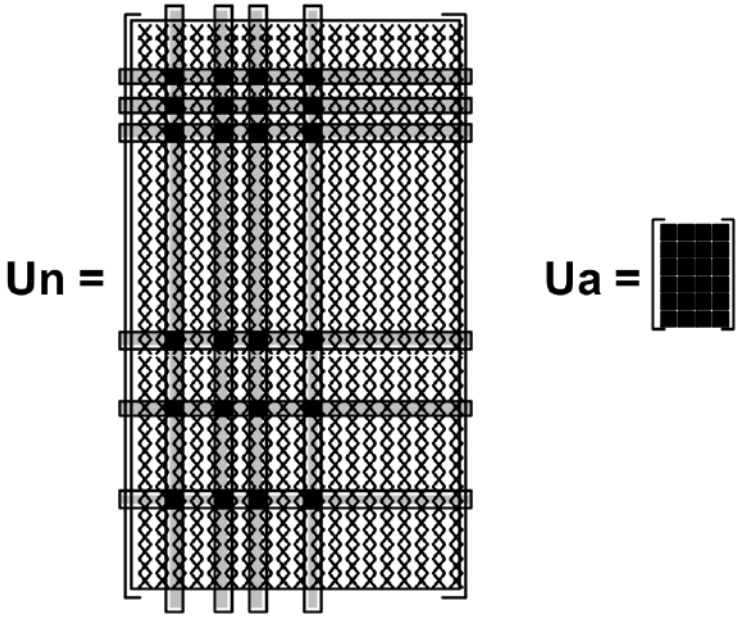

Figure 3.2: Schematic representation of the reduction of the complete modal matrix in the active degrees of freedom. Source: AVITABILE (1998)

$$\{\tilde{q}_p(t)\} = \left([\Phi_{ap}]^T[\Phi_{ap}]\right)^{-1}\{X_p(t)\} \tag{3.30}$$

Merging Eq.3.28 into Eq.3.30:

$$\{X_s(t)\} = [R]\{X_a(t)\}\ ,\ [R] = [\Phi_{dp}][\Phi_{ap}]^{\dagger} \tag{3.31}$$

Where R is the SEREP condensation matrix.

Furthermore, the transformation matrix T can be calculated by substituting Eq. 3.28 in Eq. 3.27:

$$\{T\} = [\Phi_p][\Phi_{ap}]^{\dagger} = \begin{bmatrix} \Phi_{ap}\Phi_{ap}^{+} \\ \Phi_{dp}\Phi_{ap}^{+} \end{bmatrix} \tag{3.32}$$

Thus,the reduced stiffness and mass matrices can be calculated using Eq. 3.33 and Eq. 3.34.

$$\left[{K_{\mathrm{a}}}^{S}\right] = \left[T\right]^{T}\left[K\right]\left[T\right] \tag{3.33}$$

$$\left[{M_{\mathrm{a}}}^{S}\right] = \left[T\right]^{T}\left[M\right]\left[T\right] \tag{3.34}$$

3.4 Experimental Mode Shapes Smoothing and Expansion Method

3.4.1 Local Correspondence Principle (LC)

The smoothing of experimental modes using subsets of numerical modes is defined by BRINCKER *et al.* (2014) as the Local Correspondence Principle (LC). The LC is derived from the mode shape sensitivity equations and it is based on the consideration that a change in a mode shape is primarily a linear combination of the surrounding modes TARPØ *et al.* (2020).

The smoothing process can be interpreted as a fitting process whereas the numerical model is adjusted to the real structure characteristics, diminishing the uncertainty between the numerical and experimental systems.

The subset of numerical modes ($[B_\phi]$) is defined according to the LC. In this method the number of mode shapes is ranked after the distance in frequency to the mode shape to be correlated. In this analysis the DOFs are divided into two sets, fitting DOFs (used in the smoothing) and observation DOFs (used to verify when over-fitting occurs).

The mode shape cluster is constructed by including an increasing number of mode shapes, from the ranking, at each cluster iteration. The optimal number of mode shapes to be used in the correlation is calculated by optimizing the MAC (the definition at the observation DOFs BRINCKER *et al.* (2014).

Considering the experimentally obtained mode shape $[\phi]$, it can be expressed as a linear combination of a subset of numerical modes, $[B_\phi]$, as defined:

$$[\phi] \approx [B_\Phi]\{z\} \tag{3.35}$$

Where $[B_\Phi]$ is the cluster of vibration modes derived from the numerical model, reduced to the number of measured DOFs. The linear relationship of Eq. 3.35 is defined by the transformation vector $\{z\}$. This transformation vector is calculated according to Eq. (3.36)

$$[\hat{z}] = [B_\Phi]^\dagger[\phi] \tag{3.36}$$

Where $[B_\Phi^+]$ is the pseudo inverse of the subset of numerical modes chosen for the fitting process. A numerical mode being correlated is analogous to stating that the experimental mode shape is being adjusted or smoothed to minimize noise in the measured DOFs. This correlation process is defined using the following equation:

$$[\hat{\phi}] = [B_\Phi][\hat{z}] \tag{3.37}$$

Here $[\hat{\phi}]$ is the numerical mode shape matrix fitted with the experimental results, $\{\hat{z}\}$ is the transformation matrix calculated according to Eq. (3.36), $[B_\Phi]$ is the subset of numerical modes and

When using the LC methodology for the correlation of models, it is important to be aware of the quality dependence on the selected nodes for the fitting and observation sets of DOF. BRINCKER *et al.* (2014)

3.4.2 Local Correspondence Principle for Modes and Coordinates (LCMC)

The LCMC method is an extension of the LC method proposed in this work. It differs from LC by verifying all possible combinations of DOFs to be used as a fitting set, therefore as a result the best set of fitting nodes and cluster of modes that yields that maximizes the smoothing MAC value can be used .

The subset of numeric modes $[B_\Phi]$, used in smoothing is defined according to the same description given in 3.4.1, but in the methodology proposed, to complement the LC (aiming at avoiding over fitting of Experimental modes), the LCMC allows, in addition to the choice of the optimum group of modes, the selection of an optimal set of degrees of freedom (compatible with those measured experimentally) used in the smoothing, in order to maximize the MAC. The selection of degrees of freedom, at each iteration during the smoothing process, is done by using combinatorial analysis, according to Eq. (3.38).

$$n = C_i^{m-r} = \frac{(m-r)!}{i!(m-r-i)!}, \text{ where, } r \geq 2 \tag{3.38}$$

In Eq. (3.38) *n, m, r and i* represent the number of possible combinations, the number of experimental degrees of freedom compatible with the reduced model, the number of degrees of freedom used to verify the fit and the number of the iteration, respectively.

3.5 Dynamic Response Prediction

The following equation of motion governs the response of a discrete system with n_{eq} DOFs.

$$[M]\{\ddot{X}(t)\} + [C]\{\dot{X}(t)\} + [K]\{X(t)\} = \{F(t)\} \tag{3.39}$$

The equation of motion described in Eq. (3.39) can only be solved by numerical integration of the n_{eq} coupled equations, as described by PAULTRE (2011). For linear systems the orthogonality properties between mode shapes yields a simplification

that can be used in the solution. A transformation by expressing the equation in terms of generalized coordinates instead of geometric coordinates, this transformation uncouples the equations going from n_{eq} simultaneous solutions to independent solutions. The exact dynamic response can therefore be obtained using the modal superposition.

Prediction of the dynamic response at unmeasured locations can be developed by making use of the modal decomposition approach. Deriving Eq. (3.26) twice, the acceleration vector, $\{\ddot{X}(t)\}$, can be written as a linear combination of the mode shape vectors $[\Phi_p]$, as shown in Eq. (3.40) ILIOPOULOS *et al.* (2016).

$$\{\ddot{X}(t)\} = [\Phi_p]\{\ddot{q}_p(t)\} \tag{3.40}$$

Where $\{\ddot{q}_i(t)\}$ is the vector of the acceleration modal coordinates for each time instance t.

The modal coordinates are calculated by using the pseudo inverse as indicated in Eq. (3.41), assuming that the number of modes p is less then the number of active DOF's ILIOPOULOS *et al.* (2016):

$$\{\hat{\ddot{q}}(t)\} = \left([\Phi_p]^T[\Phi_p]\right)^{-1}[\Phi_p]^T\{\ddot{X}_p^{\text{meas}}(t)\} = [\Phi_p]^{\dagger}\{\ddot{X}_p^{\text{meas}}(t)\} \tag{3.41}$$

The acceleration prediction at unmeasured locations, $\{\ddot{X}_p^{\text{pred}}(t)\}$ can be obtained by including the desired degrees of freedom in the modal matrix $[\Phi_p]$:

$$\{\ddot{X}_p^{\text{pred}}(t)\} = [\Phi_p]\{\hat{\ddot{q}}(t)\} = [\Phi_p][\Phi_p]^{\dagger}\{\ddot{X}_p^{\text{meas}}(t)\} \tag{3.42}$$

It is important to note that, as described by PAULTRE (2011), the main component of responses presents important contributions only for the first few mode shapes. Hence, taking into account uniquely those modes as a truncated eigenvector basis would save unnecessary calculations with minimal effect in comparison to the response obtained with the complete modal basis PAULTRE (2011). This type of calculation with a truncated eigenvector basis yields a sufficiently small error if a sufficient mode basis is considered PAULTRE (2011).

3.6 Criteria Used for Model Assessment

The criteria used for the verification of the reduced model derive from the experimental modal analysis by comparing the reduced modal matrix and the complete modal matrix. These criteria will also be used to correlate the reduced model with experimentally obtained data. After the definition of the criteria for modal assurance, this work also defined correlation factors used for the assessment of the predicted time

series signal for unmeasured DOF.

3.6.1 Model Assurance Criteria (MAC)

As defined in MENDONÇA *et al.* (2019), MAC is essentially a regression correlation coefficient used to measure the consistency between two vectors. The MAC value ranges from 0 to 1, where 0 represents inconsistency or orthogonality between vectors, and 1 represents perfect consistency (difference only by the scale factor).

Considering the assessment of two different vibration mode vectors, $[\Phi_A]$ and $[\Phi_B]$, the MAC between these modes is given by ALLEMANG (2002):

$$MAC\left(\Phi_A, \Phi_B\right) = \frac{\left|[\Phi_A]^T[\Phi_B]\right|^2}{\left([\Phi_A]^T[\Phi_A]\right)\left([\Phi_B]^T[\Phi_B]\right)} \tag{3.43}$$

3.6.2 Co-Ordinate Modal Assurance Criterion (COMAC)

According to FRISWELL e MOTTERSHEAD (1995) and EWINS (2000b), MAC is an important tool in mode correlation, but may pose a challenge in correlation of modes that are closely spaced in frequency or when the selected locations for measurement or modeling are insufficient. To this extent, a variant of MAC, called a co-ordinate MAC or COMAC, can be used for error finding. COMAC values reflect the discrepancy between the compared modal forms and can be calculated as follows:

$$COMAC(i) = \frac{\left(\sum_{j=1}^{L}\left[\Phi_A\right]_{i,j}\left[\Phi_B\right]_{i,j}\right)^2}{\left(\sum_{j=1}^{L}\left[\Phi_A\right]_{i,j}^2\right)\left(\sum_{j=1}^{L}\left[\Phi_B\right]_{i,j}^2\right)} \tag{3.44}$$

Where L e i represent respectively the number of modes being compared and the coordinate being evaluated and $[\Phi_A]$ e $[\Phi_B]$ represent the modal matrices being correlated. COMAC values close to 1 indicate that all mode coordinates associated with degree of freedom i are equal, values below 0.9 indicate discrepancy in the evaluated degree of freedom.

3.6.3 Relative Difference Between Modes (RD)

The Relative Difference between modes (RD) assesses the level of variances in amplitudes of each degree of freedom between the modes being compared and is calculated as follows:

$$DR(i,j) = \left|\frac{\left[\Phi_A\right]_{i,j} - \left[\Phi_B\right]_{i,j}}{\left[\Phi_A\right]_{i,j}}\right| \quad \text{, if} \quad \left[\Phi_A\right]_{i,j} = \left[\Phi_B\right]_{i,j} \rightarrow DR(i,j) = 0 \tag{3.45}$$

Where, $[\Phi_A]$ e $[\Phi_B]$ represent the modal matrices being compared and indexes i and j represent the degree of freedom and the mode being evaluated respectively. Values close to 0 indicate that the amplitudes of the degrees of freedom analyzed are alike.

3.6.4 Time Response Assurance Criterion (TRAC)

The time response assurance criterion (TRAC) is a correlation for one DOF over the time of the predicted signal $\{\ddot{X}_p^{\text{pred}}(t)\}$ with the measured signal in the time domain $\{\ddot{X}_p^{\text{meas}}(t)\}$ ILIOPOULOS *et al.* (2016).

$$TRAC = \frac{\left[\{\ddot{X}_p^{\text{meas}}(t)\}^T\{\ddot{X}_p^{\text{pred}}(t)\}\right]^2}{\left[\{\ddot{X}_p^{\text{meas}}(t)\}^T\{\ddot{X}_p^{\text{meas}}(t)\}\right]\left[\{\ddot{X}_p^{\text{pred}}(t)\}^T\{\ddot{X}_p^{\text{pred}}(t)\}\right]} \tag{3.46}$$

3.6.5 Frequency Response Assurance Criterion (FRAC)

The frequency response assurance criterion (FRAC) is a correlation for one DOF over all frequencies of the predicted complex frequency domain $\ddot{X}_p^{\text{pred}}(f)$ with the measured complex frequency domain signal $\ddot{X}_p^{\text{meas}}(f)$ ILIOPOULOS *et al.* (2016).

$$FRAC = \frac{\left[\{\ddot{X}_p^{\text{meas}}(f)\}^H\{\ddot{X}_p^{\text{pred}}(f)\}\right]^2}{\left[\{\ddot{X}_p^{\text{meas}}(f)\}^H\{\ddot{X}_p^{\text{meas}}(f)\}\right]\left[\{\ddot{X}_p^{\text{pred}}(f)\}^H\{\ddot{X}_p^{\text{pred}}(f)\}\right]} \tag{3.47}$$

3.6.6 Mean Absolute Error (MAE)

Mean Absolute Error in the time domain (MAE_{TD}) is defined as the mean absolute error over n_s data samples in the time domain ILIOPOULOS *et al.* (2016).

$$MAE_{TD} = \frac{1}{n_t}\sum_t \left|\{\ddot{X}_p^{\text{meas}}(t)\} - \{\ddot{X}_p^{\text{pred}}(t)\}\right| \tag{3.48}$$

Mean Absolute Error in the frequency domain (MAE_{FD}) is defined as the mean absolute error over n_f data samples in the frequency domain ILIOPOULOS *et al.* (2016).

$$MAE_{FD} = \frac{1}{n_f}\sum_f \left|\{\ddot{X}_p^{meas}(f)\} - \{\ddot{X}_p^{pred}(f)\}\right| \tag{3.49}$$

3.6.7 Root Mean Squared error($RMSE$)

The root-mean-square error is a mean of calculating the deviation between two samples, the predicted and the measured. It is defined as the square root of the second sample moment of the deviations between the observed and predicted values.

It can be calculated for the signal in the time domain as in Eq. (3.50) or in the frequency domain as in Eq. (3.51).

$$\mathrm{RMSE_{TD}} = \sqrt{\frac{\sum_t \left(\{\ddot{X}_{\boldsymbol{p}}^{meas}(t)\} - \{\ddot{X}_p^{pred}(t)\} \right)^2}{n_t}} \tag{3.50}$$

$$\mathrm{RMSE_{FD}} = \sqrt{\frac{\sum_f \left(\{\ddot{X}_p^{meas}(f)\} - \{\ddot{X}_p^{pred}(f)\} \right)^2}{n_f}} \tag{3.51}$$

Chapter 4

Methodology for Response Prediction Using the Modal Expansion Method

The methodology presented in this chapter describes the process in which the work was developed in order to fulfill the objectives proposed in section 1.3, mainly dynamic response prediction. The methodology was applied to an experimental example of an aluminum beam in two different case studies, using different boundary conditions each time in order to validate its results. Then it was used in a real industry situation to test it with real world conditions.

In Fig. 4.1 a flowchart of the process detailed in this chapter can be seen for the aluminum beam case study and in Fig. 4.2 for the interstage piping system case study.

4.1 Finite Element Model

The starting point for the application of the methodology is building a Finite Element Model that represents as close as possible the geometry and properties of the structure of interest.

This model has many implications on the full process, the first is to be the preliminary source of natural frequencies and mode shapes. This is very important for the next step of the methodology, as it lays the foundations for a good planning of the experimental procedures. The mode shapes resulted from the FEM model are to be used alongside professional experience to identify the coordinates of the structure where, for the most important mode shapes, the displacement amplitudes are higher. These positions are therefore the best places in the structure to position the accelerometers in order to avoid nodes of certain mode shapes.

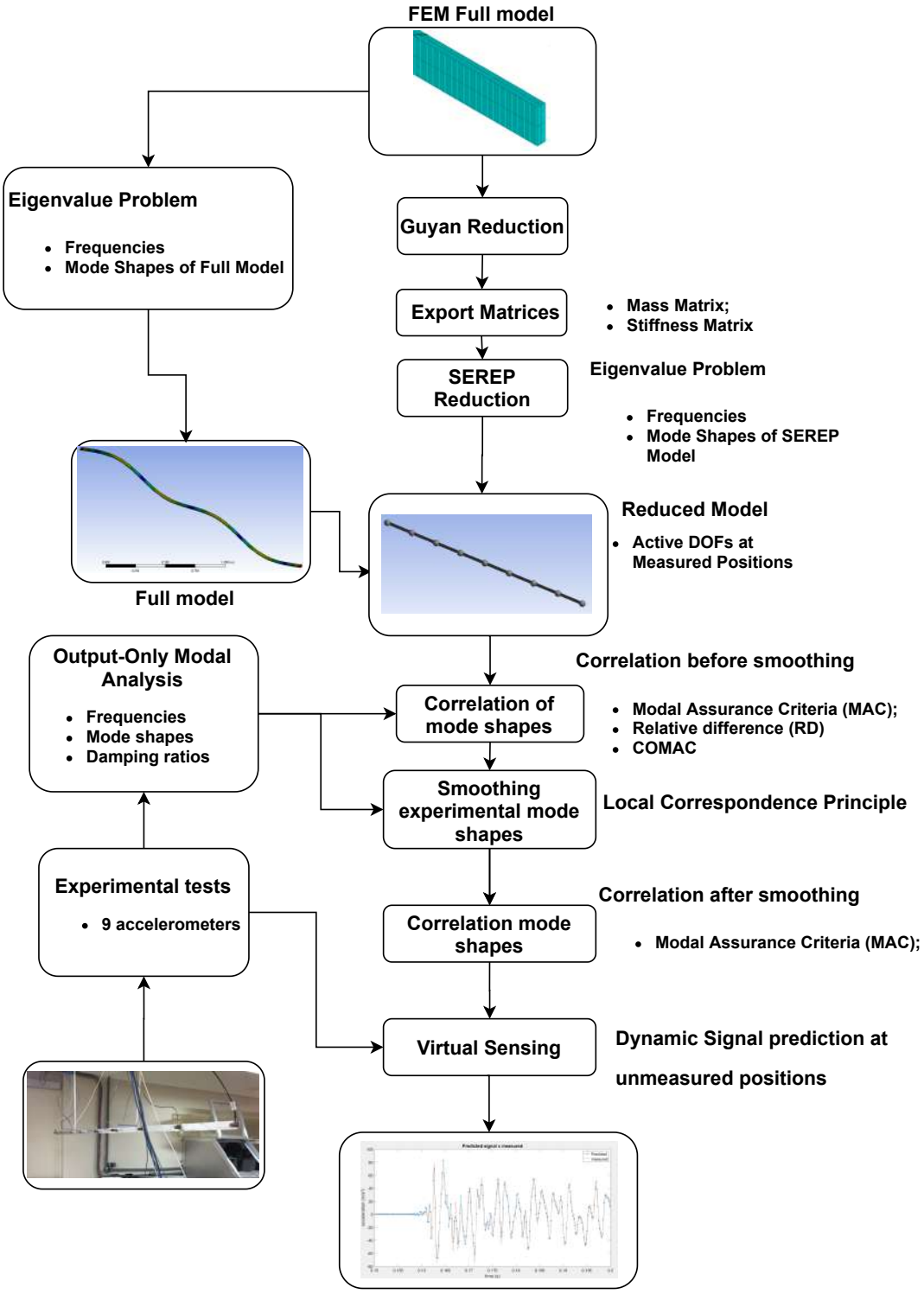

Figure 4.1: Diagram with the steps applied in the methodology for the aluminum beam

The FEM model is also the source for the Mass an Stiffness matrices, that should be exported from the FE software to be manipulated externally, using algorithms

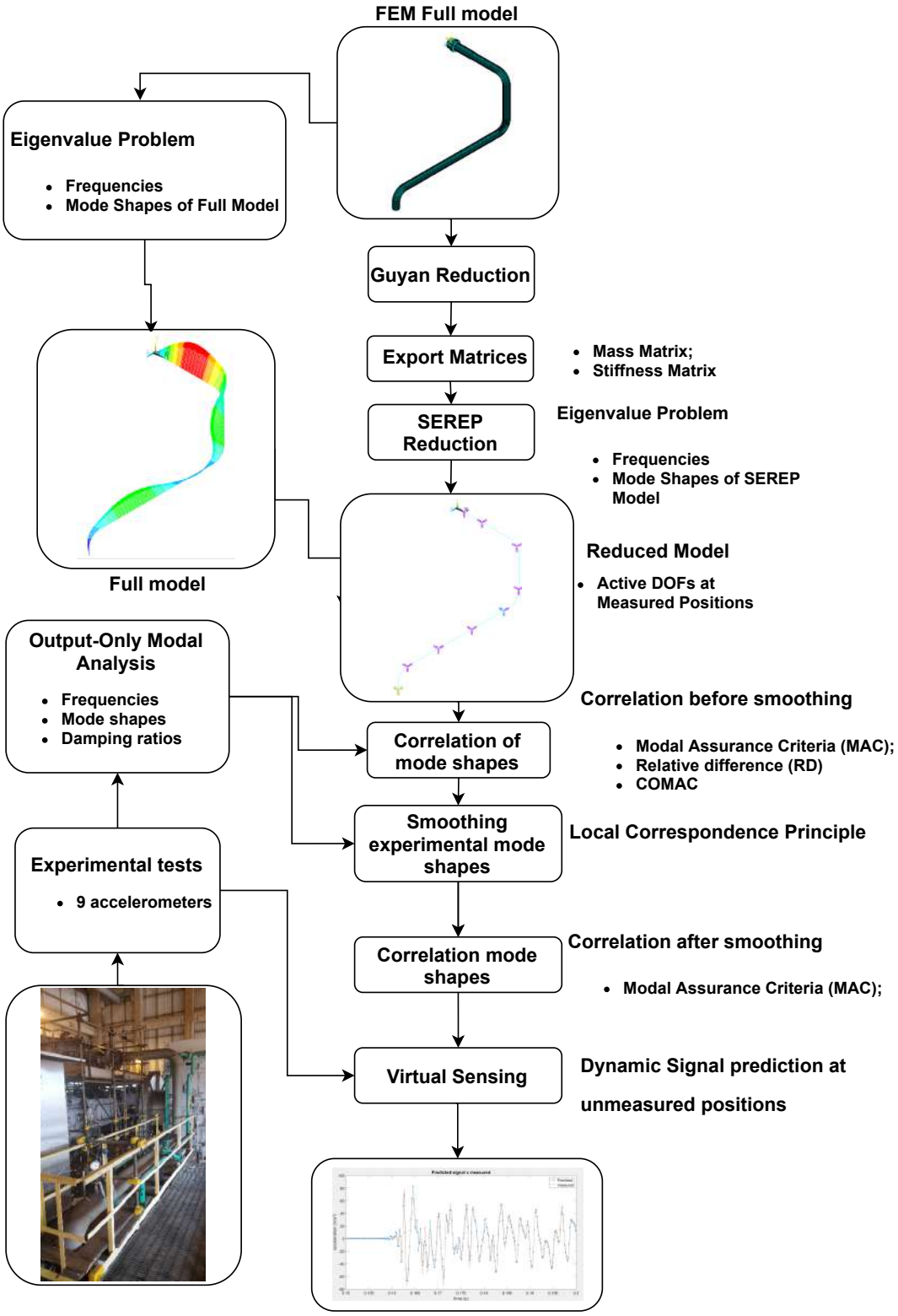

Figure 4.2: Diagram with the steps applied in the methodology for the pipe system

for reduction, smoothing and virtual sensing. The unit system used in the modelling shall be carefully chosen in accordance to the system size as the processing of the matrices can induce numerical errors if numbers are too small depending on model

properties and mesh sizes.

In order to construct a reliable and optimized model to be used in the following steps of the analysis it is of paramount importance that the model is constructed carefully together with appropriate mesh convergence test.

In this work the software used to develop the full FEM was ANSYS APDL 2020 Student. The full FEM model is defined as the model with all the degrees of freedom necessary for the mesh convergence. This model will be further processed in the reduction steps throughout the methodology herein proposed.

4.2 Experiment and O-OMA

The next step in the analysis is the experiment on the real structure in operational conditions. The focus of the method presented are structures where it is not viable or feasible to measure the forces acting on the structure during an experiment, therefore only the output data is collected.

With the signal output from the experiment, an O-OMA shall be performed. As mentioned in section 3.2, the O-OMA method applied is in the frequency domain as EFDD. The O-OMA returns the estimated modal parameters of the structure in operational conditions: natural frequencies and mode shapes (usually complex) are the parameters of interest.

As the experimental mode shapes obtained are usually complex, following will be described the procedure used to transform them to real values.

A major limitation of the operational modal analysis, output-only, occurs in the estimation of the modal matrix. Since the excitation force is not measured, the modal shapes are not mass normalized. The lack of this standardized matrix restricts the use of modal parameters in applications such as load estimation. Methods such as Mass Addition (MA) are commonly used to estimate normalization factors, in this method, previously known masses are added at defined points. As MA uses the modal parameters obtained for the system with and without the added masses, it requires many tests and careful planning of the experiment RAINIERI e FABBROCINO (2014).

This dissertation uses a simplified methodology for normalizing experimental modes, proposed by AENLLE e BRINCKER (2013), that uses the mass matrix of a finite element model. A good estimation to the normalization factor is given by Eq: (4.1).

$$\hat{\alpha}_{O-OMA} = \frac{1}{\sqrt{[\phi_i]^T_{O-OMA} \cdot [M]_{FEM} \cdot [\phi_i]_{O-OMA}}} \tag{4.1}$$

This normalization factor is then used to M-orthonormalize the experimental modal

matrix as given:

$$[\Psi]_{O-OMA} = [\phi]_{O-OMA} \cdot [\hat{\alpha}]_{O-OMA} \tag{4.2}$$

Where $[\phi]_{O-OMA}$ is the unscaled modal matrix, $[\Psi]_{O-OMA}$ is the mass scaled or M-orthonomalized experimental modal matrix and $\hat{\alpha}_{O-OMA}$ is the normalization factor.

4.2.1 Complex to Real Operation to the Experimental Mode Shapes

As revised in section 3.2, O-OMA usually returns complex frequencies and complex mode shapes due to measurement noise. Since there is a necessity to compare the experimentally obtained complex modes to the numerical modes from finite element undamped model, a complex-to-real operation to the experimental mode shapes as described bellow must be performed.

RAINIERI e FABBROCINO (2014) indicates that complex modes are often obtained from modal tests due to measurement noise. However, the degree of complexity is usually moderate. Taking into account that O-OMA provides only unscaled mode shapes, there is the necessity for simple approaches to scaling and complex-to-real conversion of the estimated mode shape vectors.

When the expected mode shapes to be obtained should be normal modes, the simplest way to apply the complex-to-real conversion is based in calculating the phase of each mode shape component and setting it equal to 0^{o} or 180^{o} depending on its initial value. If the phase angle lies in the first or in the fourth quadrant it is set equal to 0^{o} ; it is set equal to 180^{o} if it lies in the second or in the third quadrant. For the sake of strictness, this method should only be used close to the normal mode, when the phase angle from 0° to 180° does not exceed 10°. However, it is often extended to all phase angles EWINS (2000a).

4.3 Model Post-Processing and Reduction

With the FEM model constructed and experimental results obtained, the next step is to perform the post-processing and reduction of the FEM model, step necessary to the continuity of the procedure as numerical obtained mode shapes are used frequently from here on.

As exporting the mass and stiffness matrices (from commercial software) of the full model for complex structures is not always recommended, due to their size and the high computational effort necessary for their processing. The methodology here applied uses a mixed reduction method in order to streamline the reduction process,

in two steps. The first stage partially reduces the model using Guyan's method (in physical space) to a number of manageable, computationally low-cost, active degrees of freedom.

The first part of the reduction is applied inside the commercial software used (in this work ANSYS APLD was used for this purpose) and as it relies heavily on the number and position of the active DOFs used in the reduction a mesh convergence test has to be applied to guarantee the quality of the reduction process. It is of paramount importance that the DOFs located on the same positions of the measured ones are included in the set of active nodes for the first reduction as they are necessary from here on.

With the first reduction completed the mass and stiffness can be exported to be manipulated outside of the FEM Software with the algorithms for the next steps. Now with a more manageable size, its processing can be done faster.

In this step great care should be taken with the ordering of the nodes and elements from the numeric model, as they can be altered internally in the commercial software for performance improvements. The reordering of the elements can be challenging depending of the FEM software used and it is relevant as the results of the numeric and experimental analysis are compared.

4.4 Model Reduction Using Guyan-SEREP

The next step of the mixed Guyan-SEREP reduction process is to apply the SEREP method completing the reduction of the model to the sensor's DOFs using the partially reduced modal, mass and stiffness matrices. As noted in section 3.3.2 the reduced model using SEREP method has exactly the same frequencies and mode shapes as the original system for the selected modes of interest. That is the reason explaining the Guyan-SEREP hybrid reduction. The methodology aim to reduce the model in the physical domain using Guyan to a degree that the results are almost unaffected and further computational effort is small and then apply SEREP.

The solution of the eigenvalue problem from the reduced mass and stiffness matrices from SEREP give the reduced mode shapes with DOFs matching the experimental mode shapes.

The reduction process can be validated using the assessment criteria presented in section 3.6. MAC, COMAC and RD are quality indicators for the correlation and can be used to analyse the mode shapes of the reduced model in comparison with the mode shapes of the full model.

4.5 Local Correspondence Principle

In the smoothing process described in section 3.4.1 it is considered that the experimental modes are a linear combination of the numerical modes. In such wise, the transformation herein described can be used in two different possibilities: (i) to estimate modal amplitudes at unmeasured locations and (ii) to smooth the measured data FRISWELL e MOTTERSHEAD (1995).

For the first possibility the model is reduced to a number of DOF considered necessary, for example, to have a good spacial representation of the mode shapes of interest. Then, the experimental modal matrix is expanded to the same degrees of freedom as the reduced numerical model through the procedure described in 3.4.1 where the number of optimal modes to yield the best MAC correlation factor is considered the optimal fitting procedure.

On the other hand, for the case of using only the degrees of freedom measured, the reduced model is taken to the same DOF considered experimentally and the algorithm for smoothing the operational data as described in 3.4.1 is used.

This fitting process optimizes only the number and mode shapes used in the process and therefore leaves an important variable outside of the analysis, that is the DOFs used in the fitting process. To fill the gap observed when using the LC method as proposed by BRINCKER *et al.* (2014), this work proposes a variation that aims to improve the quality of the results.

4.5.1 Local Correspondence for Modes and Coordinates

As described in section 3.4.2 the proposed variant of the Local Correspondence Principle uses repeated iterations of the possible combinations of degrees of freedom. Each combination of DOF is processed using the LC algorithm and after all possibilities are calculated, and the one that yielded the highest MAC value is considered the optimal fitting.

The smoothing process can be correlated to the non-smoothed and full numerical model results using the assessment criteria presented in section 3.6, MAC, COMAC and RD. The results can indicate the improvement obtained from the LC and/or LCMC method applied.

4.6 Dynamic Response Prediction

With the experimental mode shapes smoothed with the numerical we have the set of mode shapes that are to be used in eq. 3.41 in conjunction with signals in the time domain for all measured positions to perform the calculation of the modal coordinates, later to be used in dynamic response prediction.

As this dissertation intends to test the usage of this method, the signal at the position where the prediction was made was also measured, although the values were not used in the prediction itself but only as a baseline for the assessment of the predicted value.

The time domain signal is first filtered to the frequency of the highest mode used in the mode shape set that is employed in the calculation of the modal coordinates. Then, as it occurred with the smoothing of the modes, the results are very dependent on the degrees of freedom and modes used in the prediction. For this reason, we use to different approaches to encounter the best combination of DOFs and modes to be used in the prediction.

For the DOFs all combinations of DOFs are used (excluding the one being estimated). For the modes, a similar approach to the LC is used: they are ranked after the distance in frequency and used in the prediction process as a set increasing from the closest (in frequency) to the most prominent mode in the response and at each iteration the next closest mode, to the main one is added.

At each iteration of DOF and mode combination the predicted signal is assessed using the criteria presented in 3.6 ($TRAC$, $FRAC$, MAE_{TD},MAE_{FD} and $RMSE$). The combination that yields the best correlation with the measured signal is considered the best estimation.

Chapter 5

Case Studies

The methodology proposed in chapter 4 was validated using an aluminum beam in two case studies tested under laboratory controlled conditions with different boundary conditions. Afterwards, the methodology was applied to a real structure, an interstage pipe of a reciprocating compressor. The results are encountered below.

5.1 Rectangular Beam in Free-Free Boundary Condition

In order to support the procedure that this dissertation proposes, experimental tests were carried out on an aluminum beam and a Finite Element Model was also built, as representative of the test structure as possible. As described below.

5.1.1 Finite Element Model (FEM)

The Finite Element Model (FEM), necessary to the execution of the proposed methodology, was developed using the ANSYS APDL software as seen in Fig 5.1.

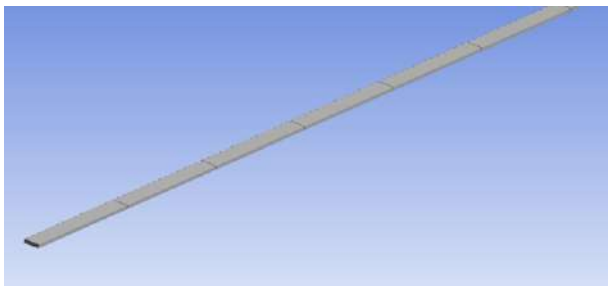

Figure 5.1: Aluminum beam finite element model.

To validate the numerical model, a mesh test was performed. The number of nodes in the model were increased and the results compared with the experimental

results to evaluate result convergence.

The test started with a 9 (nine) nodes model and its dynamic result was compared with the experimental results. The number of nodes doubled every step until reaching 2,304 nodes and the results in frequency were close enough to those obtained experimentally. From these results, it is possible to identify this number of nodes as a value in which the model's convergence has been achieved. The natural frequencies obtained in the mesh convergence test can be seen in Tab. 5.1

Table 5.1: Mesh convergence by comparison of numerical and experimental natural frequencies.

Modes	FEM - Number of Nodes									Experimental	Difference
	9	18	36	72	144	288	576	1152	2304	Steel tip	(%)
1	6.6141	6.5144	6.4887	6.4806	6.4783	6.4973	6.4994	6.5253	6.7717	6.260	-7.6
2	19.492	18.367	18.088	18.018	18	18.003	18.005	18.01	18.069	17.528	-3.0
3	41.465	36.493	35.323	35.035	34.963	34.949	34.946	34.95	34.982	34.430	-1.6
4	78.322	62.353	58.898	58.066	57.86	57.811	57.799	57.796	57.806	56.966	-1.5
5	139.5	96.173	88.056	86.157	85.69	85.575	85.546	85.539	85.55	85.136	-0.5
6	263.53	143.64	126.19	122.26	121.3	121.06	121.01	120.99	121	118.940	-1.7
7	569.24	194.9	163.84	157.16	155.55	155.16	155.06	155.03	155.03	153.996	-0.7
8		301.53	233.35	219.72	216.49	215.69	215.49	215.44	215.43	212.215	-1.5
9		388.13	284.73	265.02	260.39	259.25	258.97	258.9	258.89	257.287	-0.6
10		536.46	359.02	328.16	321.04	319.29	318.86	318.75	318.73	314.253	-1.4
11		725.69	438.1	393.13	382.94	380.45	379.83	379.67	379.64	376.227	-0.9
12		1012.5	532.18	467.42	453.03	449.54	448.67	448.46	448.4	443.835	-1.0
13		1463.1	635.28	545.15	525.61	520.89	519.71	519.42	519.35	518.955	-0.1
14			767.96	640.74	613.87	607.42	605.82	605.42	605.33	596.580	-1.4
15			876.47	714.22	680.88	672.91	670.94	670.45	670.33	669.196	-0.2
16			1145.4	884.39	833.19	821.1	818.11	817.37	817.19	793.770	-2.9
17			1281	968.01	907.8	893.63	890.14	889.27	889.06	877.654	-1.3
18			1512.1	1097.1	1020.5	1002.6	998.22	997.12	996.85	973.432	-2.3
19			1756.6	1223.8	1129.4	1107.5	1102.2	1100.8	1100.5	1077.975	-2.0
20				1366.2	1249.7	1223	1216.5	1214.8	1214.4	1196.289	-1.5
21				1511	1369.7	1337.5	1329.7	1327.7	1327.2	1304.587	-1.7
22				1691.8	1517.1	1477.8	1468.2	1465.8	1465.2	1415.390	-3.4
23				1813.9	1614.1	1569.5	1558.6	1555.9	1555.3	1556.866	0.1
24					1889.9	1828.5	1813.6	1809.9	1809	-	-
25					1992	1924.5	1908.2	1904.2	1903.1	-	-

The model with the number of nodes necessary for convergence of results is herein named the full model.

5.1.2 Experimental Setup

The experiment carried out was the impact test. In this experiment, an instrumented hammer was used to apply impacts to the aluminum beam, whose intensities were measured. The impacts were undertaken transverse to the beams largest dimension. The beam, properly instrumented with accelerometers distributed along its length, generated results that allowed the identification of dynamic parameters through the use of modal analysis techniques. As the process validated would be used in situations were the excitation force is not always available, although the tests were made with an impact hammer and the forces were available for the modal analysis, they were not used as the O-OMA was performed. A comparison between the modal

parameters obtained using the different approaches EMA and O-OMA can be seen in details in ALBUQUERQUE *et al.* (2019).

The aluminum beam with the accelerometers installed can be seen in Fig.5.2. Its dimensions are presented in the table 5.2.

Table 5.2: Dimensions of aluminum beam

Dimensions	Data
Thickness	6.17 mm
Width	25.42 mm
Length	2145 mm

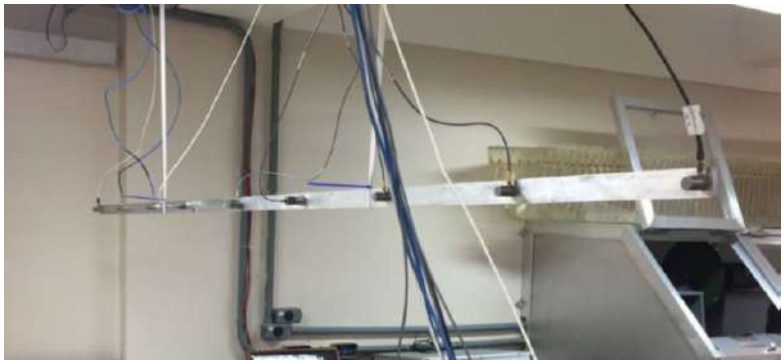

Figure 5.2: Rectangular beam suspended in Free-Free boundary condition and instrumented with 09 accelerometers.

The nine accelerometers used are of the piezoelectric type, their specifications, as well as the respective masses also included in the FEM can be seen in the table 5.3

Table 5.3: Accelerometers specification

Índice	**Sensor**	**Sensibility**	**Mass**
1	Kistler	100 mV/g	9 g
2	Kistler	100 mV/g	9 g
3	Kistler	100 mV/g	9 g
4	Kjaer	9,72 mV/g	17 g
5	PCB	100 mV/g	27 g
6	Kjaer	9,65 mV/g	17 g
7	Kistler	100 mV/g	9 g
8	Kistler	100 mV/g	9 g
9	Kistler	100 mV/g	9 g

Figures 5.3 and 5.4 show a schematic representation of the installation position of each accelerometer along the length of the beam and an image showing the installation detail, respectively. As can be seen, the accelerometers were positioned keeping

them equidistant from each other. As the total length of the beam is 2145mm, between them we obtain a distance of approximately 268.1mm.

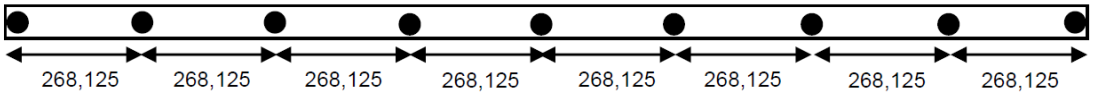

Figure 5.3: Schematic of the positioning of accelerometers.

Figure 5.4: Detailed view of the sensor positioning

In Fig. 5.5 the procedure used to apply the impacts on the beam can be seen. The hammer used is a Brüel and Kjaer type 8200. This hammer, which can be seen in Fig. 5.6, has tips with three different materials capable of exciting different frequency bands.

Each of the nine DOF were impacted 10 (ten) times, with each of the three tips available, totaling 270 impacts.

The modal parameters identification was made using the data obtained by the *National Instruments* NI 9234 acquisition board, processed as in Fig. 5.7.

Next section will present the processing results of the signals obtained in this experiment.

5.1.3 Output-Only Modal Analysis (O-OMA)

Only vibration responses were used in the Enhanced Frequency Domain Decomposition (EFDD) algorithm. The idea was to simulate practical situations where it is

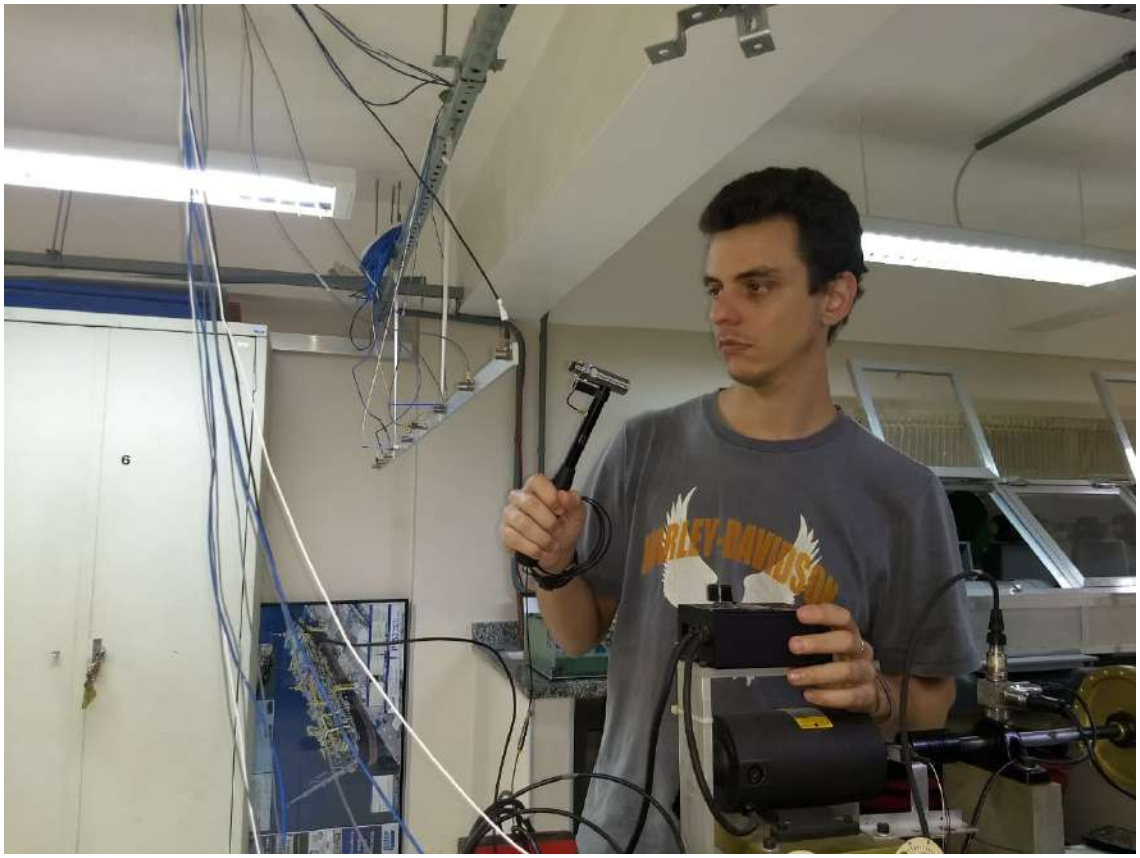

Figure 5.5: Aluminum beam being excited by impact hammer.

Figure 5.6: Impact Hammer Brüel e Kjaer model 8200.

not always possible to measure the excitation forces. Details of this analysis can be found in (BUSSON *et al.*, 2019).

The analysis of the range up to 1500 Hz encountered 22 (twenty two) modal parameters. Table 5.4 shows these natural frequencies. The first 4 (four) experimental mode shapes can be seen in Fig. 5.10.

Figure 5.7: Data acquisition board from *National Instruments* model NI 9234.

Table 5.4: Modal parameters estimated using EFDD

Vibration Modes	Frequency[Hz]	Vibration Modes	Frequency[Hz]	Vibration Modes	Frequency[Hz]
1	6.26	9	257.26	17	879.63
2	17.53	10	314.25	18	974.06
3	34.42	11	376.40	19	1078.49
4	56.97	12	443.85	20	1198.08
5	84.81	13	518.77	21	1303.98
6	119.19	14	596.57	22	1417.92
7	153.81	15	669.14		
8	212.28	16	793.77		

5.1.4 Model Reduction using Guyan-SEREP

With the FEM of the aluminum conveniently constructed and converged, this full model was used as a initial stage of the study, as it was the source from where the mass and stiffness matrices were withdrawn.

The mass and stiffness matrices were then used as input data to perform a eigenvalue solution from which the results were used in the model reduction (in modal space). The goal of the reduction was matching the number of degrees of freedom of the reduced model with the experimental ones.

The full model was reduced to 9 (nine) active nodes - located in the same physical position where the accelerometers were placed. As shown in Fig. 5.8, the first four mode shapes were plotted for the numerical full modes and the numerical SEREP reduced modes. The MAC number between the SEREP reduced and the full numerical modal model is indicated above each plot. As can be seen, there is a perfect match between full and reduced mode shapes, which leads to a MAC value of 1. Figure 5.9 presents the MAC matrix for the 7 (seven) numerical mode shapes.

All assessment criteria used to compare the reduced and full numerical models indicated that the reduction process to the 9 (nine) DOF were successful and a good correlation between the full model and reduced was achieved. The MAC numbers corresponds to 1 (one) for all modes assessed.

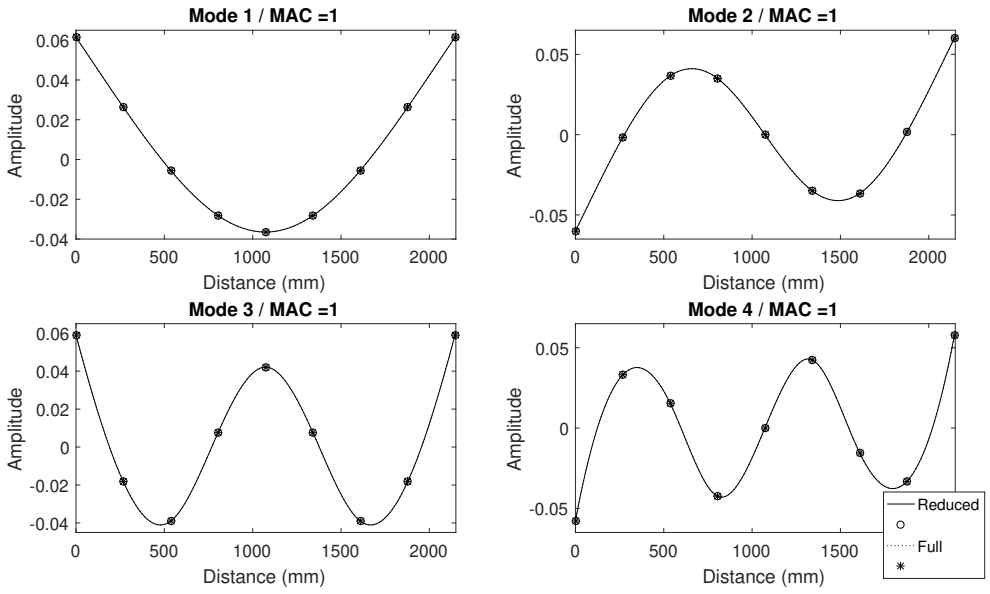

Figure 5.8: SEREP reduced and full numerical mode shapes comparison.

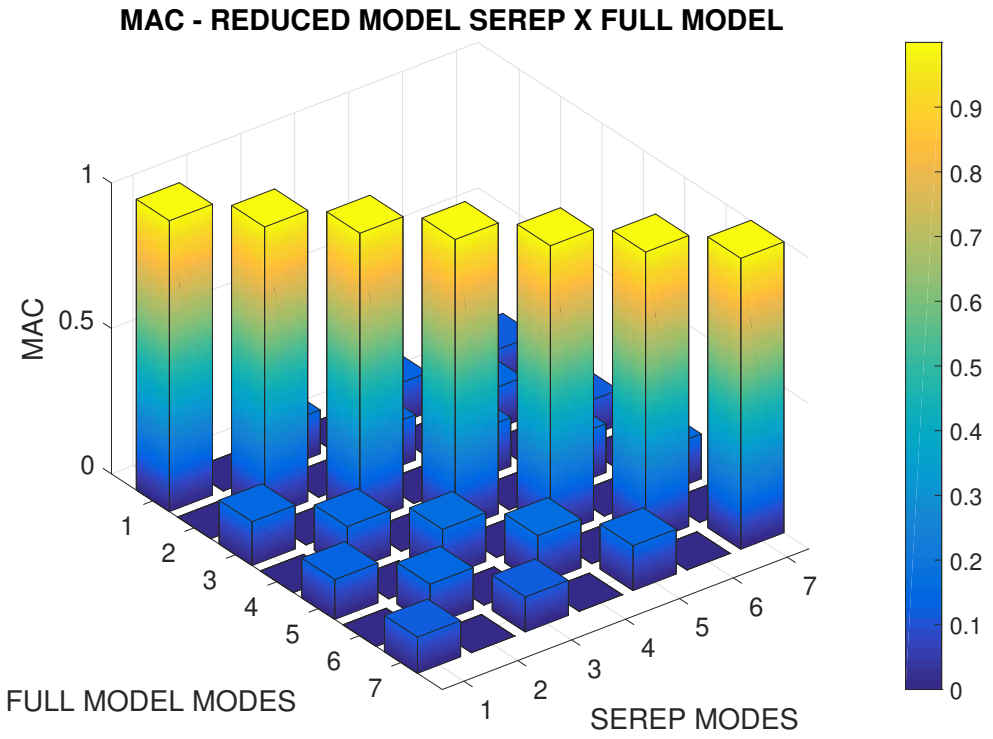

Figure 5.9: MAC for SEREP reduced and full numerical mode shapes comparison.

The efficiency illustrated above permits reduction process use as a comparable base for smoothing with the experimental data. Fig. 5.10 shows the first four mode shapes where the numerical SEREP and the experimental mode shapes were plotted. As can be seen in Fig. 5.11 all MAC values are above 0.97 and mode shapes are very similar as expected for this high MAC values. Fig. 5.12 presents the COMAC and

RD between experimental and reduced models on each accelerometer DOFs and for 7 (seven) mode shapes. In general, the COMAC of all DOFs was above 0.97, except for the DOF no.4. Also, the RD stayed below 0.2% for all DOFs and mode shapes considered in the analysis.

This result was expected, since as stated in BRINCKER e VENTURA (2015), a free - free test is good because it is well defined, but bad in the sense that the FEM simply correlates too well with the experiment.

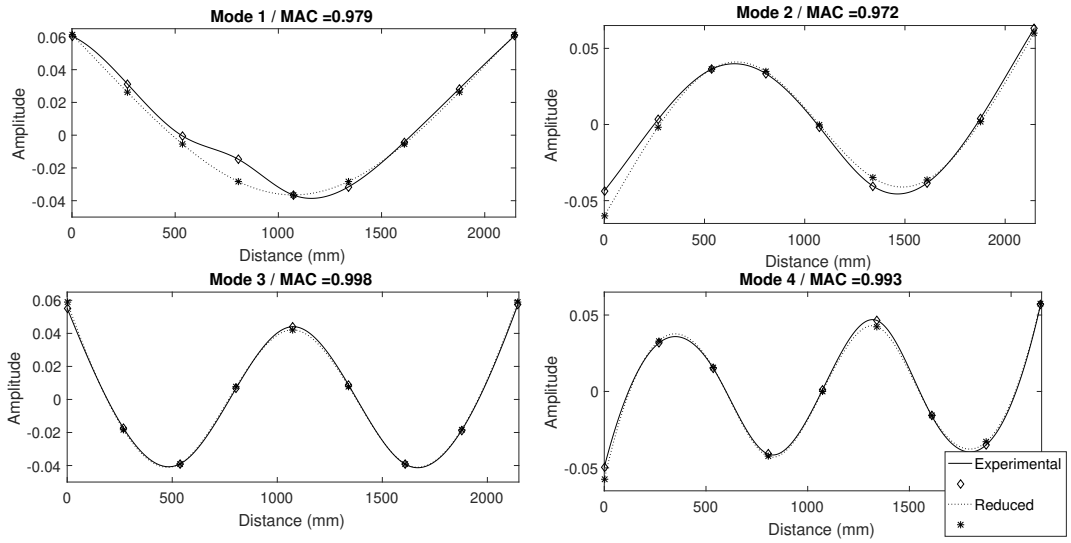

Figure 5.10: Experimental and FE reduced mode shapes.

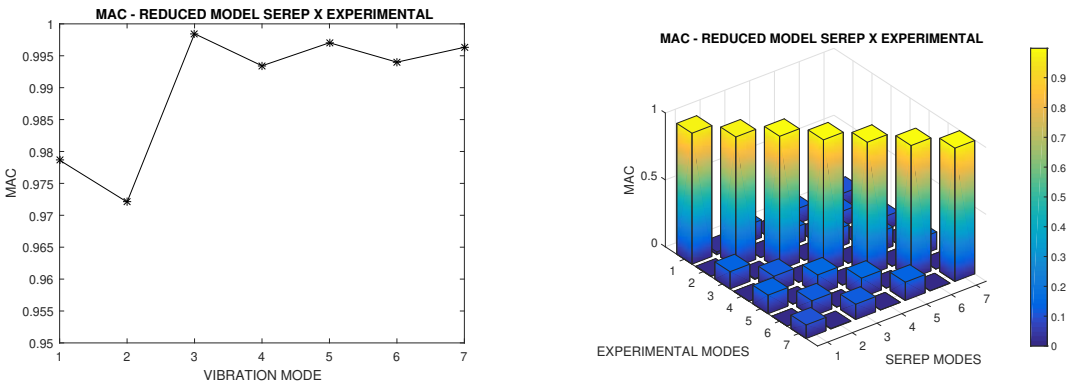

(a) MAC diagonal values

(b) MAC correlation

Figure 5.11: MAC for SEREP and experimental modes.

For the other 15 (fifteen) experimental mode shapes such comparisons cannot be made directly, because the 9 (nine) accelerometers (DOFs) cannot spatially represent these higher modes, i.e., there is a spatial aliasing. Although these measured modes are spatially incomplete, it is still possible to calibrate them, as shown by LIU (2011).

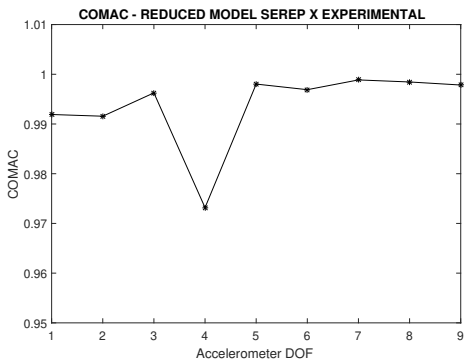

(a) COMAC

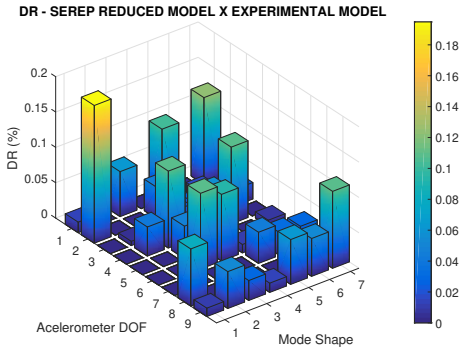

(b) RD

Figure 5.12: COMAC and RD between SEREP and experimental modes

5.1.5 Modal Expansion and Smoothing Using Experimental Mode Shapes

Smoothing between numerical and experimental modes reduces the differences between numerical and experimental DOF's amplitudes. It tends to increase MAC and COMAC values and decrease RD values.

The LC is based on the selection of an optimum base of numerical modal vectors. As an example of this process, Fig 5.13 presents on the left the increasing MAC number for the fitting DOFs as the number of modes increases, while on the right, for the observation DOFs, the MAC number reaches a maximum and then decreases, indicating that any number of modes above the one where the maximum occurred yields a correlation that can be considered over fitting. For the fifth mode presented in Fig. 5.13, 4 (four) modes were used as a base for the fitting process.More details on how the LC works can be seen in (BRINCKER *et al.*, 2014).

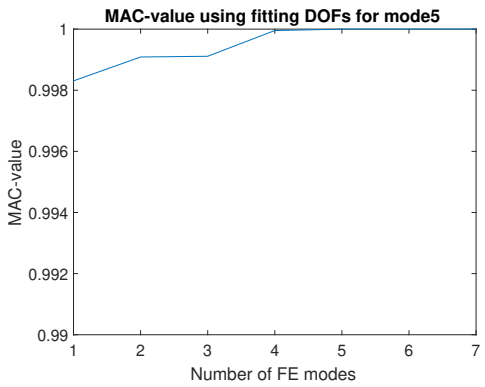

(a) MAC values using fitting DOFs for the fifth mode.

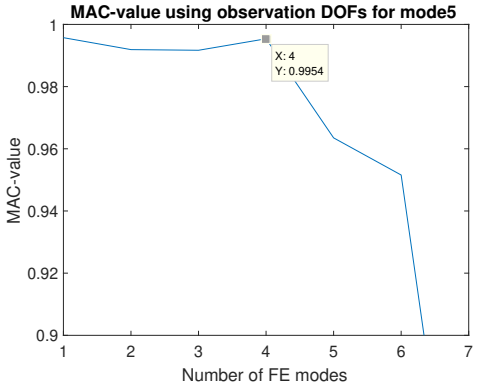

(b) MAC values using observation DOFs for the fifth mode.

Figure 5.13: LC estimate of optimum number mode shapes for correlation.

The fitted (calibrated or smoothed) mode shapes can be seen in Fig.5.14, plotted

along with the non-fitted (numerical) and the experimental mode shapes for comparison purposes. MAC values appearing in the plots are between the fitted and the experimental mode shapes, and, in general, a clear improvement can be seen, mainly for the 2^{nd} mode shape, as showed in Fig.5.15.

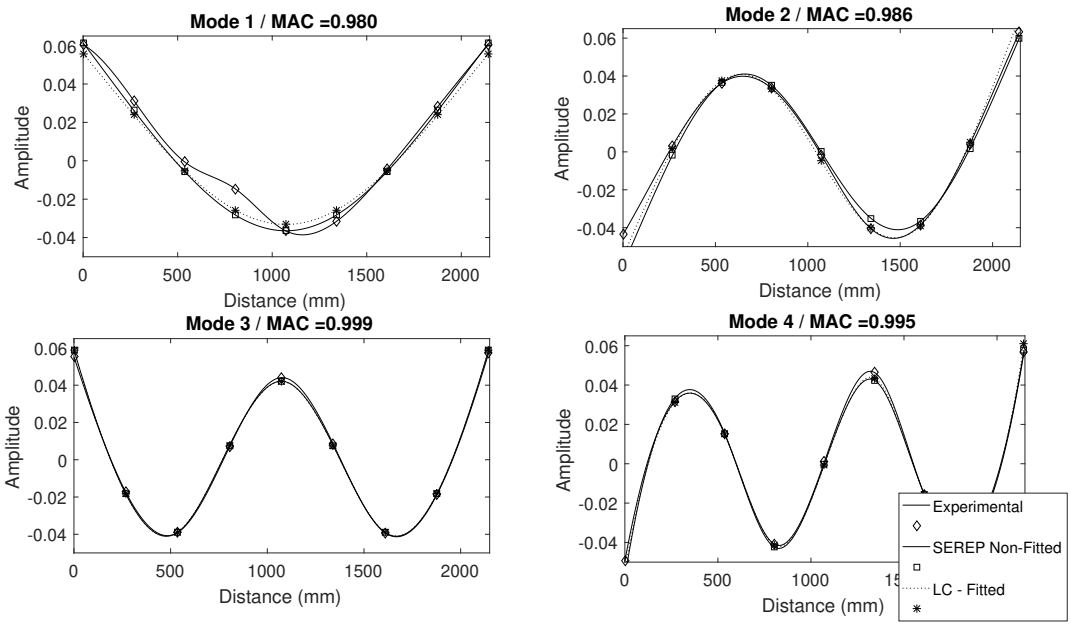

Figure 5.14: Modal plots for calibrated, non-fitted and experimental mode shapes.

The improvements achieved with the LC methodology in comparison with the results obtained with the non-fitted reduced procedure can be observed in Fig. 5.15 for lower frequency modes and in Fig. 5.16 for higher frequency modes. The MAC results show a clear improvement on the correlation of the LC fitted model in comparison with the non-fitted reduced model.

The smoothing process could have been carried out for each mode shape separately, but in this work, one chose to fit all the 22 (twenty-two) modes using the same 4 (four) fitting DOFs (numbers 2, 4, 7 and 8) and keeping the same 5 observation DOFs (numbers 1, 3, 5, 6 and 9), since the results obtained were satisfactory, as shown above.

5.1.6 Virtual Sensing

As mentioned in section 5.1.2, the beam's modal parameters were identified considering the impacts on all 9 (nine) DOFs. Thus, it was possible to identify all 22 (twenty-two) bending mode shapes, in the range of 0.1 to 1500 Hz. For the virtual sensing procedure, only the response signals measured due to the impact on DOF 5 were chosen, as shown schematically in Fig.5.17. In addition, dynamic response predictions were evaluated for DOF 9 and the acceleration signal measured in this DOF

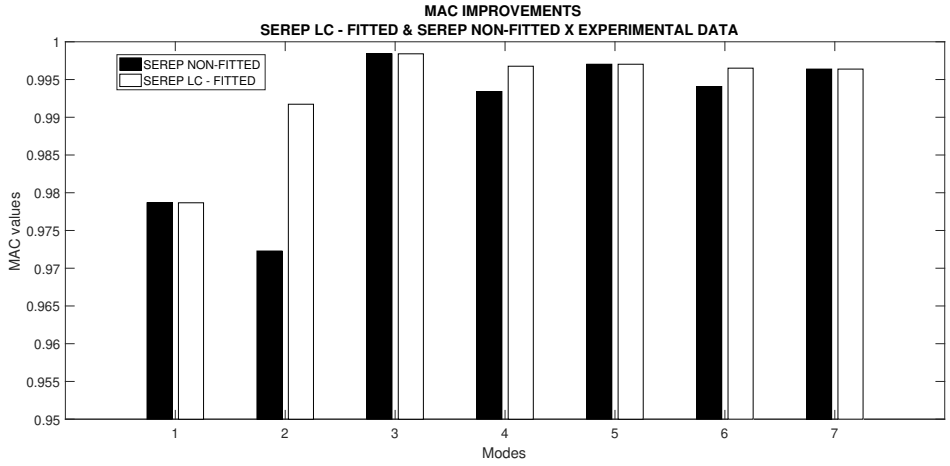

Figure 5.15: MAC improvements from LC correlation procedure.

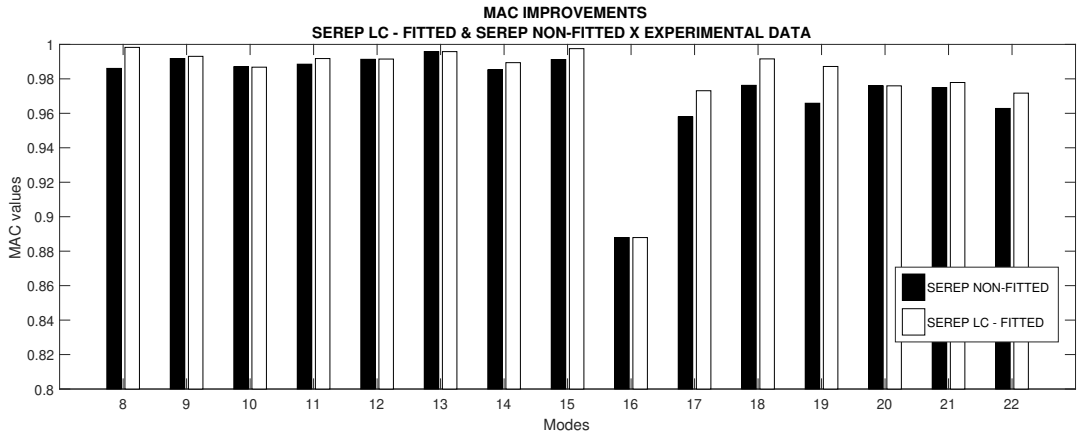

Figure 5.16: MAC improvements from LC correlation procedure for higher modes.

were used as a reference to assess the accuracy of the predictions. Two situations were analyzed: (i)the possibility of obtaining good results if only one accelerometer and one mode shape are used. And, (ii)the influence to the prediction errors if more accelerometers are used.

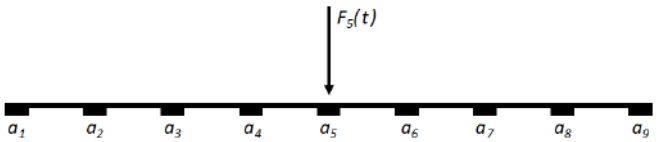

Figure 5.17: Rectangular beam configuration(F_i: force, a_i: accelerometer).

Response Prediction in DOF 9 using the Acceleration Measured in DOF 1

An impact on DOF 5 did not excite the even vibration modes, that is, the 2^{nd}, 4^{th}, 6^{th}, 8^{th}, 10^{th} and so forth, until the 22^{nd} mode shape. It can be seen in Fig. 5.15 that, in the 2^{nd} and 4^{th} mode shapes, DOF 5 behaves as a node, and it is so for all even mode shapes.

When attempting to predict the vibration signal in DOF 9 using all 22 mode shapes, the result is disastrous, as it should be, because the modal participation factor of the impact force is not taken into account in the response measurements. This means that the modal matrix that should be used in Eqs. (3.41) and (3.42) must be obtained experimentally, considering only the impacts on DOF 5. For this case, no even vibration modes would be identified.

Figure 5.18 shows the measured and predicted signals in DOF 9 in the time domain. Figure 5.19 shows the same signals in the frequency domain. In this case, only the acceleration measured in DOF 1 (a1) was used for the prediction, and all 11 odd mode shapes (1^{st}, 3^{rd}, 5^{th}, 7^{th} and so on) were used. Note that both TRAC and FRAC have values close to 1, and the mean absolute errors (MAE) and the RMS errors are small, which shows the high accuracy in the prediction.

On the other hand, if in Figs. 5.22 and 5.23, we look at the first line in the axis number of accelerometers, we find that using only the first mode, the prediction is already quite accurate for the entire frequency range, with TRAC and the FRAC close to 1 and RMS error around $3 \times 10^{-3} m/s^2$. It should be noted that increasing the number of modes used in the modal matrix manifests no significant accuracy improvement. In Figs. 5.22 and 5.23, the axis named Number of Accelerometers represents the number of measurements used to estimate the modal coordinates, being 1 for a_1; 2 for a_1 and a_2; 3 for a_1, a_2 and a_3; up to 8 (a_1, a_2, a_3, a_4, a_5, a_6, a_7 and a_8). The acceleration measurement a_9 was used only for evaluating the predictions accuracy. The Number of Modes axis shows the number of odd mode shapes used in the predictions.

Response Prediction in DOF 9 using Multiple Acceleration Measurements

Figures 5.20 and 5.21 show the measured and predicted signals for DOF 9, in the time and frequency domains. In this case, 3 accelerometers (a_1,a_2 and a_3) and 9 odd (1^{st}, 3^{rd}, 5^{th}...17^{th}) mode shapes were used. Note that the TRAC and FRAC are close to 1, indicating that both signals have the same shape and, from the amplitude standpoint, mean absolute (MAE) and the RMS errors are low, which shows the high accuracy of the predicted signal. It can be seen in Fig. 5.22 (a) and

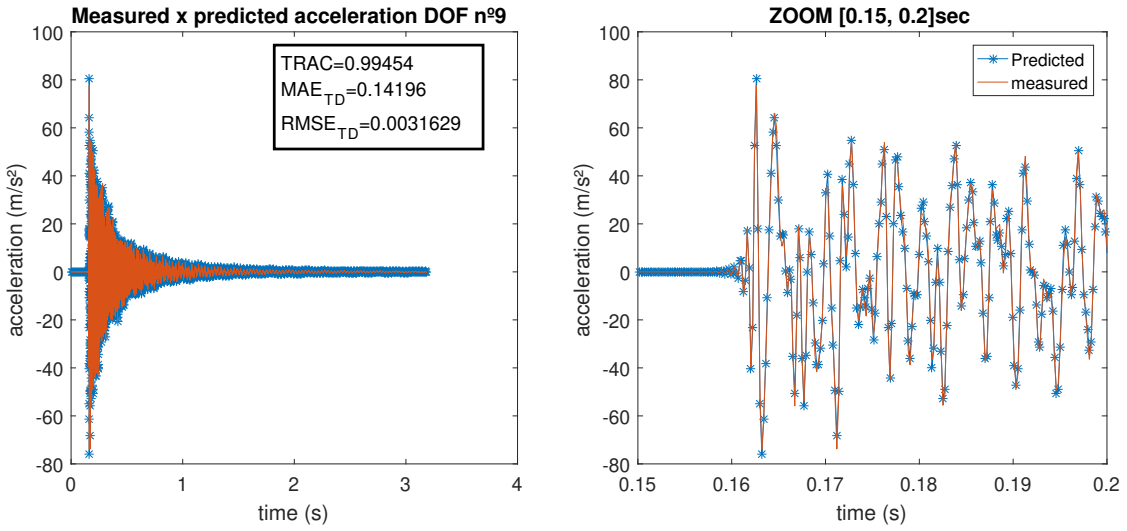

Figure 5.18: Time domain comparison of predicted and measured accelerations at the ninth DOF.

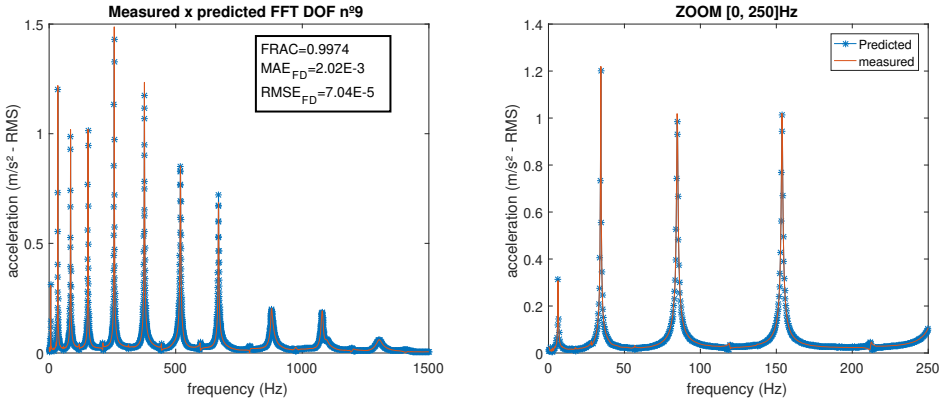

Figure 5.19: Frequency domain comparison of predicted and measured accelerations at the ninth DOF.

(b) that TRAC and FRAC are between 0.5 and 0.994. That is, for large number of accelerometer used, the predicted response signal, in time and frequency domains, has low accuracy with few modes but increases as more modes are added to the process. The difference is due to the amplitudes, as can be seen in Fig. 5.23 (a) and (b). In the time and frequency domains, the RMS error was minimal when 3 accelerometers and 9 odd vibration modes were used.

An advantage of the modal expansion method in predicting responses is that it only uses the modal matrix and does not depend on natural frequencies and damping ratios, as can be seen in the Eqs. (3.41) and (3.42). Other methods, such as the Kalman Filter, need those information MAES *et al.* (2014).

Another advantage of this method is that there is no need to normalize the modal matrix, since this is implicitly taken into account at the time of modal coordinates estimation, as shown in Eq. (3.41). The modal matrix normalization affects only

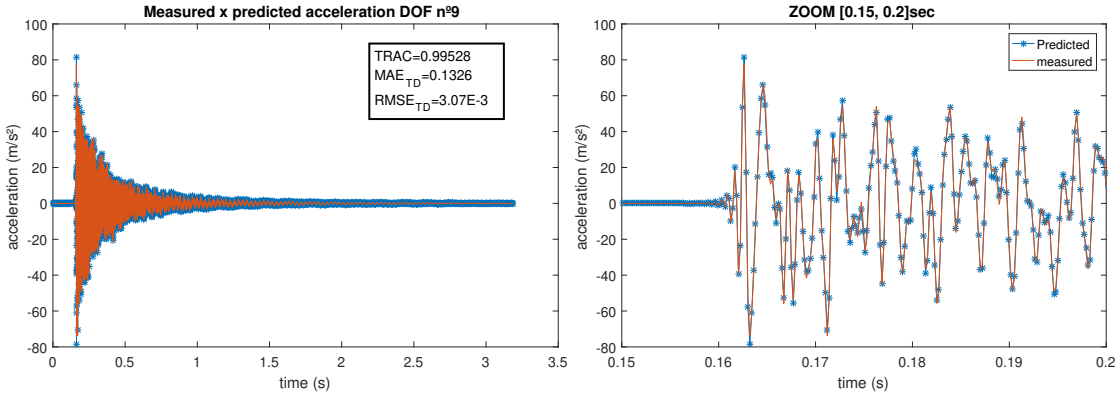

Figure 5.20: Time domain comparison of predicted and measured accelerations at the ninth DOF.

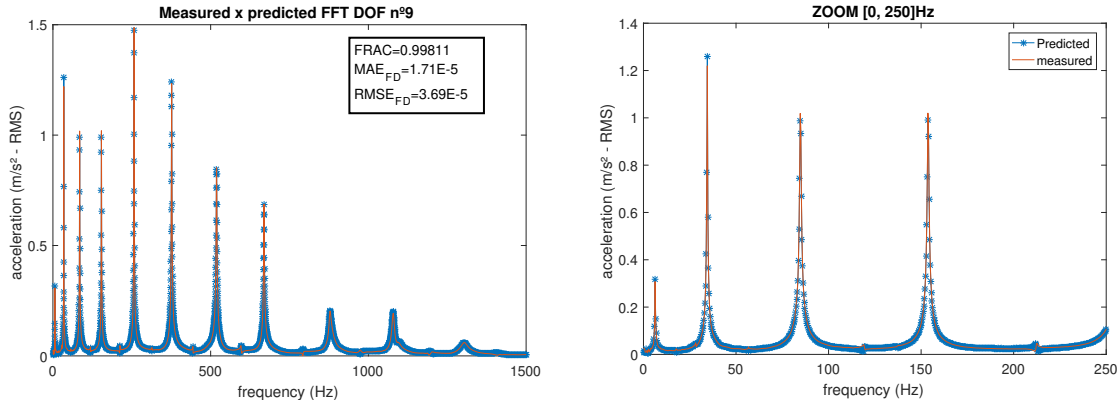

Figure 5.21: Frequency domain comparison of predicted and measured accelerations at the ninth DOF.

the amplitudes of the modal coordinates.

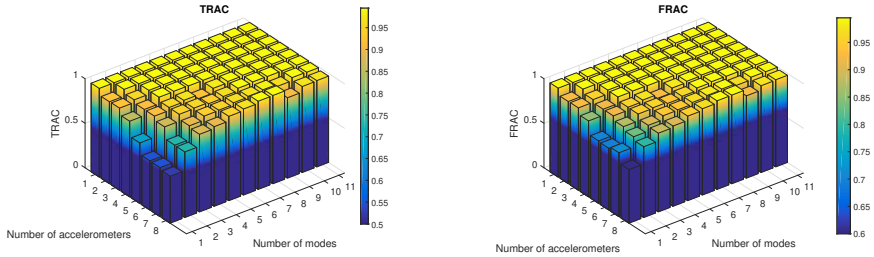

(a) TRAC (b) FRAC

Figure 5.22: Comparison between predicted and estimated signals.

5.1.7 Results Discussion

In this case study a calibrated or smoothed expanded modal model of a rectangular aluminum beam suspended in air was used to estimate acceleration amplitudes in non-instrumented locations.

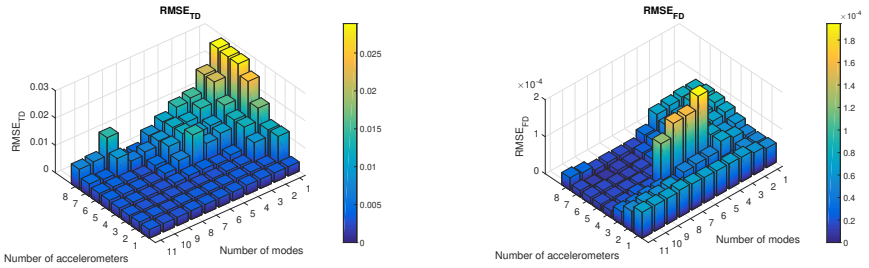

(a) $RMSE_{TD}$ (b) $RMSE_{FD}$

Figure 5.23: Root mean squared error on time and frequency domains.

The numerical modal model, obtained through the FEM, was necessary (i) to serve as a basis for smoothing the experimental modal matrix; (ii) for obtaining a mass matrix to M-orthonormalize the experimental modal matrix (this step is not necessary for response prediction, but it is crucial when predicting forces); and (iii) to serve as a basis to correct the spatial aliasing of higher experimental mode shapes.

A clear improvement can be seen on the MAC correlation when the fitting process is undertaken, meaning that numerical model when fitted become closer to the experimental model. Thus, when used the fitted modal model to expand the dynamic measurements onto non measured degrees of freedom are more prone to yield more accurate results.

The correlation process, based on the LC principle, showed to be dependent on the choice of fitting DOFs. Therefore, on the next case study the improvement of this method proposed in this work, the LCMC, will be used as it allows the optimization of the fitting DOFs for each mode shape to be calibrated.

It can be concluded that modal parameters should be identified and used for virtual sensing in a specific operational condition. In general, modal parameters obtained in one operational condition should not be used to predict the dynamic response in another operating condition, because some vibration modes may or may not be excited in the new operational condition, which can lead to erroneous predictions.

Finally, to validate the improvements that can be achieved with the LCMC smoothing method proposed in this dissertation, a test was undertaken in this case study. The improvements can be seen in Fig. 5.24.

As can be seen the MAC values showed better results with the proposed LCMC method and therefore for the next case studies it will be the method of choice for the smoothing process.

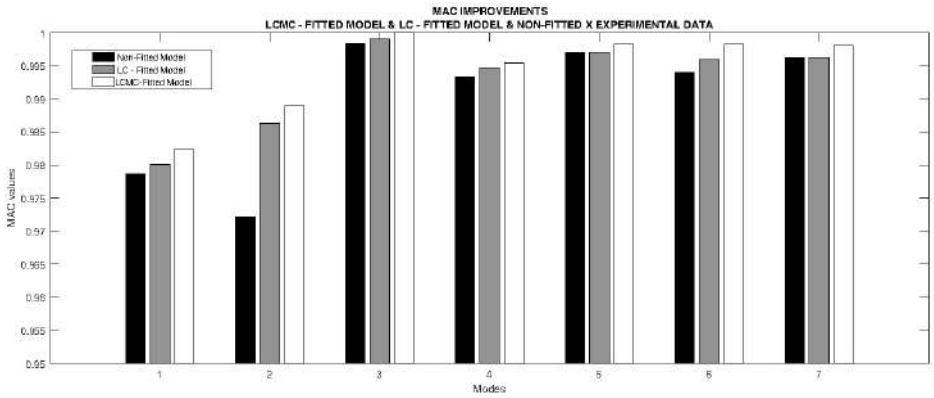

Figure 5.24: MAC improvements comparing LC and LCMC smoothing methods.

5.2 Rectangular Cantilever Beam

The second case study here presented is based on the same aluminum beam used on the first case study, but considering in this case a different boundary condition. The same methodology was applied as described below.

5.2.1 Finite Element Model (FEM)

A numerical FEM was developed at first to have a preliminary notion of the modal parameters of the beam, mainly to avoid positioning the sensors over the nodes where the displacement will be zero, spoiling the measurement.

For the FEM model an important assumption is that the system is undamped. This assumption is pertinent because the proposed method is not interested in a system's response in the resonance regions, where it would be crucial to consider damping effects.

The dimensions of the beam are the same from the previous and can be seen on 5.2, the difference being that in this case a clamp was installed 835 mm from one end of the beam in order to introduce the cantilever boundary condition.

The model was developed in the same finite element commercial software and the construction started with keypoints that were assigned to match the sensors coordinates and the clamped point, as shown in table 5.5. A line segment between each keypoint was assigned and further subdivided to build the mesh. The optimized subdivision of these segments was determined afterwards by a mesh test.

The sensors were modeled as mass elements, in this case each accelerometer used weighted 50g. The sensors mass was assigned to the nodes in each of the last 5 keypoints in Table 5.5 to match their coordinates in the experiment.

The number of nodes in the model was assessed using a mesh test as in the previous case study. A mesh test was performed to determine an optimized mesh

Table 5.5: FEM model keypoints position in relation to the beam clamped point.

Keypoints	Coordinates [m]
#1	-0.835
#2	0.0
#3	0.11
#4	0.41
#5	0.72
#6	1.01
#7	1.31

size, i.e. a size where it can be considered the solution converged. The convergence criteria applied is a relative average relative difference between frequencies of successive mesh steps reaches a value below $0,1\%$. The mesh step size was determined by the number of subdivisions for each of the 6 line segments, these subdivisions were determined as a constant multiplied by the length of the segment, so the variable is the constant which started with 6 and doubled each iteration. Only the first 10 eigenvalues were used for this test, Tab. 5.6 shows the comparison between number of subdivisions for the line segments and its respective eigenvalue solutions.

Table 5.6: Mesh convergence by comparison of Natural frequencies (f (Hz)) and number of line segment subdivisions (N).

f \ N	6	12	25	50	100	200
#1	2,4341	2,4323	2,4315	2,4313	2,4313	2,4313
#2	7,5634	7,5461	7,5413	7,5402	7,5399	7,5399
#3	15,490	15,272	15,181	15,164	15,160	15,158
#4	44,833	43,038	42,313	42,178	42,142	42,132
#5	51,493	48,281	47,473	47,297	47,253	47,242
#6	93,526	85,841	82,940	82,399	82,256	82,220
#7	170,49	140,96	134,14	132,69	132,33	132,24
#8	196,71	166,46	154,03	152,03	151,51	151,37
#9	307,37	241,4	218,66	214,79	213,77	213,51
#10	436,42	295,22	266,67	260,82	259,40	258,96
Avg. Rel. diff.	-	10,67%	3,88%	0,42%	0,20%	0,03%

Based on the criteria and analyzing Tab. 5.6 a mesh size resultant of the subdivision of the line segments in 100 has been determined as an optimized mesh size

for the geometry of the study case, since further smaller subdivisions would not give results with an average relative difference greater than $0,1\%$. This subdivision resulted in a mesh size of 215 nodes with elements of about 10 mm in length each.

5.2.2 Experimental Setup

A cantilever aluminum beam, instrumented with accelerometers and used for modal tests. It has a full length of 2,145mm, however, the length of the segment which the accelerometers were positioned is 1,310mm from the clamped point to the top.

The following equipment were used in the tests:

- B&K Impact Hammer (Model 8200)
- 05 Uniaxial Accelerometers
- National Instruments Data Acquisition Card (Model NI 9233)
- 01 Notebook for Data Acquisition

R. S. MINETTE (2014) For signal acquisition, A *National Instruments'*® system was used with software *Labview® 8.0*. The system has a analogic-digital converter of 24 bits with sampling rate from 2 kHz to 50kHz for each channel, up to 32 channels (NI-9178 model with boards USB NI-9233). The system also has an analogic filter anti-aliasing.

The accelerometer used was a piezo-electric type with 100 mV/g sensibility, acquisition range from 2 Hz to 10 kHz, waterproof from manufacturer PCB-IMI, model 624B11. The signal acquisition system as well as the accelerometer used can be seen in Fig. 5.25.

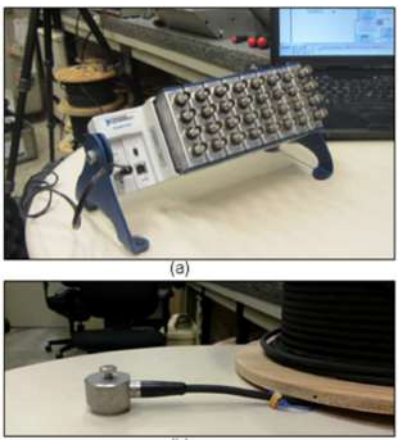

Figure 5.25: Measuring Instruments: a) A/D NI® board b) Waterproof piezo-electric accelerometer.

These 5 (five) accelerometers were positioned so that the distances between two consecutive sensors were equivalent. As the free length of the beam is 1,310mm, the distances between the sensors is 300mm, being the first accelerometer installed 110mm from the fixation point. A multiple reference impact testing was performed using an instrumented hammer with a steel tip mounted. Fifteen impacts were applied near the clamped point, as shown in Fig. 5.26.

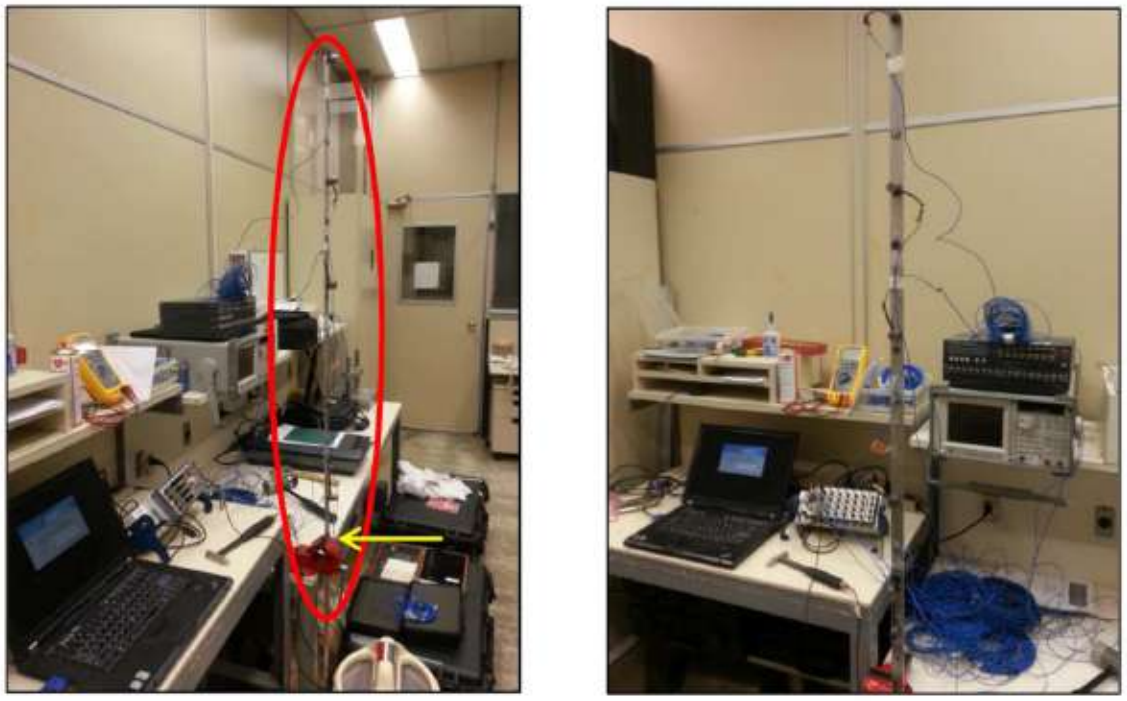

Figure 5.26: Rectangular beam in cantilever boundary condition and instrumented with 05 accelerometers.

Firstly, the output-only modal analysis results were presented. Then, the reduction process was validated through MAC, COMAC and RD by comparing the SEREP reduced and the full numerical model. Next, results for model correlation using the LC method were presented, as well as the improvement in the correlation, using MAC as a criteria. Finally, results of virtual sensing the vibration response at the DOF no. 5, which is at the end of the beam, were presented.

5.2.3 Output-Only Modal Analysis (O-OMA)

The beam was clamped in its base and all excitation impacts were applied near the clamped point, as shown is Figure 5.27.

The first 5 (five) natural frequencies obtained from the analysis are shown in Table 5.7. The first mode had to be identified manually. This can be explained by the fact that the impacts were applied near the clamped point, therefore exciting higher modes. The consequence is that lower frequency modes showed lower energy

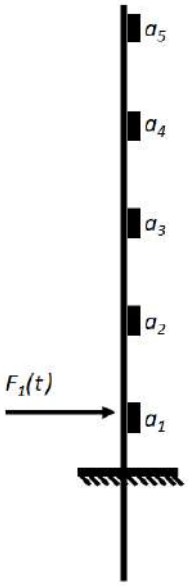

Figure 5.27: Rectangular beam configuration(F_i: force, a_i: accelerometer).

in the spectrum and might be harder to identify.

Only vibration responses were used in the Enhanced Frequency Domain Decomposition (EFDD) algorithm. The objective was to simulate practical situations where it is not always possible to measure the excitation forces. Details of this analysis can be found in MARTINS VIEIRA (2020). Table 5.7 shows the first 5 (five) natural frequencies. The corresponding experimental mode shapes can be seen in Fig. **??**.

Table 5.7: Natural frequencies estimated using EFDD

Modes	Frequency[Hz]
1	2.39
2	14.82
3	41.22
4	81.19
5	136.96

5.2.4 Model Reduction using Guyan-SEREP

First of all, the aluminum beam FEM was conveniently constructed and converged. Its large number of nodes makes exporting mass and stiffness matrices manipulation time consuming, specially for application of SEREP modal reduction and for the smoothing process. Therefore, as the software has a built-in Guyan reduction algorithm available, it was used to decrease the matrices sizes, carefully applying the reduction without loss of dynamic characteristics.

A sensitivity test was carried out to guarantee the maintenance of the dynamic properties during this reduction process. In this test, the number of *active* nodes required to maintain the dynamic characteristics was evaluated.

Whether the Guyan method is applied to get a complete reduction to the few nodes of interest, substantial errors may be obtained since the number and selection of active DOFs have influence on the solution. Thus, the number of active degrees of freedom chosen for Guyan was optimized to obtain eigenvalues close to the eigenvalues obtained from the solution of the full model. In all cases the nodes related to the sensors were included. The stop criterion was when the average relative difference between two subsequent solutions reaches a value below $0,1\%$. Tab. 5.8 shows the number of active degrees of freedom and the related frequency values.

Table 5.8: Analysis of the influence of the number of active degrees-of-freedom in the Guyan natural frequency results.

	Number of Active DOF					
Vibration Modes	5	11	16	26	57	91
#1	2,3782	2,3781	2,3781	2,3781	2,3781	2,3781
#2	-	7,1375	6,8915	6,8862	6,8854	6,8854
#3	14,7364	14,877	14,8719	14,8717	14,8706	14,8706
#4	37,5596	41,2862	41,2083	41,1765	41,1593	41,1589
#5	55,0133	48,2337	47,3733	46,2462	46,0064	46,0065
#6	91,0793	81,24	81,1551	81,1136	81,0306	81,0271
#7	-	151,266	144,1323	132,8619	127,8839	127,8832
#8	-	-	157,484	148,5908	147,1813	147,1224
#9	-	228,4923	213,8304	213,1786	210,1728	210,0402
#10	-	-	-	269,6793	253,2336	253,2478
Avg. Rel. Diff.	-	6,80%	2,09%	1,82%	1,29%	0,01%

Examining Tab. 5.8 it has been concluded that 57 active degrees of freedom are the minimum number in which the solution does not diverge over $0,1\%$ since the average difference between frequencies with 91 active DOF and 57 active DOF observed was only $0,01\%$.

The next step was to perform the reduction process in the FEM software, considering the optimal 57 nodes, and then extracting the mass and stiffness matrices to be manipulated externally using *Matlab* to perform the further reduction.

The Guyan reduced model was used to obtain mass and stiffness matrices that were then used as input data to perform a eigenvalue solution from which the re-

sults were used in the model reduction (in modal space), the goal of the reduction is matching the number of degrees of freedom of the reduced model with the experimental ones.

The model was reduced to 5 (five) active nodes (located in the same physical position where the accelerometers were placed). It can be seen in Fig. 5.28 the first five mode shapes where the numerical SEREP reduced and the numerical full model mode shapes were plotted. The MAC number between the SEREP reduced and the full numerical modal model is indicated above each plot. As can be seen, there is a perfect match between full and reduced mode shapes, which leads to a MAC of 1. Figure 5.29 presents the MAC matrix for the 5 (five) numerical mode shapes.

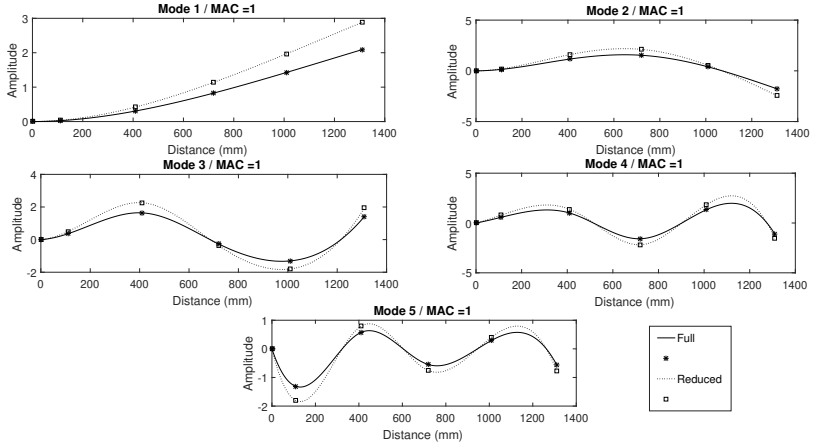

Figure 5.28: SEREP reduced and full numerical mode shapes comparison.

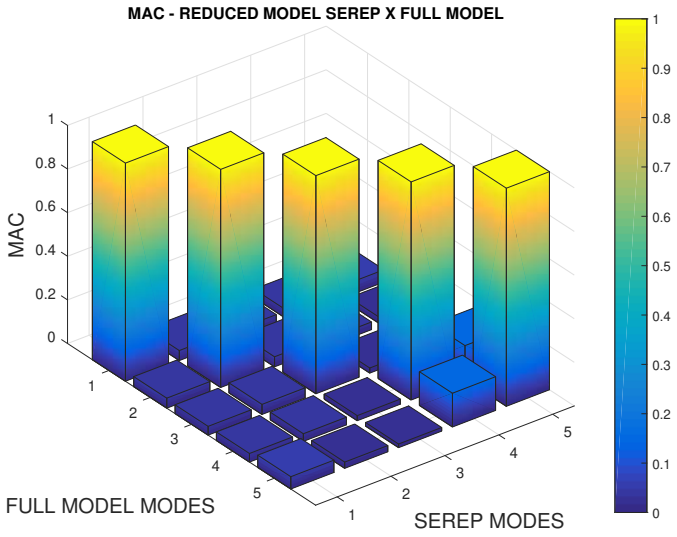

Figure 5.29: MAC for SEREP reduced and full numerical mode shapes.

All assessment criteria used to compare the reduced and full numerical models indicated that the reduction process was successful for the five DOF and a good

correlation between the full model and reduced was achieved. The MAC numbers are 1 (one) for all modes assessed.

The efficiency illustrated above permits reduction process use as a comparable base for smoothing with the experimental data. In Fig. 5.30 can be seen the first five mode shapes where the numerical SEREP and the experimental mode shapes were plotted. As can be seen in Fig. 5.31 all MAC values are above 0.9 and mode shapes are very similar as expected for this high MAC values. Fig. 5.32 presents the COMAC and RD between experimental and reduced models on each accelerometer DOFs and for 5 mode shapes. It can be seen that, in general, the COMAC of all DOFs was above 0.94. Also, the RD stayed below 0.8% for all DOFs and mode shapes considered in the analysis.

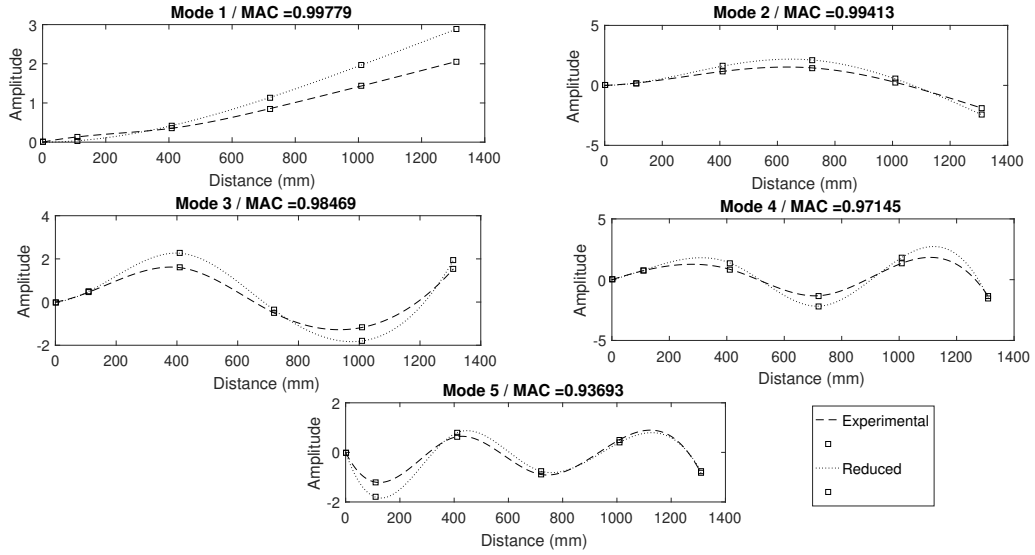

Figure 5.30: Experimental and SEREP reduced mode shapes comparison.

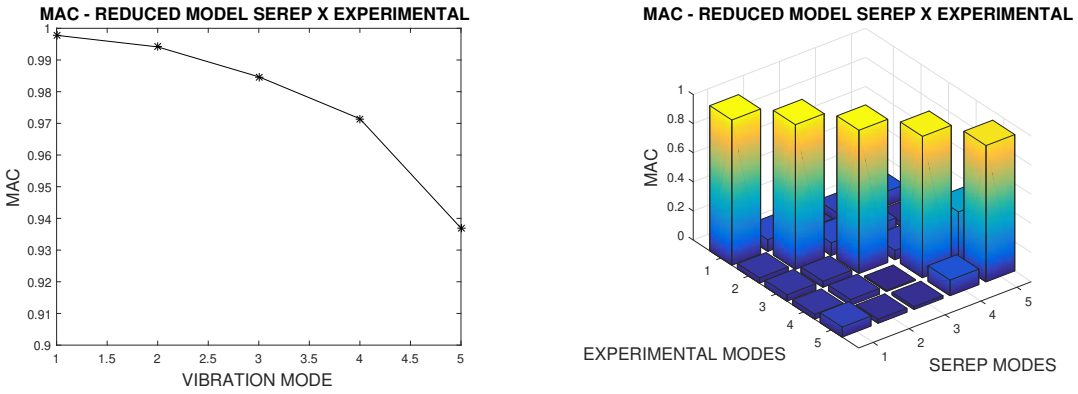

Figure 5.31: MAC for SEREP and experimental modes.

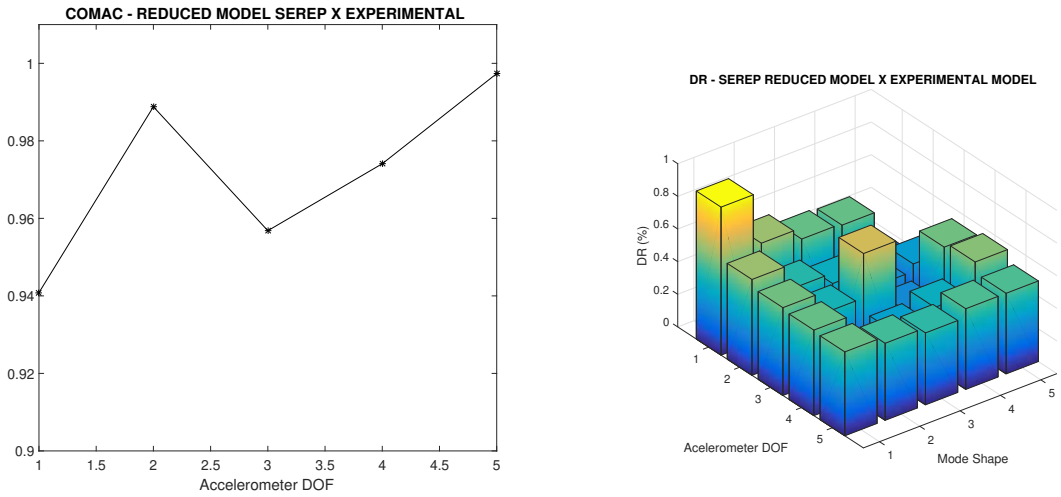

Figure 5.32: COMAC and RD between SEREP and experimental modes

5.2.5 Smoothing of the Experimental Modal Matrix

The same conclusion taken from the free-free case study happens here and the smoothing of the experimental modes with numerical data caused the differences between the numerical and experimental DOFs amplitudes to be minimized. This will tend to increase MAC and COMAC values and decrease RD values. As in the previous case study it was concluded that greater care should be taken with the choice of DOF for the smoothing process, in these case study the proposed LCMC method was applied.

The fitted (calibrated or smoothed) mode shapes can be seen in Fig.5.33, plotted along with the non-fitted (numerical) and the experimental mode shapes for comparison purposes. MAC values appearing in the plots are between the fitted and the experimental mode shapes, and, in general, a clear improvement can be seen.

The improvements achieved with the LCMC methodology in comparison with the results obtained with the non-fitted reduced procedure can be observed in Fig. 5.34. The MAC results show a clear improvement on the correlation of the LCMC fitted model in comparison with the non-fitted reduced model.

5.2.6 Virtual Sensing

As mentioned in section 5.2.3, the beam's modal parameters were identified considering the impacts near the clamped point. Thus, it was possible to identify the first five bending mode shapes, in the range of 0.1 to 140 Hz. For the virtual sensing procedure, the response signals measured due to the impact on DOF 1 was used, as shown schematically in Fig.5.27. In addition, dynamic response predictions will be evaluated at DOF 5 and the acceleration signal measured in this DOF will be

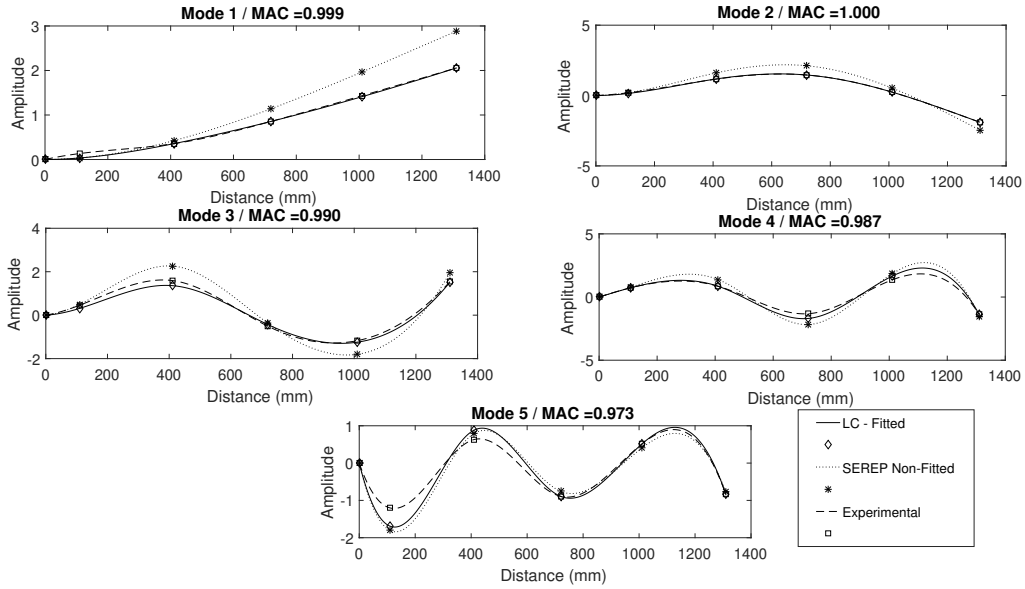

Figure 5.33: Modal plots for calibrated, non-fitted and experimental mode shapes.

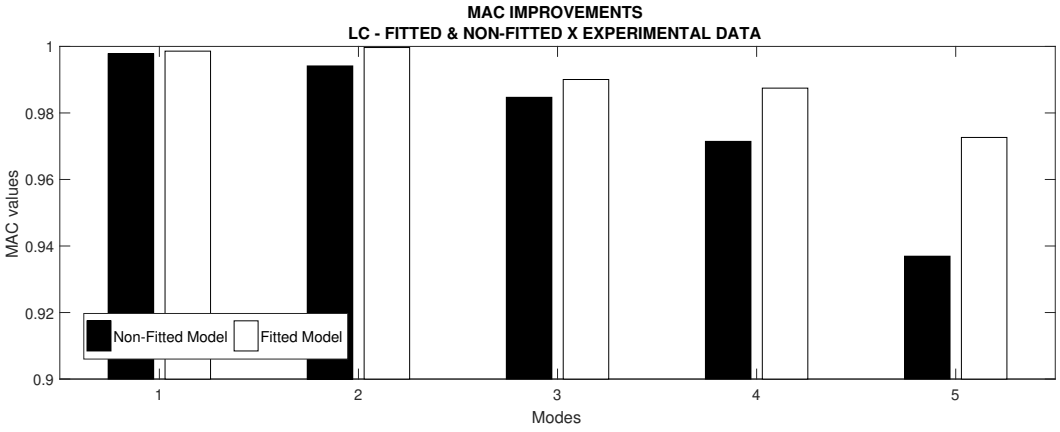

Figure 5.34: MAC improvements from LC correlation procedure.

used as a reference to assess the accuracy of the predictions. Two situations were analyzed: (i)The possibility of obtaining good results if only one accelerometer and one mode shape are used. And, (ii)The influence to the prediction errors if more sensors and mode shapes are used.

Response Prediction in DOF 5 using the Acceleration Measured in DOF 4

Figure 5.35 shows the measured and predicted signals in DOF 5, in the time domain. Figure 5.36 shows the same signals, now in the frequency domain. In this case, only the acceleration measured in DOF 4 (a4) was used for the prediction, and the second to fifth mode shapes (2^{nd},3^{rd},4^{th} and 5^{th}) were used. Note that both TRAC

and FRAC have values above 0.95, and the mean absolute errors (MAE) and the RMS errors are small, which shows the high accuracy in the prediction.

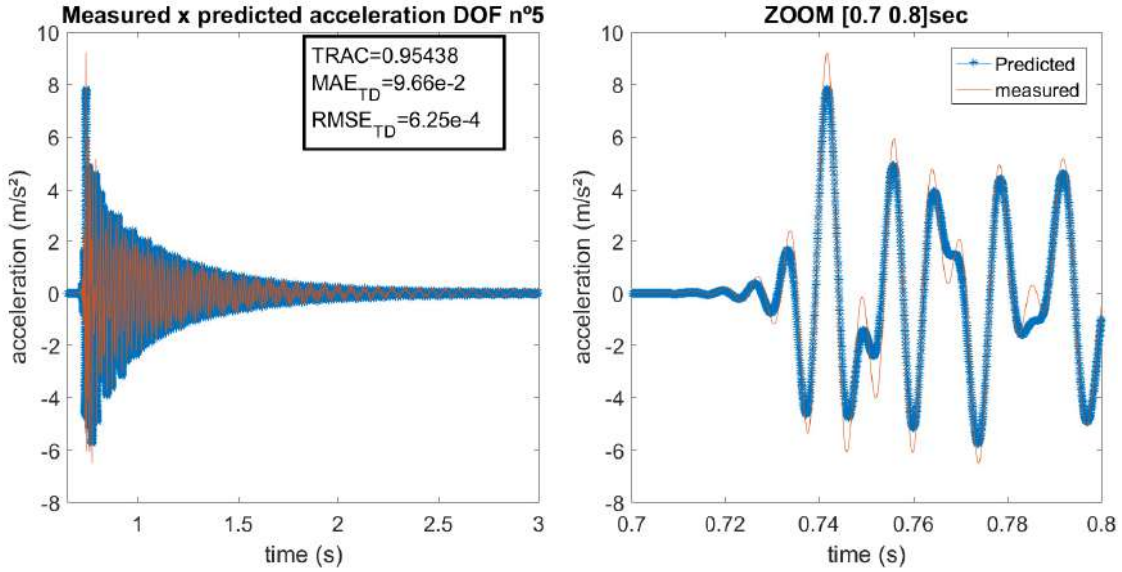

Figure 5.35: Time domain comparison of predicted and measured accelerations at the fifth DOF.

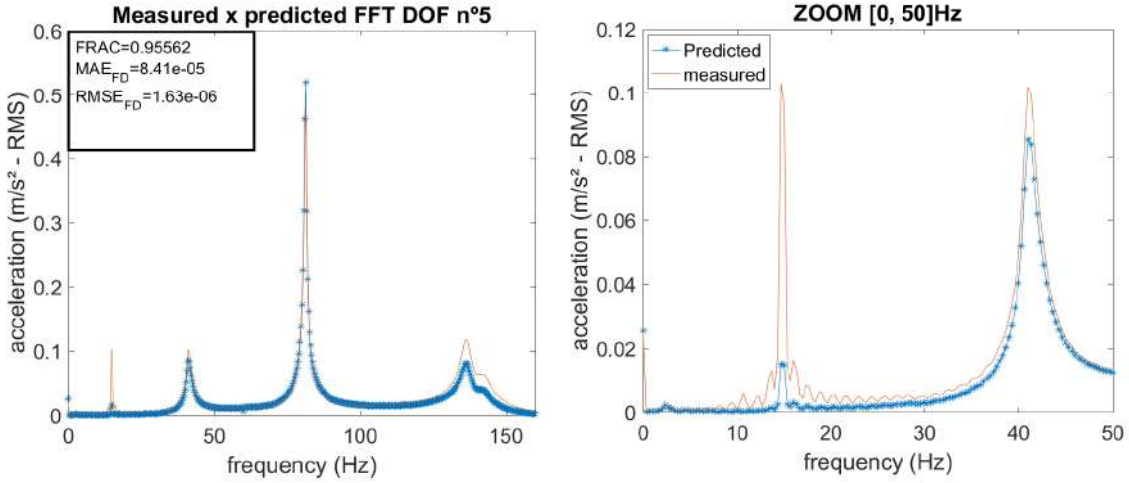

Figure 5.36: Frequency domain comparison of predicted and measured accelerations at the fifth DOF.

5.2.7 Response Prediction in DOF 5 using Multiple Acceleration Measurements

Figures 5.37 and 5.38 show the measured and predicted signals for DOF 5, in the time and frequency domains. In this case, the method used to choose the number of accelerometers and modes in the prediction was to calculate the correlation for

the prediction signals with the measured in all combinations possible with the available accelerometers and modes. Then, the assessment criteria were optimized one by one and the RMS in the time domain yielded the best result. The combination of accelerometers and modes that minimized the $RMSE_{TD}$ was using 2 (two) accelerometers (a_1 and a_4) and 2 (3^{rd} and 5^{th}) mode shapes. Note that the TRAC and FRAC are above 0.98, indicating that both signals have the same shape and, from the amplitude viewpoint, mean absolute (MAE) and the RMS errors are low, which shows the high accuracy of the predicted signal.

An advantage of the modal expansion method in predicting responses is that it only uses the modal matrix and does not depend on natural frequencies and damping ratios, as can be seen in the Eqs. 3.41 and 3.42. Other methods, such as the Kalman Filter, need those information MAES *et al.* (2014).

Another advantage of this method is that there is no need to normalize the modal matrix, since this is implicitly taken into account at the time of modal coordinates estimation, as shown in Eq. 3.41. The modal matrix normalization affects only the amplitudes of the modal coordinates.

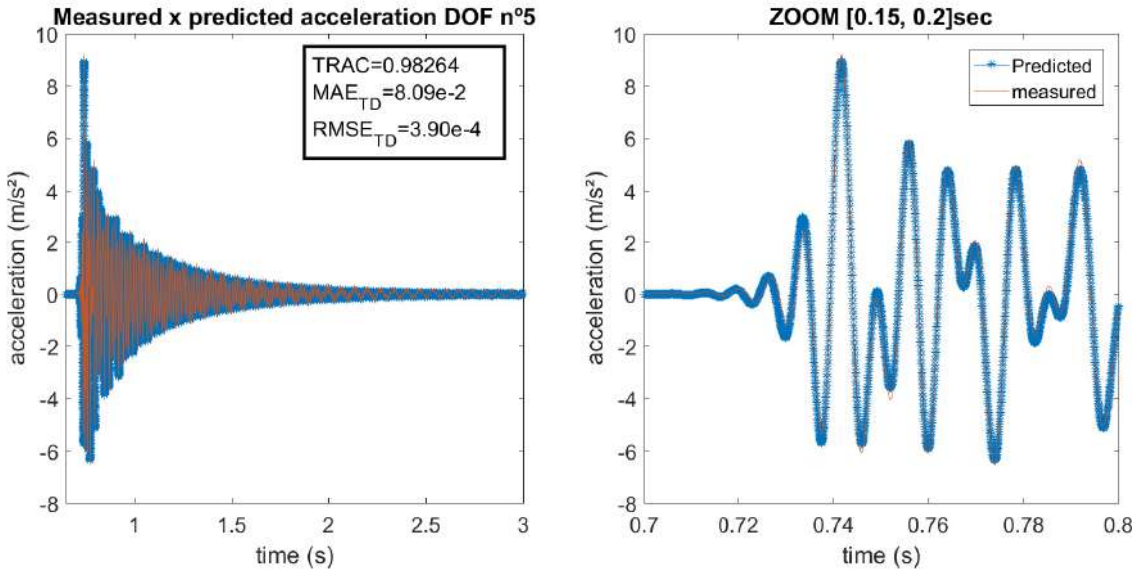

Figure 5.37: Time domain comparison of predicted and measured accelerations at the fifth DOF.

5.2.8 Results Discussion

In this case study, a calibrated or smoothed expanded modal model of a cantilever aluminum beam was used to estimate acceleration amplitudes in DOF 5.

The numerical modal model, obtained through the FE method, was necessary (i) to serve as a basis for smoothing the experimental modal matrix; (ii) for obtaining a mass matrix to M-orthonormalize the experimental modal matrix (this step is not

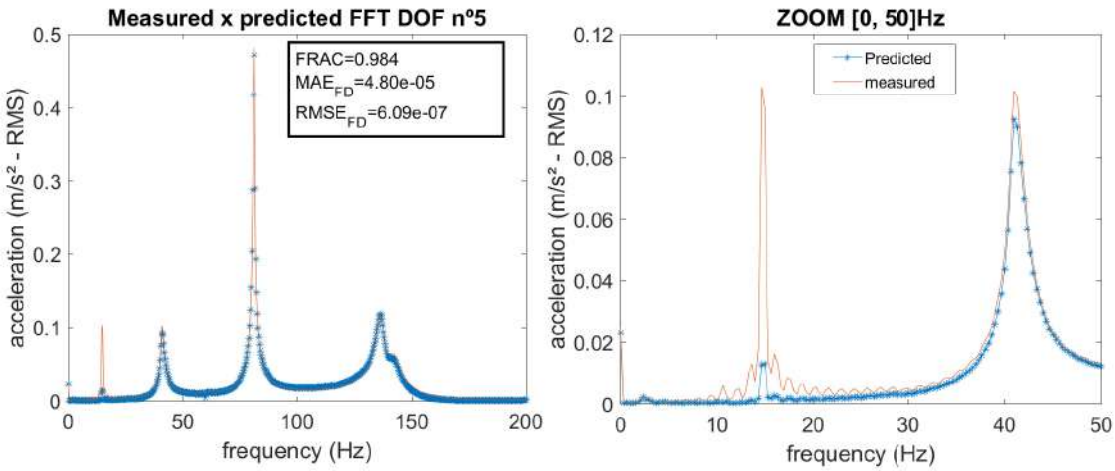

Figure 5.38: Frequency domain comparison of predicted and measured accelerations at the fifth DOF.

necessary for response prediction, but it is crucial when predicting forces) and (iii) to serve as a basis to correct the spatial aliasing of higher experimental mode shapes.

The SEREP reduction procedure achieves the goal of fully reducing the system keeping exactly the same natural frequencies and mode shapes from the original system. The MAC between the reduced model mode shapes from this method compared to the full model were all close to 1 and all relative difference (RD) values were below 1%. These results conclude the efficiency of the reduction procedure.

The smoothing process, based on the LCMC principle, showed to be successful and yielded very good improvement in the correlation with the experimental results.

An advantage of the modal expansion method, in predicting responses, is that it only uses the modal matrix and does not depend on natural frequencies and damping ratios. This method is fast, easy to implement and effective. The virtual sensing, both in the time and frequency domains, showed good agreement with the measured acceleration signals.

The optimization process used to select the accelerometers and modes for the signal prediction resulted in a selection of accelerometers with signals that don't represent all amplitude response, thus resulting in predicted signal that for some frequencies are below the real measurement amplitude, as can be seen in Fig. 5.38. For future works this could be improved by using a more robust optimization technique to select the attributes for the prediction process, for example, by using other optimization algorithms or machine learning in the process.

5.3 Interstage Compressor Pipe System

As the methodology was validated using the two case studies presented before, with controlled conditions in laboratory tests, the next step of this work was to apply

the same procedure in a real application case. This case study is the application of the methodology to an interstage DN10 pipe connecting the discharge of the first stage of a reciprocating compressor to the pulsation damper from the second stage suction as can be seen in Fig. 5.39 taken from the process plant 3D model. In the image, the blue marked pipe is the section that was modeled using ANSYS software and the red dots indicate the positions where accelerometers were installed.

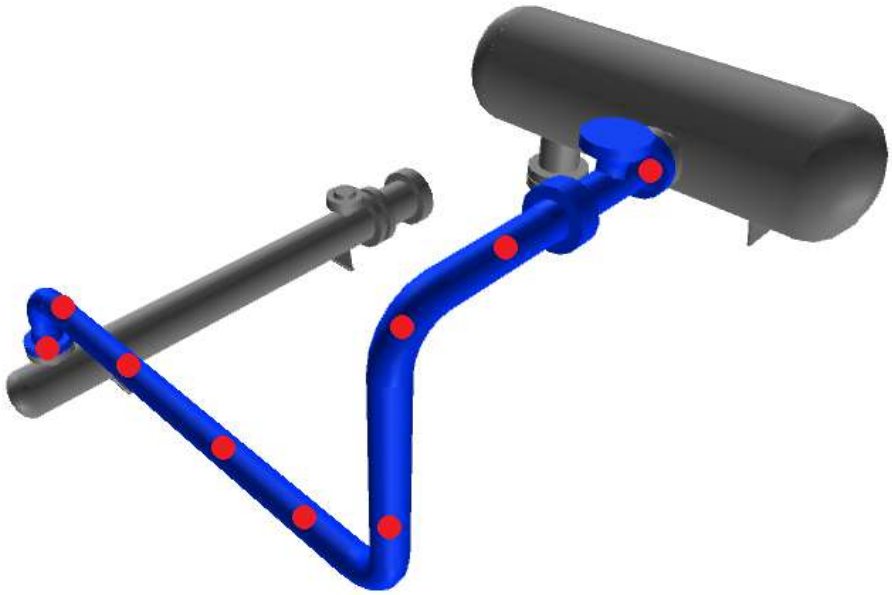

Figure 5.39: Second stage suction pipe, image taken from the 3D model of the process plant. Accelerometer installation positions marked in red.

5.3.1 FEM Model

As described in chapter 4, a preliminary model was developed to indicate the best positions for sensor placement, avoiding positioning of sensor over node points of the lower frequency and more relevant mode shapes. Fig. 5.40 shows the dimensions of the DN10 pipe, object of analysis in this case study.

The full model consisted of 715 (seven-hundred and fifteen) nodes, including nodes positioned at the measured locations. The number of nodes used was calculated using a mesh test with a convergence criteria related to the natural frequencies. As this case study is a three-dimensional structure, it took in consideration all translations and rotational degrees of freedom, therefore 6 (six) DOFs for each node. A two-dimensional, derived from the beam element, pipe element (PIPE288) was used. In Fig. 5.41 the model can be seen with the element cross-section represented in the plot, therefore even though a two-dimensional element was used the model image appears three-dimensional.

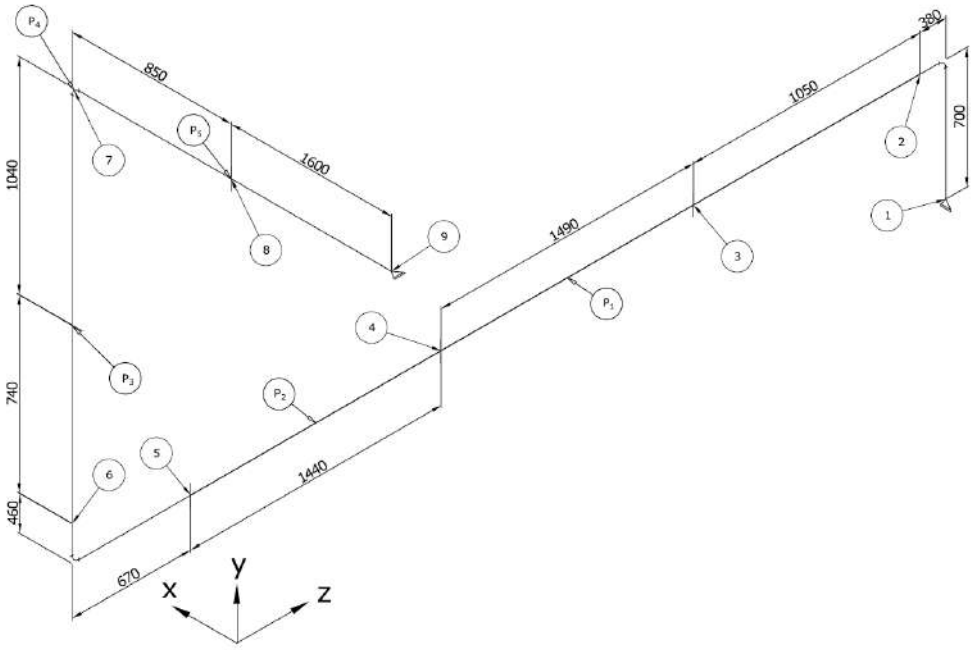

Figure 5.40: Pipe dimensions and identification of accelerometer and impact positions.

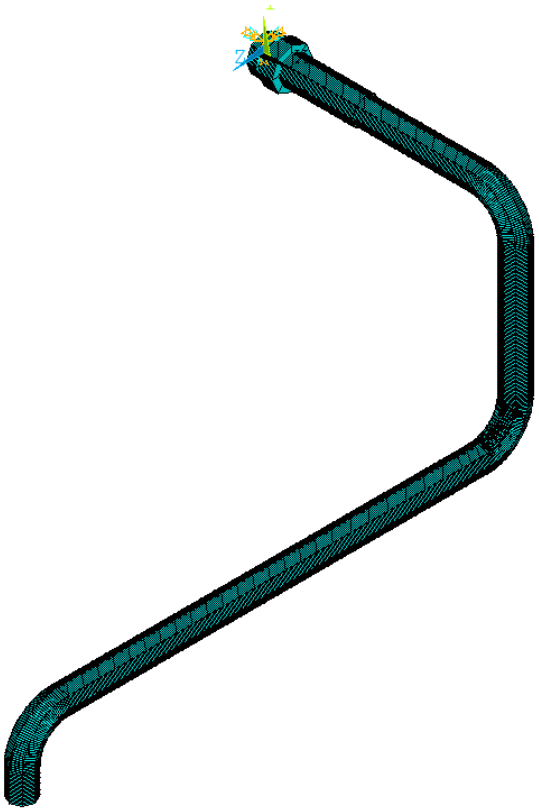

Figure 5.41: Finite element full model.

The model boundaries consisted of three interfaces. The first is the flanged connection to the interstage heat exchanger (point #1 shown in Fig 5.39. The

second is a hold down support located on point #5 as identified in Fig. 5.39 and in the picture shown in Fig. 5.42. the third is the connection to the pulsation damper (point #10 shown in Fig 5.39

Figure 5.42: Intermediary pipe support.

The boundary condition for the pulsation damper presents a lower stiffness than what normally would be considered in these cases, that is a rigid anchorage at the pipe end. As the vessel can be considered a compliant structure for its characteristics of larger diameter and thin shell construction, an approximation of its rigidity on the flange connection to the pipe was estimated. The estimation of the values was performed using the FEM shown in Fig. 5.43. A unitary displacement was applied individually at each DOF of the flange and the resulting reaction was considered as the system rigidity on that direction.

The other boundary conditions used were zero displacement for all three direction for the intermediate support (UX=UY=UZ = 0) and an anchor point at the connection to the interstage heat exchanger as it is a more robust structure (UX=UY=UZ=RX=RY=RZ = 0).

The FEM model constructed yielded very satisfactory results. In table 5.9, the natural frequencies calculated numerical for the full model can be seen in comparison with the experimentally obtained values as well as the difference between them.

5.3.2 Experimental Setup

The experiments were undertaken on the second stage suction line of the hydrogen make-up compressor of a diesel hydrotreating unit at Presidente Bernardes Refinery - Cubatão-SP (RPBC). The hydrogen make-up system consists of two reciprocating compressors, A and B (doubly redundant). The measurements were concentrated on compressor A, initially inactive, while compressor B operated to supply the unit's hydrogen demand.

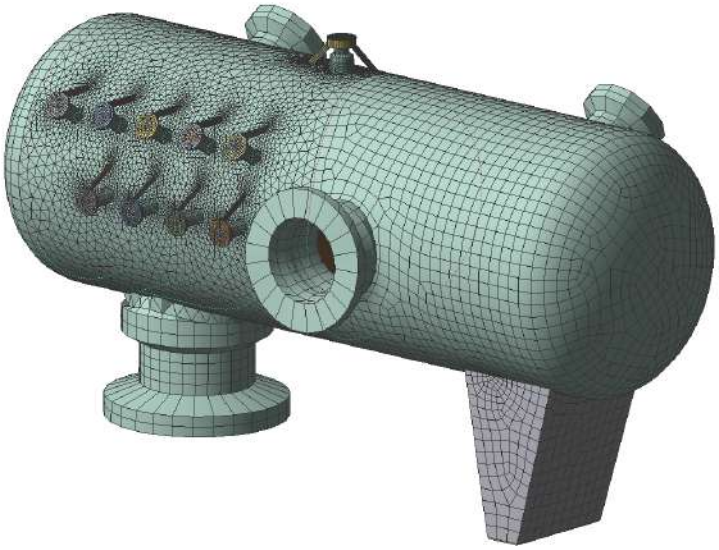

Figure 5.43: Pulsation damper model for boundary condition stiffness calculation.

Table 5.9: Difference between numerical and experimental natural frequencies.

Mode	Numerical Natural Frequency [Hz]	Experimental Natural Frequency [Hz]	Difference [%]
1	30.94	29.904	3.46%
2	44.31	42.187	5.04%
3	48.46	48.135	0.67%
4	69.7	68.635	1.55%
5	88.97	89.661	0.77%
6	107.78	108.13	0.32%
7	118.25	120.14	1.57%
8	125.69	126.07	0.30%
9	137.23	131.94	4.01%
10	159.8	156.13	2.35%
11	181.87	176.35	3.13%

The data acquisition system was installed along the pipe. Numbers from 1 to 10 shown in Fig. 5.40 indicate the positions where the accelerometers were installed. In table 5.10 the number of accelerometers used at each position, the manufacturer and directions measured can be seen.

In addition to the sensors used, a *National Instruments* data acquisition system composed of a series of c-DAQ NI 9234 and a PCB impact hammer was also used.

In Fig. 5.44 the second stage pipe with the accelerometer installed can be seen.

The experiment was performed in two parts. The first part consisted of an impact test condition, similar to the one applied in the first case study. Impact tests were carried out at 5 (five) different points: P1 and P2, with impacts in the X and Y directions; P3, in the X and Z directions; P4, in the Z direction; and P5, in the Y

Table 5.10: Description and location of the sensors used.

Item	Number of Acc	Manufacturer	Direction
1	2	PCB	X & Z
2	2	Kistler	X & Z
3	2	Kistler	X & Y
4	2	Kistler & PCB	X & Y
5	2	Kistler & PCB	X & Y
6	2	SKF	X & Z
7	2	PCB	X & Z
8	3	PCB	X & Y & Z
9	3	PCB	X & Y & Z
10	2	PCB	Y & Z

and Z directions. The impact points locations are identified in Fig. 5.40.

In the second part the following conditions were applied in the machine while vibration signals were being collected: compressor ramp start, steady-state measurement and ramp stop. The acquisitions were made with the compressor operating in re-circulation condition, to avoid interference from the test with the operation of the unit, at 30% of its capacity, without load. All measurements were performed with an acquisition rate of 2 KHz. Impact tests were measured for 50 seconds; the measurement throughout the start-up, for 150 seconds; steady-state, for 100 seconds; and during the stop, for 100 seconds.

5.3.3 Output-Only Modal Analysis (O-OMA)

Using the data obtained with the experiment described before, the Modal parameters were estimated using the OMA analysis, using the EFDD method. The natural frequencies were estimated from the SVD plot of each measurement, assessed to the frequency of 250Hz. Fig. 5.45 presents the results for impacts on positions P1 and P2 in X direction.

From the singular value decomposition (SVD) plot it can be seen that although during the impact testes compressor A was not operational, the harmonics from the operation of compress B, located in the proximity were also collected as the high level of vibrations the machine generated were transmitted through the support base and structures, this imposed an additional challenge to the identification of the natural frequencies.

The modal parameters estimated can be seen on table 5.11.

Figure 5.44: Second stage suction pipe with accelerometer installed highlighted with red circles.

5.3.4 Model Reduction using Guyan-SEREP

With the FEM completed and presenting natural frequencies that are close to the experimentally obtained the next stage of the analysis was to perform the model reduction, making the number of DOF compatible with the measurements available, a necessary procedure for the next steps of smoothing and virtual sensing.

The first step of the reduction was undertaken using the FE software built-in function, that uses the Guyan reduction method. This stage of the reduction is very dependent on the selected active degrees of freedom, therefore great care was taken to allow the downsizing of the data to be exported from the software without loosing

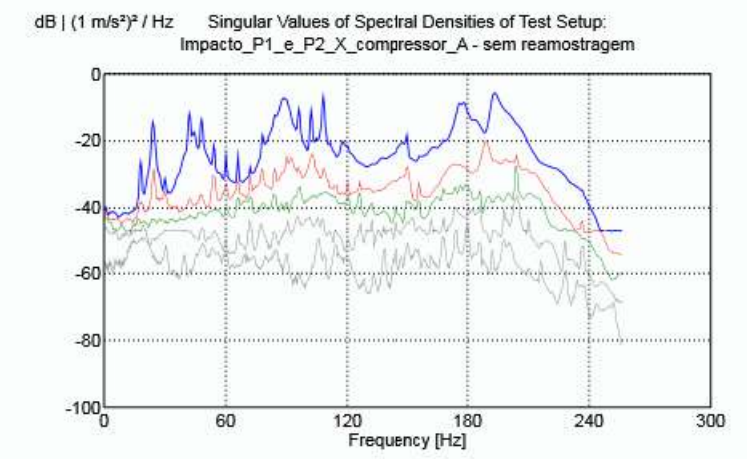

Figure 5.45: SVD - Impacts in P1 and P2, X direction.

Table 5.11: Modal Parameters estimated using EFDD.

Mode	EFDD Natural Frequency [Hz]	Damping [%]
1	29.904	0.561
2	42.187	0.793
3	48.135	0.339
4	68.635	0.110
5	89.661	0.875
6	108.13	0.203
7	120.14	0.066
8	126.07	0.010
9	131.94	0.055
10	156.13	0.069
11	176.35	0.328

important dynamic characteristics.

A total number of 70 (seventy) active nodes were necessary in this first step of the reduction. As each node has 6 (six) DOF the exported mass and stiffness matrices were of the size 420×420. Fig. 5.46 shows the FEM with the active nodes highlighted.

The exported mass and stiffness matrices were then manipulated using Matlab. A great amount of adjustment was necessary from the routines developed for this case study when comparing with the one used in the rectangular beam as this example is a three-dimensional example with displacements occurring simultaneously.

As can be seen in Fig. 5.40 the experiment consisted of sensor installation in 9 (nine) different positions. The final objective of the reduction process was to make the numerical mode equivalent in number of DOF with the experimental data, for a consistent comparison. With the same objective, the experimental data could also be expanded to match the size of the numerical model.

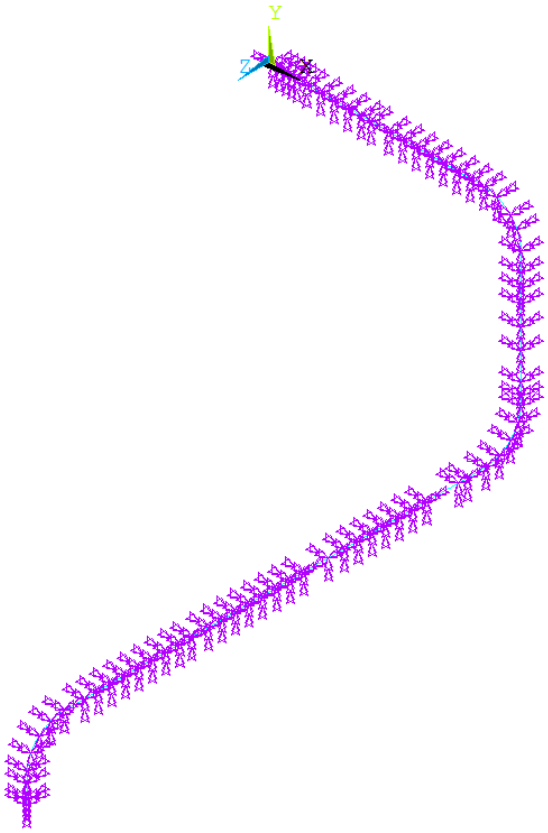

Figure 5.46: Guyan reduction model showing active DOFs.

In this analysis the reduction was selected so that the resulting data, necessary for the virtual sensing calculation, was smaller and demanded less computational resources.

The MAC criteria was applied to compare the mode shapes from the reduced model Guyan-SEREP against the full model to validate the reduction procedure. The MAC plot for this comparison is shown in Fig. 5.47. All values for the main diagonal are 1 (one), showing an excellent correlation between the mixed Guyan-SEREP reduced model and the full model, thus validating the reduction procedure. These results are in line with the plots of the mode shapes as it could be seen that the modes are almost the same. The mode shapes from the first to fourth modes for the full and reduced models can be seen in Figs. 5.61 to 5.64.

As a last assessment of the reduction procedure, the correlation between the numerical reduced and the experimental mode shapes was made. The criteria used for this assessment were MAC, COMAC and RD.

MAC values can be seen in Fig. 5.52 on the left plot, the diagonal values of the MAC matrix and on the right, the bar plot showing the complete MAC matrix.

The COMAC and RD values for the correlation between reduced and experimental modes can be seen in Fig. 5.53.

Analyzing the correlation results between reduced an experimental data shown

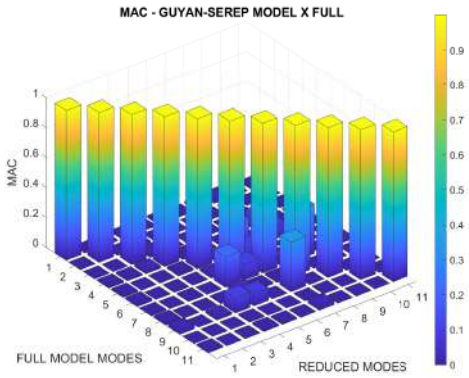

Figure 5.47: MAC for reduced and full modes.

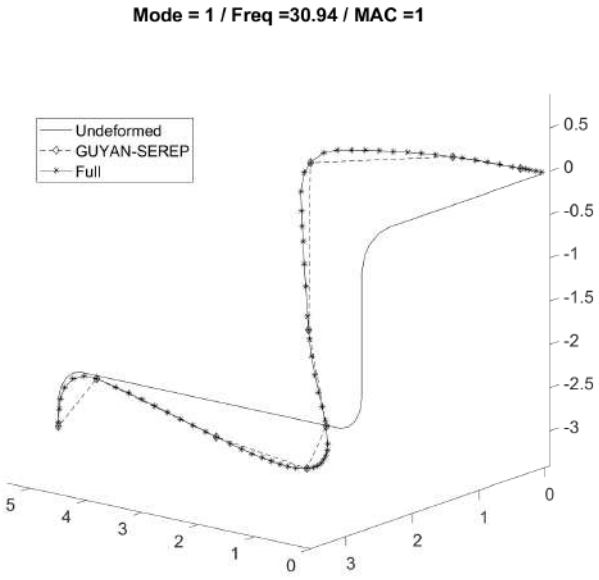

Figure 5.48: Guyan-SEREP reduced and full mode shape for the first mode.

on Figs 5.52 and 5.53 it is possible to conclude that although the numeric and experimental natural frequencies are very close to each other, the mode shapes are not.The mode shapes from the first to fourth modes for the experimental and reduced models can be seen in Figs. 5.54 to 5.57.

The difference between numerical and experimental mode shapes can be explained by the complexity of the structure object of this case. It is composed of boundary conditions that are highly nonlinear and difficult to model and therefore these differences between the numerical model and the real structure end up as differences in mode shapes. One approach that could be used in these situations is the *model updating*, where some parameters of the numerical model are optimized to make it as close as possible to the real structure. In this work this was not the approach used, we used the *local correspondence principle* for modes and coordinates

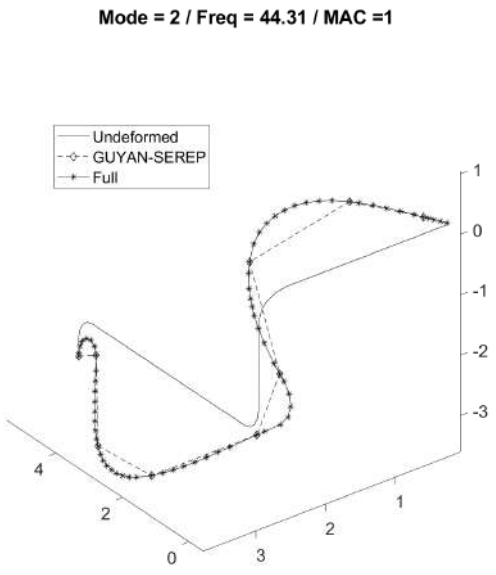

Figure 5.49: Guyan-SEREP reduced and full mode shape for the second mode.

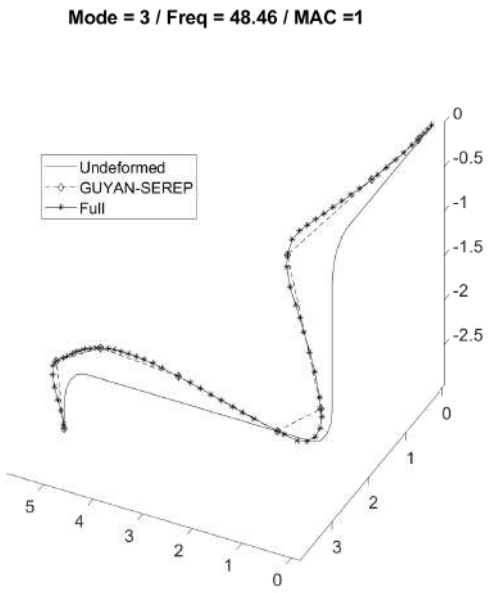

Figure 5.50: Guyan-SEREP reduced and full mode shape for the third mode.

as a smoothing solution to the differences as can be seen on the next section.

5.3.5 Modal Smoothing Using Experimental Mode Shapes

As we could see in the first two case studies, the smoothing of the experimental modes diminishes the differences between numerical and experimental data. As the first cases were experiments made in a controlled environment with very known

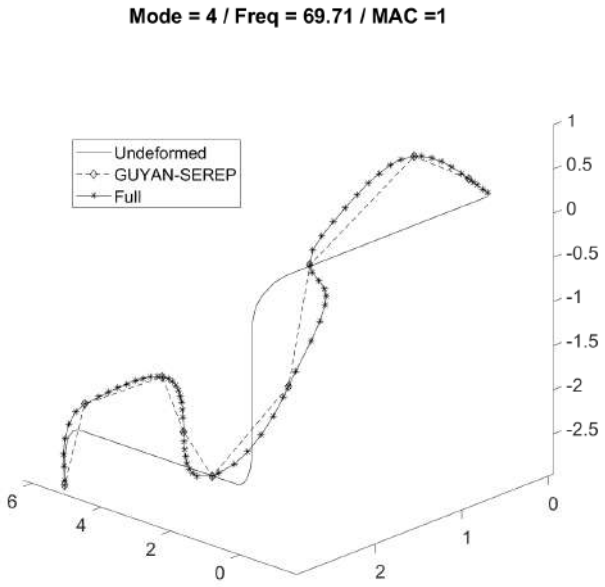

Figure 5.51: Guyan-SEREP reduced and full mode shape for the fourth mode.

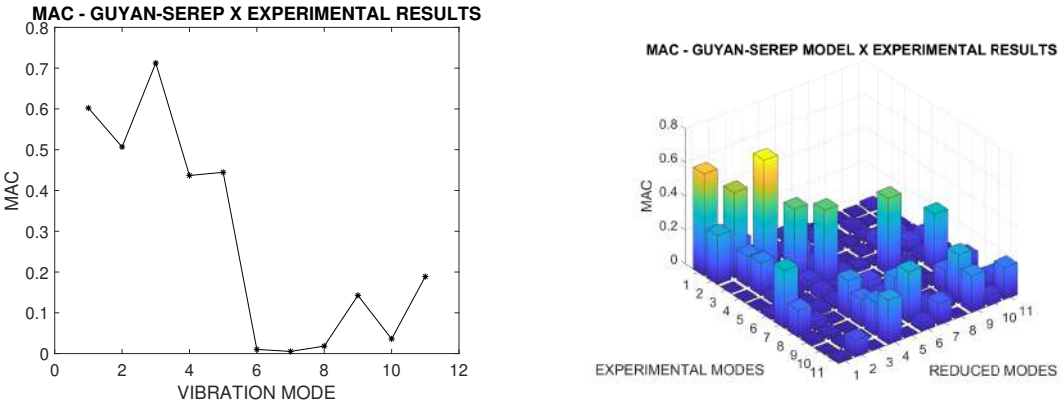

Figure 5.52: MAC for reduced and experimental modes.

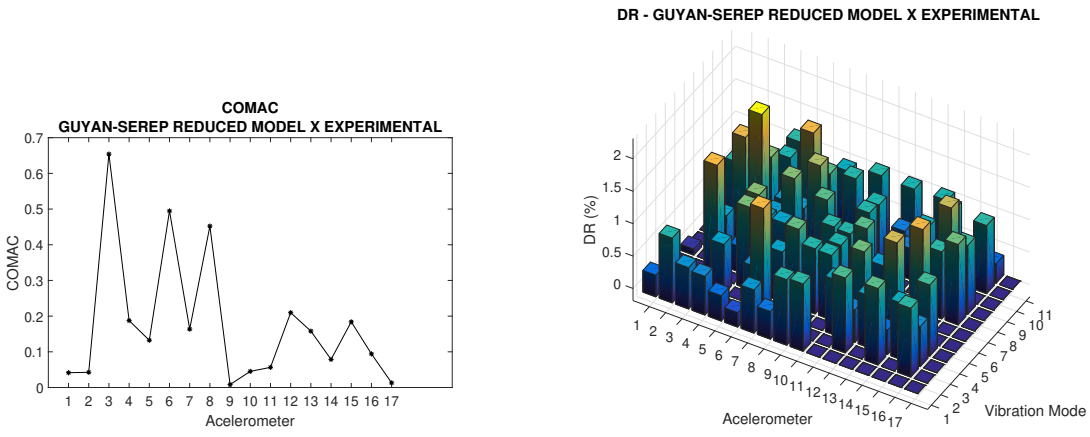

Figure 5.53: MAC for reduced and experimental modes.

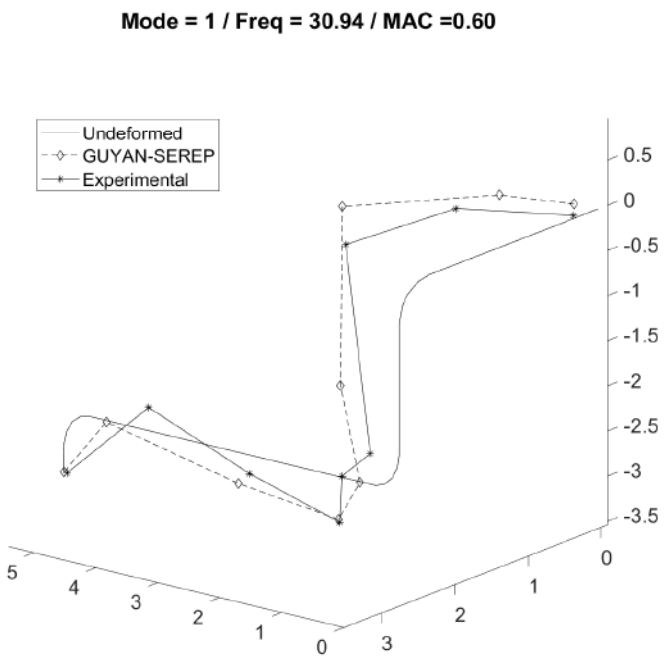

Figure 5.54: Guyan-SEREP reduced and experimental mode shape for the first mode.

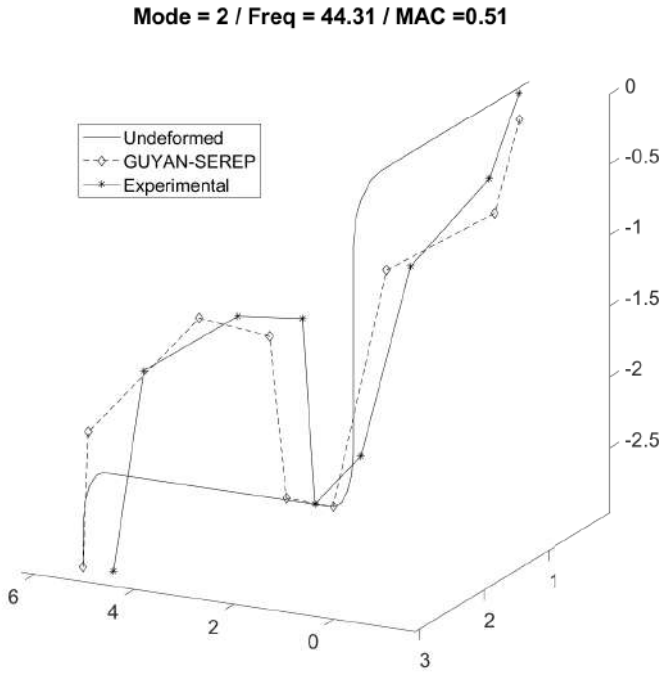

Figure 5.55: Guyan-SEREP reduced and experimental mode shape for the second mode.

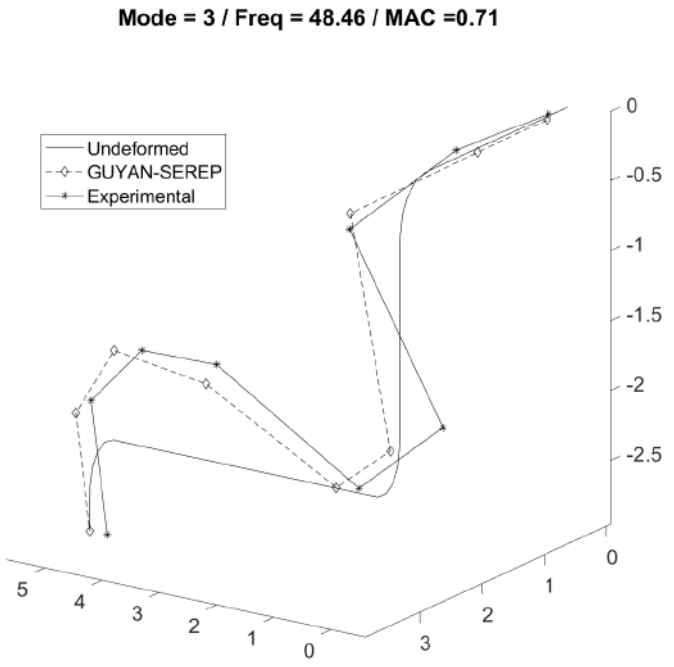

Figure 5.56: Guyan-SEREP reduced and experimental mode shape for the third mode.

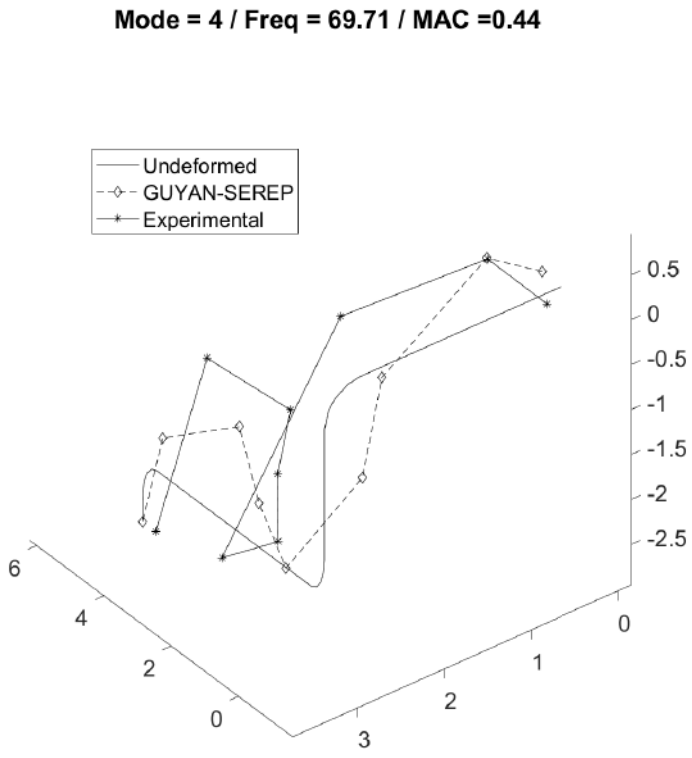

Figure 5.57: Guyan-SEREP reduced and experimental mode shape for the fourth mode.

boundary conditions, the differences started small and were improved. In this case the differences were greater and this smoothing process is extremely important.

The smoothing process was performed using the LCMC method using the 11 (eleven) mode shapes and the 17 (seventeen) degrees of freedom of the reduced modal model coinciding with the accelerometers positions and directions.

Fig. 5.58 shows the MAC values between the smoothed mode shapes and the experimental ones.

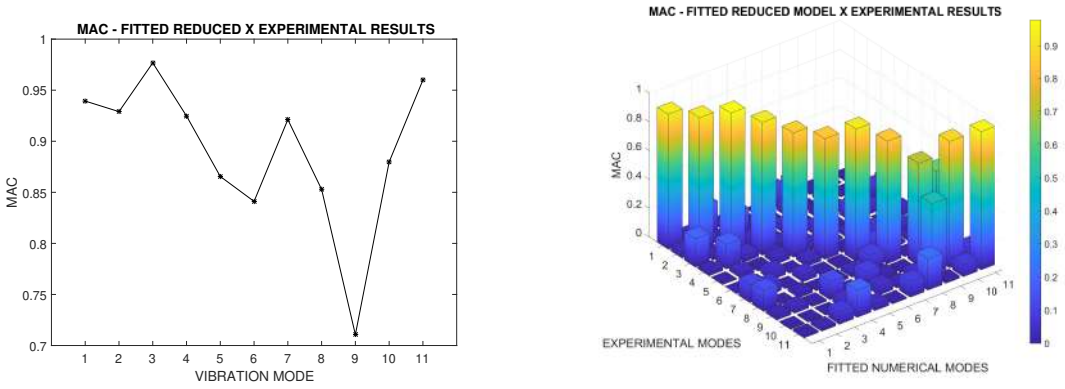

Figure 5.58: MAC for Fitted and experimental modes.

Fig 5.59 show the COMAC and RD correlation between Smoothed and Experimental results.

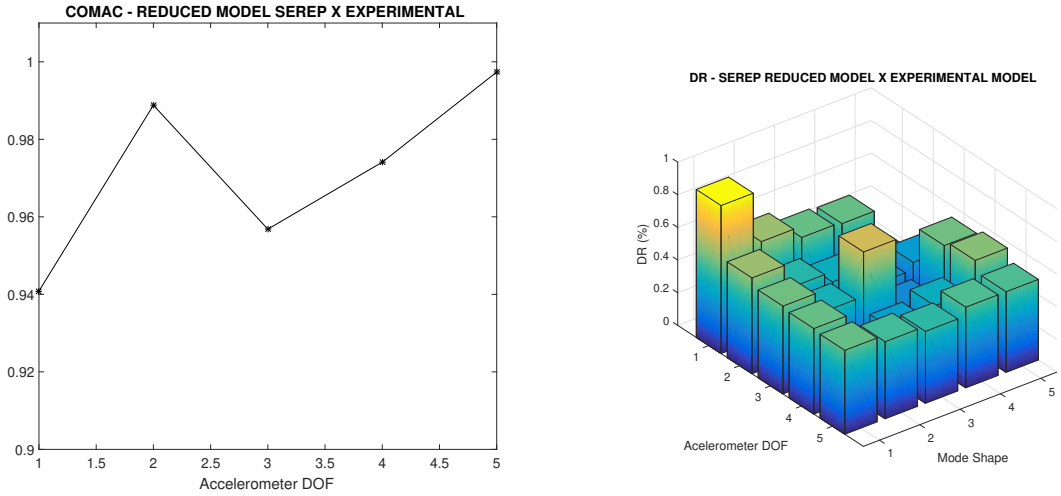

Figure 5.59: COMAC and RD between fitted and experimental modes

From the correlations shown above, in comparison to the results shown for the reduction and experimental correlation shown on section 5.3.4, the improvements after the smoothing using the LCMC method are very considerable. The comparison between MAC values for each mode shape for the reduced/Experimental and Smoothed/Experimental can be seen in the comparison presented in Fig. 5.60.

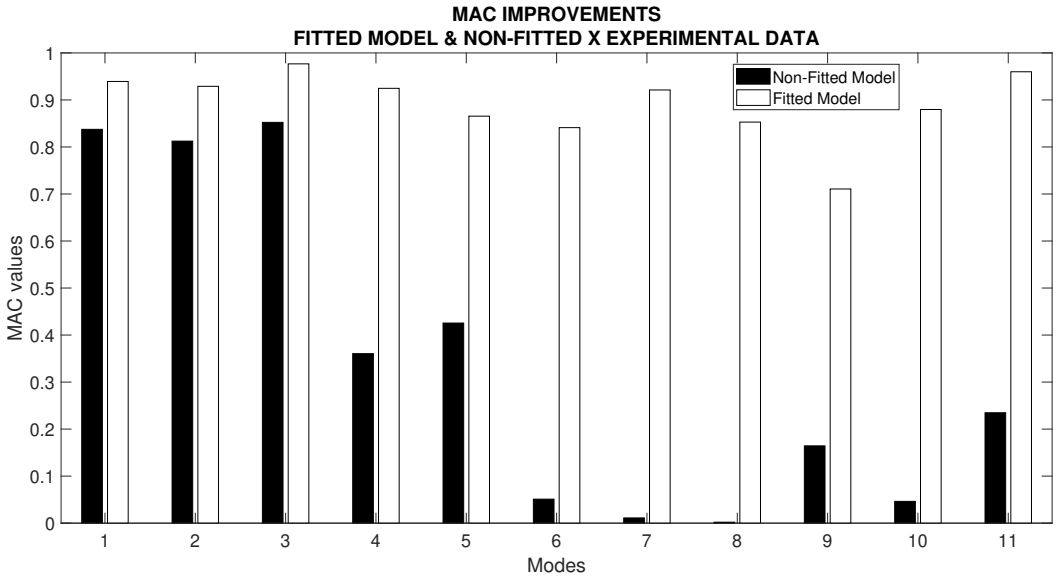

Figure 5.60: MAC improvements from LCMC correlation procedure.

The smoothed mode shapes, along with the experimental ones can be seen from the first to fourth modes in Figs. 5.61 to 5.64.

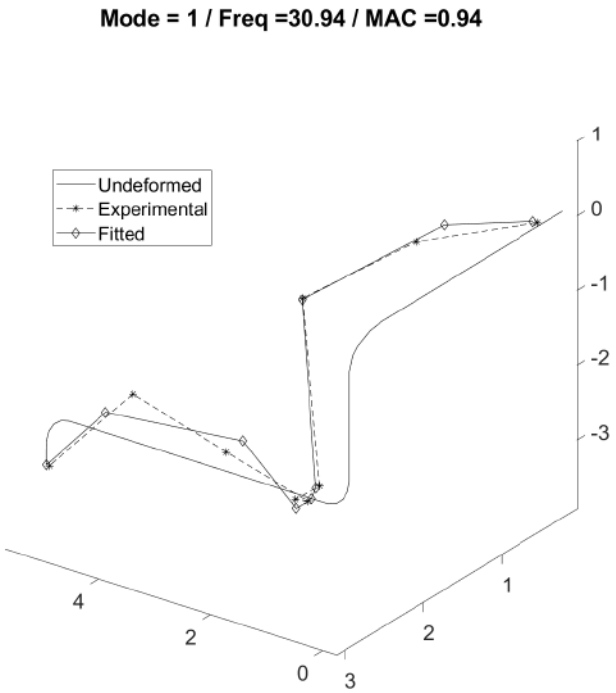

Figure 5.61: Experimental and Fitted mode shape for the first mode.

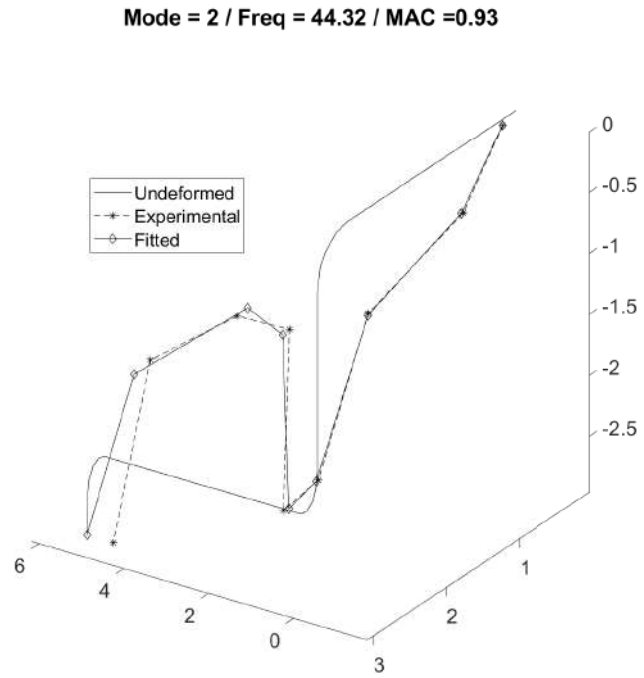

Figure 5.62: Experimental and Fitted mode shape for the second mode.

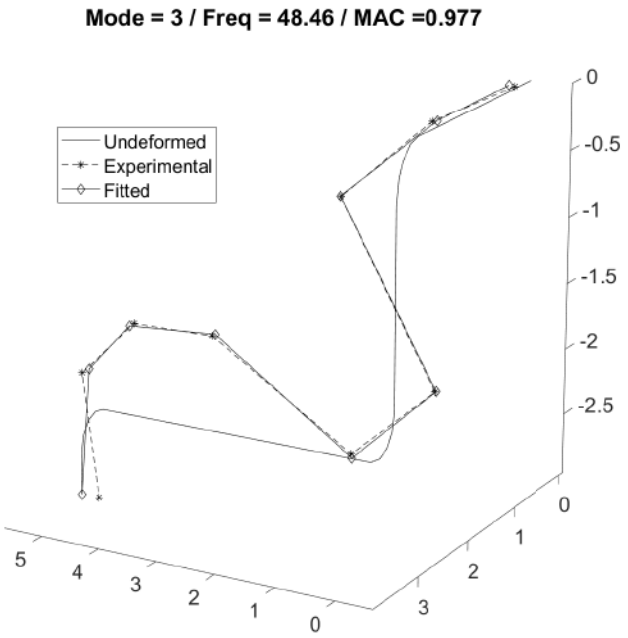

Figure 5.63: Experimental and Fitted mode shape for the third mode.

5.3.6 Virtual Sensing

With the correlated mode shapes, the next step in the analysis was to perform the dynamic response prediction. As the modes that were numerically obtained and smoothed range to 180Hz, the vibration signals used in the virtual sensing

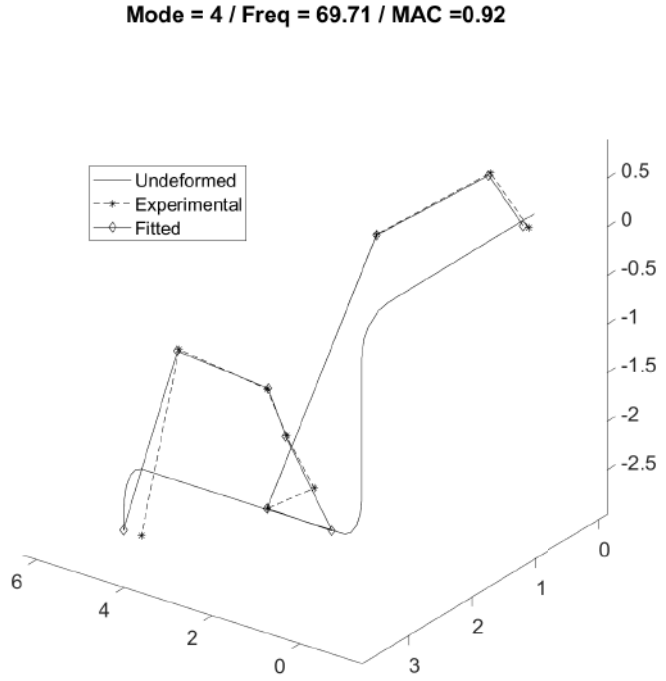

Figure 5.64: Experimental and Fitted mode shape for the fourth mode.

methodology were first filtered to this value.

The virtual sensing was undertaken in two conditions: (a) The first was using data from the impact tests and (b) using data from the steady-state machine operation, where the excitation came from the normal operation of the reciprocating compressor.

In this case study the number of degrees of freedom and modes available to combine and test in the search for the best combination of DOF and mode set can become very computational demanding, especially when taking into account that for the impact tests all possible combinations of DOF, modes should be made for the available signal of each impact position considered.

For estimating the time that would take to consider the all combinations possible of DOF and modes for the dynamic prediction of each DOF we tested an example using one degree of freedom. It took 5,0000 seconds (around 14 hours) to calculate the best possibility. Considering that there are 9 impact tests and 17 degrees of freedom to be calculated, it would take 2,140 hours (almost 90 days) to finish the processing. To overcome this difficulty, an approach based on the consideration used to create the mode set cluster used in the LC method was used.

In the approach proposed to create the combinations to be calculated, the DOFs are used in all combinations possible as usual, but the modes are ranked after the distance in frequency and used in the prediction process as a set increasing from the closest (in frequency) to the most prominent mode in the response and at each

iteration the next closest mode, to the main one is added. Using this approach we were able to predict the dynamic response at all combinations of DOF using all impacts within 6 hours.

Dynamic Response Prediction Using Impact Test Data

For the dynamic response prediction using the acceleration time series obtained during the impact tests the best result was for the prediction of the signal in sensor positioned in location 7 from Fig. 5.40 in the X direction. The combination that yielded the highest TRAC correlation value between the predicted signal and the actual measurement was the usage of the signal from DOFs 4; 9; 11; 15 and 17 and the mode shapes: 1; 2; and 3.

The result is seen in Fig. 5.65 in time domain and in Fig. 5.66 in the frequency domain. High values of TRAC and FRAC combined with low values of MAE and RMS errors indicate the high accuracy of the prediction.

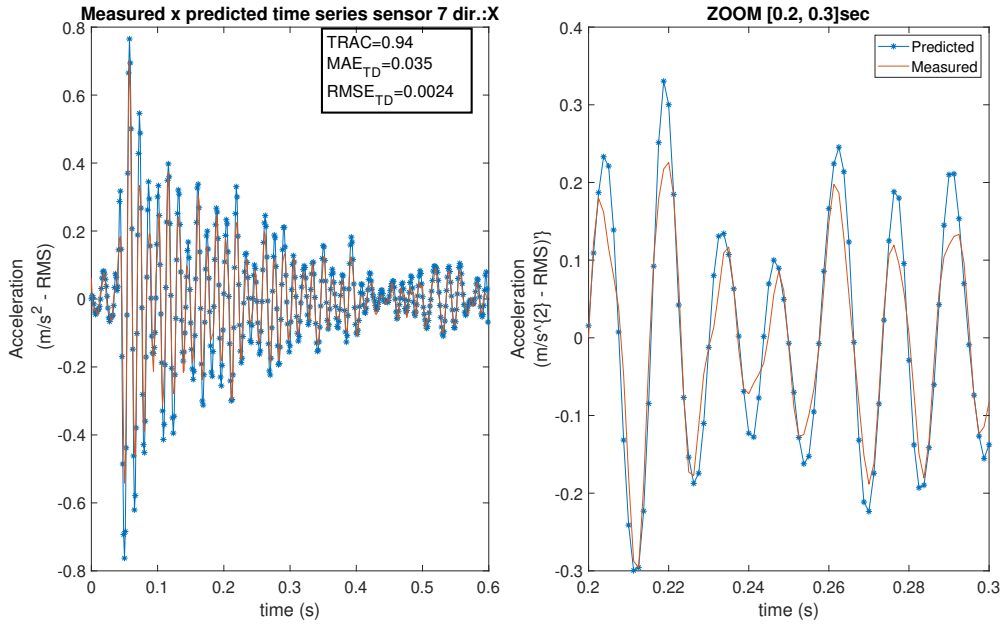

Figure 5.65: Time domain comparison of predicted and measured accelerations at sensor 7 direction X, impact given at point P4 in Z direction.

Another example of predicted DOF that yielded excellent results is the sensor in location 7 from Fig. 5.40. Nevertheless, in this case, for the Y direction. The combination that yielded the highest TRAC correlation value between the predicted signal and the actual measurement was the using the signal from DOFs 2; 4; 9; 12 and 16 and the mode shapes: 1 and 2.

The result can be seen in Fig. 5.67 in time domain and in Fig. 5.68 in the frequency domain. As the results presented before, high values of TRAC and FRAC

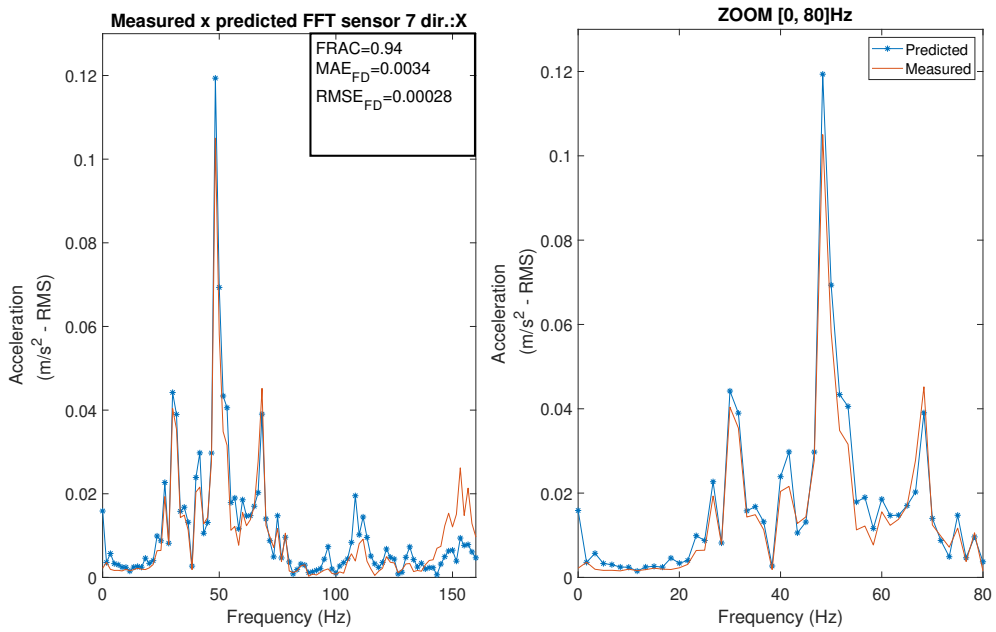

Figure 5.66: Frequency domain comparison of predicted and measured accelerations at sensor 7 direction X, impact given at point P4 in Z direction.

combined with low values of MAE and RMS errors were also encountered, hence another successful prediction.

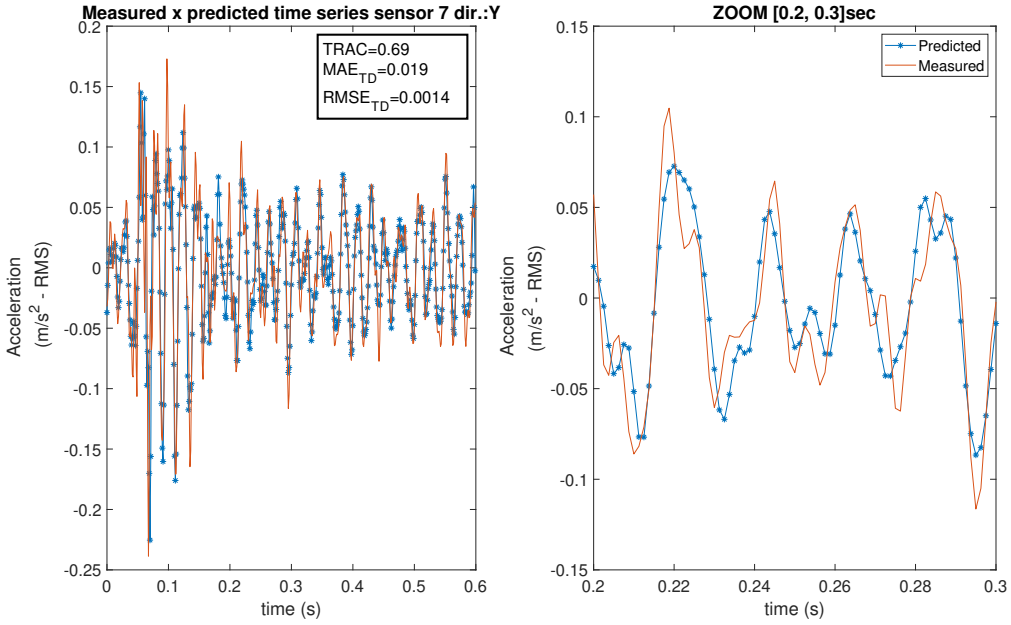

Figure 5.67: Time domain comparison of predicted and measured accelerations at sensor 7 direction Y,impact given at point P4 in Z direction.

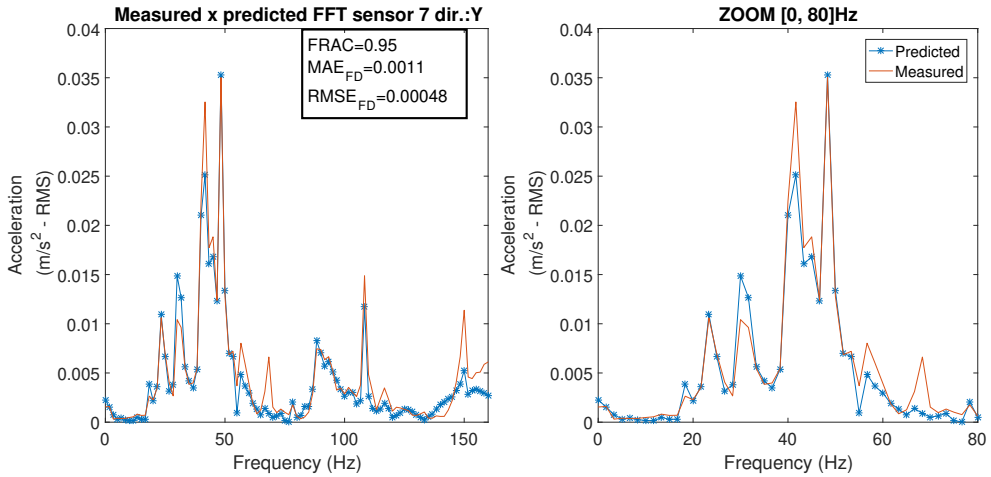

Figure 5.68: Frequency domain comparison of predicted and measured accelerations at sensor 7 direction Y, impact given at point P4 in Z direction.

Dynamic Response Prediction Using Steady-State Operation Data

For the dynamic response prediction using the acceleration time series obtained during the steady-state operation the best result was also for the prediction of the signal in sensor positioned in location 7 from 5.40 in the X direction. The combination that yielded the highest TRAC correlation value between the predicted signal and the actual measurement was the using the signal from DOFs 1; 3; 5; 6; 7; 8; 9; 10; 11; 12 and 15 and the mode shapes: 1; 2; 3; 4; 5; 6; 7; 8 and 9.

The result can be seen in Fig. 5.69 in time domain and in Fig. 5.70 in the frequency domain. High values of TRAC and FRAC combined with low values of MAE and RMS errors indicates the high accuracy of the prediction.

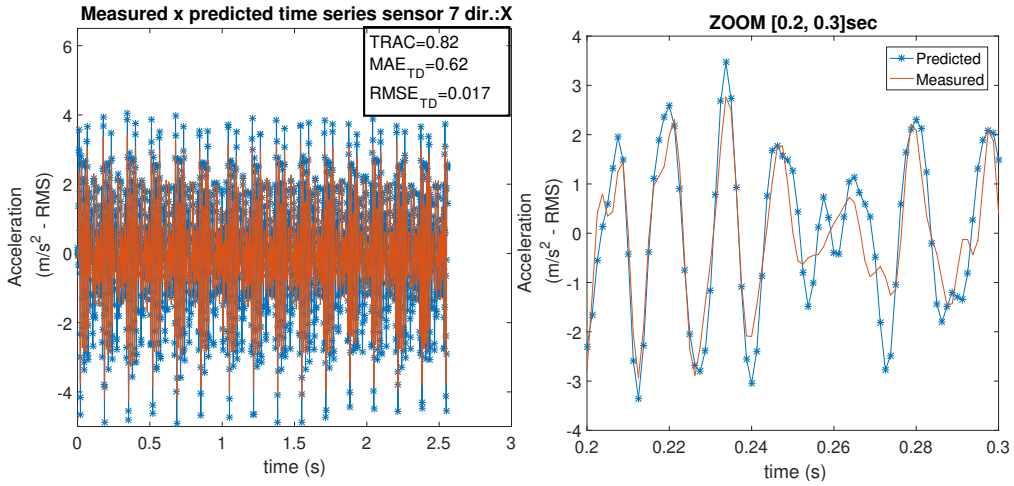

Figure 5.69: Time domain comparison of predicted and measured accelerations at sensor 7 direction X.

For the steady-state operation data, another example of predicted DOF that yielded excellent results is for the sensor in location 7 from Fig. 5.40, but in this

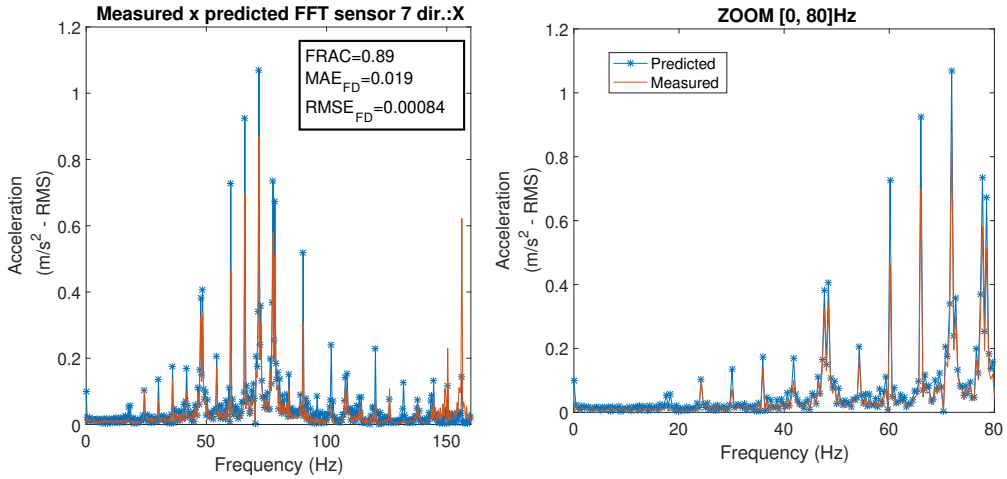

Figure 5.70: Frequency domain comparison of predicted and measured accelerations at sensor 7 direction X.

case for the Y direction. The combination that yielded the highest TRAC correlation value between the predicted signal and the actual measurement was the using the signal from DOFs 4; 6; 7; 8; 12 and 16 and the mode shapes: 1; 2; 3; 4; 5 and 6.

The result can be seen in Fig. 5.71 in time domain and in Fig. 5.72 in the frequency domain. As the results presented before, high values of TRAC and FRAC combined with low values of MAE and RMS errors were also encountered, resulting in a successful prediction.

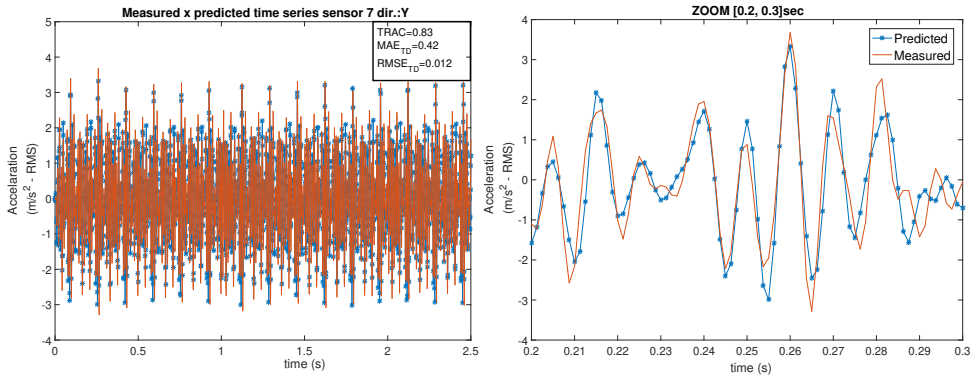

Figure 5.71: Time domain comparison of predicted and measured accelerations at sensor 7 direction Y.

5.3.7 Results Discussion

In this case study, a real operational structure was instrumented and tested to validate the methodology presented and verified before with laboratory tests. The FEM model presented challenges that were not faced in the previous tests, mostly because of the increased complexity of the system, adding an intermediary support with friction and boundary conditions that are difficult to estimate numerically. Although

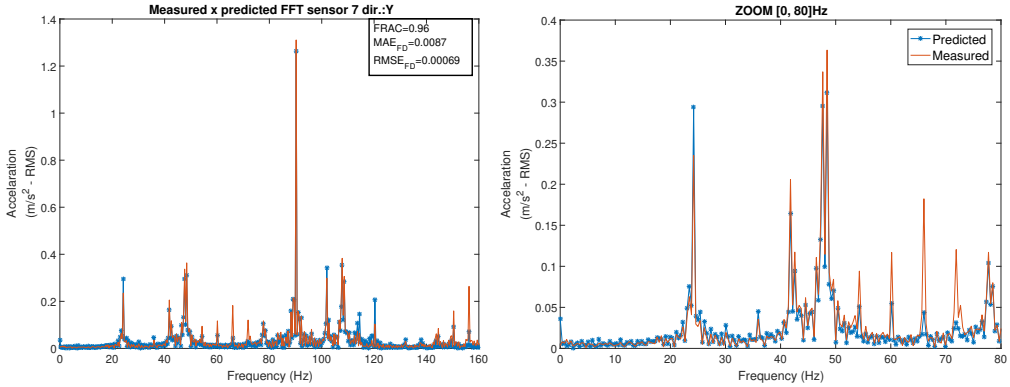

Figure 5.72: Frequency domain comparison of predicted and measured accelerations at sensor 7 direction Y.

the FEM full model presented good correlation between the natural frequencies with the experiment, the modal correlation was not adequate.

The fitting process was successful in smoothing the mode shapes between numerical and experimental data. A clear improvement could be seen in the correlation criteria (MAC, COMAC and RD) after the smoothing process.

As the previous case studies, the correlation process was very dependent on the choice of fitting DOFs and this example would also benefit from a better optimization algorithm capable of a more efficient choice of these parameters.

This structure also presented a more pronounced challenge in the virtual sensing methodology, as the number of DOFs and modes available for the algorithm were greater. The time to process all the possible combinations was very high and computational demanding. This is then a promising part for improvement in future study by for example using Machine Learning to optimize the selection of combinations.

The virtual sensing methodology both in time and frequency domain showed good correlation between the predicted and measured signal. Therefore it can be concluded that both the virtual sensing methodology could be validated and also the smoothing of the mode shapes, as they are an important input to the procedure.

Chapter 6

Conclusions and Recommendations

In this dissertation three case studies were undertaken for the application of the proposed methodology for dynamic response prediction. For the first case, an aluminum beam in free-free boundary condition, the validation of the methodology was successful. A clear improvement could be seen on the MAC correlation when the fitting process was undertaken, meaning that numerical model when fitted become closer to the experimental model. Thus, when used the fitted modal model to expand the dynamic measurements onto non measured degrees of freedom are more prone to yield more accurate results. For this first case the LC fitting method was used and it was possible to observe the dependence on the choice of the fitting DOFs. This observation provoked the development of an method that is capable of yielding better fitting results than the LC, it is defined here as the LCMC method. For the first case the dynamic response predictions were successful and yield results with good correlation between predicted and measured signals.

The second case study, based on the same aluminum beam used on the first case but with a cantilever boundary condition, was undertaken to validated the methodology at a different boundary condition. In this case the Guyan-SEREP reduction achieved the goal of fully reducing the system keeping the dynamic properties. The MAC between the reduced model mode shapes from this method compared to the full model were all close to 1 and all relative difference (RD) values were below 1%. These results conclude the efficiency of the reduction procedure. The smoothing process, based on the LCMC principle, showed to be successful and yielded very good improvement in the correlation with the experimental results. The virtual sensing, both in the time and frequency domains, showed good agreement with the measured acceleration signals.

The third and main case study of this work was the application of the methodology to an interstage DN 10 pipe of a reciprocating compressor. In this case the FEM model presented challenges, mostly because of the increased complexity of the system, adding boundary conditions difficult to represent numerically. Although the

FEM full model presented good correlation between the natural frequencies with the experiment, the modal correlation was not adequate. For this reason the fitting process was very important and successful in smoothing the mode shapes between numerical and experimental data. A clear improvement could be seen in the correlation criteria (MAC, COMAC and RD) after the smoothing process. The virtual sensing methodology both in time and frequency domain showed good correlation between the predicted and measured signal. Therefore it can be concluded that both the virtual sensing methodology could be validated and also the smoothing of the mode shapes, as they are an important input to the procedure.

In this work acceleration amplitudes were estimated at unmeasured locations using smoothed and expanded modal model for three case studies. The estimated dynamic responses were successful for the three cases presented. This was demonstrated by the high correlations factors between predicted and measured signals in time and frequency domains.

The quality of dynamic response prediction found to be very dependent on the position of the response being predicted. The number and position of the signals used in the prediction made great difference on the results, as well as the number of modes considered in the prediction.

The numerical model (FEM) was necessary to serve as a basis for the smoothing process, for obtaining the mass matrix to M-orthonormalize the experimental modal matrix (this step will be crucial at future works for the prediction of forces acting on structures) and serve as a fitting basis to correct spatial aliasing by expansion of experimental data.

The Guyan-SEREP reduction process proposed showed good correlation with the FEM full model with the advantage of yielding smaller exported mass an stiffness matrices, resulting in more computational efficient processing with similar quality results.

A clear improvements could be seen on the MAC correlation for the three case studies when the smoothing process was undertaken. A more pronounced improvement could be seen on the pipe as it had more differences between FEM and experimental results.

An advantage of the modal expansion method, in predicting responses, is that it only uses the modal matrix and does not depend on natural frequencies and damping ratios. This method is fast, easy to implement and effective. The virtual sensing, both in the time and frequency domains, showed good agreement with the measured acceleration signals.

The smoothing process with the LCMC method proposed in this work resulted in an effective selection of combinations for modes and DOFs and avoided over-fitting. This was demonstrated by the improvements in MAC values, after smoothing. How-

ever, as the proposed method relies on calculating the results for all possible combinations of DOFs and modes to choose the best, it resulted in a very computational expensive task especially for systems with more degrees of freedom.

Following are the topics recommended for further work:

- Evaluate artificial intelligence and optimization algorithms to improve performance for the definition of best combination of modes and degrees of freedom to be used in the smoothing process by discarding combinations of DOFs and modes that have no relevant influence on the mode shape being smoothed.

- Evaluate optimization and artificial intelligence algorithm to help select the best locations to install sensors in order to optimize the dynamic response prediction.

- The virtual sensing method should be extended to predict full-field stress and strain of structures, allowing the evaluation of fatigue in locations difficult to measure, for example, the ones used in offshore structures, especially those that need high reliability

- Another approach that would result in great improvement for the analysis would be using model updating techniques to optimize the numerical model and make it as close as possible to the experiment, for instance, in order to identify faults in structures and/or equipment.

- Extend virtual sensing methodology using artificial intelligence and optimization algorithm to estimate forces and moments acting on structures to be used in troubleshooting and design improvements of structures.

References

AENLLE, M. L., BRINCKER, R., 2013, "Modal scaling in operational modal analysis using a finite element model", *International Journal of Mechanical Sciences*, v. 76, pp. 86–101. ISSN: 00207403. doi: 10.1016/j.ijmecsci.2013.09.003. Disponível em: <http://dx.doi.org/10.1016/j.ijmecsci.2013.09.003>.

AENLLE, M. L., BRINCKER, R., 2014, "Modal Scaling in OMA Using the Mass matrix of a Finite Element Model", *Catbas F. (eds) Dynamics of Civil Structures*, v. 4, n. Conference Proceedings of the Society for Experimental Mechanics Series, pp. 263–270. doi: 10.1007/978-3-319-04546-7_30. Disponível em: <http://link.springer.com/10.1007/978-3-319-04546-7{_}30>.

ALBUQUERQUE, L. C., GUTIÉRREZ, R. H., HUAMANI, J. A., et al., 2019, "MODAL PARAMETER IDENTIFICATION OF A RECTANGULAR BEAM USING EXPERIMENTAL AND OUTPUT-ONLY MODAL ANALYSES Polyreference Least Square Complex Frequency Domain (p-LSCF)", .

ALLEMANG, R. J., 2002, "The Modal Assurance Criterion – Twenty Years of Use and Abuse", v. 1, n. February.

AVITABILE, P., 1998, "Overview of Analytical and Experimental Modal Model Correlation Techniques Modal Model Correlation Techniques", ISSN: 10641246.

AVITABILE, P., 2005, "Model reduction and model expansion and their applications Part 1 - Theory", *Conference Proceedings of the Society for Experimental Mechanics Series*. ISSN: 21915644.

BALMÈS, E., 1999, "Sensors, degrees of freedom, and generalized modeshape expansion methods '", *Imac*, pp. 1–8. ISSN: 10466770.

BRINCKER, R., VENTURA, C. E., 2015, *Introduction to Operational Modal Analysis*. Chichester, UK, John Wiley & Sons, Ltd. ISBN: 978-1-119-96315-8. doi: 10.1002/9781118535141.

BRINCKER, R., SKAFTE, A., LÓPEZ-AENLLE, M., et al., 2014, "A local correspondence principle for mode shapes in structural dynamics", *Mechanical Systems and Signal Processing*, v. 45, n. 1, pp. 91–104. ISSN: 08883270. doi: 10.1016/j.ymssp.2013.10.025. Disponível em: <http://dx.doi.org/10.1016/j.ymssp.2013.10.025>.

BUSSON, L., MONTEIRO, U. A., GUTIÉRREZ, R. H., et al., 2019, "OUTPUT-ONLY MODAL PARAMETER IDENTIFICATION RECTANGULAR BEAM USING MIMO AND SIMO TESTS OF Output-Only Modal Analysis". In: *IBERO-LATIN AMERICAN CONGRESS ON COMPUTATIONAL METHODS IN ENGINEERING*, Natal, RN - Brazil.

CHEN, Y., JOFFRE, D., AVITABILE, P., 2018, "Underwater Dynamic Response at Limited Points Expanded to Full-Field Displacement Response", v. 140, n. October, pp. 1–9. ISSN: 15288927. doi: 10.1115/1.4039800.

CHIPMAN, C., AVITABILE, P., 2012, "Expansion of transient operating data", *Mechanical Systems and Signal Processing*, v. 31 (aug), pp. 1–12. ISSN: 08883270. doi: 10.1016/j.ymssp.2012.04.013. Disponível em: <http://dx.doi.org/10.1016/j.ymssp.2012.04.013>.

EWINS, D. J., 2000a, *Modal Testing: Theory, Practice and Application*. 2nd ed. ed. London. ISBN: 0863800173.

EWINS, D. J., 2000b, "Model validation: correlation for updating", *Sadhana - Academy Proceedings in Engineering Sciences*, v. 25, n. 3, pp. 221–234. ISSN: 02562499. doi: 10.1007/BF02703541.

FRISWELL, M. I., MOTTERSHEAD, J. E., 1995, *Finite element model updating in structural dynamics*. London. ISBN: 0-7923-3431-0. doi: 10.1007/978-94-015-8508-8.

GUYAN, R. J., 1965, "Reduction of stiffness and mass matrices", *AIAA Journal*, v. 3, n. 2, pp. 380–380. ISSN: 0001-1452. doi: 10.2514/3.2874.

IEA, 2017. "Data and Statistics - Total primary energy by source". November. Disponível em: <https://www.iea.org/data-and-statistics?country=WORLD&fuel=Energy%20supply&indicator=Total%20primary%20energy%20supply%20(TPES)%20by%20source>.

ILIOPOULOS, A., SHIRZADEH, R., WEIJTJENS, W., et al., 2016, "A modal decomposition and expansion approach for prediction of dynamic responses on a monopile offshore wind turbine using a limited number of vibration sensors", *Mechanical Systems and Signal Processing*, v. 68-69, pp. 84–104. ISSN: 10961216. doi: 10.1016/j.ymssp.2015.07.016.

ILIOPOULOS, A. N., DEVRIENDT, C., ILIOPOULOS, S. N., et al., 2014, "Continuous fatigue assessment of offshore wind turbines using a stress prediction technique", *Health Monitoring of Structural and Biological Systems 2014*, v. 9064, pp. 90640S. ISSN: 1996756X. doi: 10.1117/12.2045576.

JACOBSEN, N. J., ANDERSEN, P., 2008, "Operational modal analysis on structures with rotating parts", *23rd International Conference on Noise and Vibration Engineering 2008, ISMA 2008*, v. 4, pp. 2491–2505.

KIDDER, R. L., 1973, "Reduction of Structural Frequency Equations", *Journal of Scientific Instruments Journal of Applied Physics Journal of Physics, Ser. E Lennert, A. E. Bell System Technical Journal*, v. 11, n. 6, pp. 892. ISSN: 0001-1452. doi: 10.2514/3.6852.

KONG, X., WU, D. J., CAI, C. S., et al., 2012, "New strategy of substructure method to model long-span hybrid cable-stayed bridges under vehicle-induced vibration", *Engineering Structures*, v. 34, pp. 421–435. ISSN: 01410296. doi: 10.1016/j.engstruct.2011.10.018.

KULLAA, J., 2016, "Virtual sensing of structural vibrations using dynamic substructuring", *Mechanical Systems and Signal Processing*, v. 79, pp. 203–224. ISSN: 10961216. doi: 10.1016/j.ymssp.2016.02.045. Disponível em: <http://dx.doi.org/10.1016/j.ymssp.2016.02.045>.

LIU, F., 2011, "Direct mode-shape expansion of a spatially incomplete measured mode by a hybrid-vector modification", *Journal of Sound and Vibration*, v. 330, n. 18-19, pp. 4633–4645. ISSN: 0022460X. doi: 10.1016/j.jsv.2011.05.003. Disponível em: <http://dx.doi.org/10.1016/j.jsv.2011.05.003>.

MAES, K., DE ROECK, G., LOMBAERT, G., 2014, "Response estimation in structural dynamics", *Proceedings of the International Conference on Structural Dynamic , EURODYN*, v. 2014-Janua, n. July, pp. 2399–2406. ISSN: 23119020.

MARTINS VIEIRA, A., 2020, *MÉTODO PARA CALIBRAÇÃO DO MODELO NUMÉRICO DE ESTRUTURAS PARA PREDIÇÃO DE AMPLI-*

TUDES DE VIBRAÇÃO. Tese de Doutorado, Universidade Federal do Rio de Janeiro.

MCKINSEY, 2020. "Mckinsey Energy Insights - Hydrotreater". september. Disponível em: <https://www.mckinseyenergyinsights.com/resources/refinery-reference-desk/hydrotreater/>.

MENDONÇA, C. O., GUTIÉRREZ, R. H., MONTEIRO, U. A., et al., 2019, "NUMERICAL AND EXPERIMENTAL CORRELATION OF RECTANGULAR BEAM USING A GUYAN-SEREP MIXED METHOD Background". In: *IBERO-LATIN AMERICAN CONGRESS ON COMPUTATIONAL METHODS IN ENGINEERING*, Natal, RN - Brazil.

NONIS, C., THIBAULT, L., MARINONE, T., et al., 2014. "Development of Full Space System Model Modes from Expansion of Reduced Order Component Modal Information". ISSN: 21915644.

O'CALLAHAN, J., AVITABILE, P., RIEMER, R., 1989, "System equivalent reduction expansion process (SEREP)", *Proceedings of the International Modal Analysis Conference - IMAC XVII*, pp. 29–37.

OGNO, M., 2013, *Identifying structural parameters of an Offshore Wind Turbine using Operational Modal Analysis*. Tese de Doutorado, Delft University of Technology.

PAULTRE, P., 2011, *Dynamic of Structures*. London. ISBN: 9781848210639.

PINGLE, P., AVITABILE, P., 2011, "Full-field dynamic stress/strain from limited sets of measured data", *Sound and Vibration*, v. 45, n. 8, pp. 10–14. ISSN: 15410161.

QU, Z.-Q., 2004, *Model Order Reduction Techniques*. London, Springer London. ISBN: 978-1-84996-924-6. doi: 10.1007/978-1-4471-3827-3. Disponível em: <http://link.springer.com/10.1007/978-1-4471-3827-3>.

R. S. MINETTE, 2014, *ANÁLISE MODAL DE BOMBAS CENTRÍFUGAS SUBMERSAS Ricardo*. Master thesis, Universidade Federal do Rio de Janeiro.

RAINIERI, C., FABBROCINO, G., 2014, *Operational Modal Analysis of Civil Engineering Structures*. New York. ISBN: 978-1-4939-0766-3. doi: 10.1007/978-1-4939-0767-0.

SESTIERI, A., D'AMBROGIO, W., BRINCKER, R., et al., 2013, "Estimation of Rotational Degrees of Freedom by EMA and FEM Mode Shapes".

Conference Proceedings of the Society for Experimental Mechanics Series, pp. 355–365. doi: 10.1007/978-1-4614-6546-1_38. Disponível em: <http://link.springer.com/10.1007/978-1-4614-6546-1{_}38>.

TARPØ, M., NABUCO, B., GEORGAKIS, C., et al., 2020, "Expansion of experimental mode shape from operational modal analysis and virtual sensing for fatigue analysis using the modal expansion method", v. 130. ISSN: 01421123. doi: 10.1016/j.ijfatigue.2019.105280.